TOPICAL REPORT
Project No.: 9-61-5329

ORNL/Sub/89-SA187/02

TITLE: FIRESIDE CORROSION TESTING OF CANDIDATE SUPERHEATER TUBE ALLOYS, COATINGS, AND CLADDINGS

Principal Investigator: S. Van Weele
Program Manager: J. L. Blough

Final Report, August 1991

Report Prepared by:

FOSTER WHEELER DEVELOPMENT CORPORATION
12 Peach Tree Hill Road
Livingston, New Jersey 07039

Prepared for:

OAK RIDGE NATIONAL LABORATORY
Oak Ridge, Tennessee 37831

Managed by:

MARTIN MARIETTA ENERGY SYSTEMS, INC.
for the
U. S. DEPARTMENT OF ENERGY

Under Contract No.:

DE-AC05-840R21400

FOSTER WHEELER DEVELOPMENT CORPORATION
Livingston, New Jersey 07039

ORNL/Sub--89-SA187/02

DE92 008500

FIRESIDE CORROSION TESTING OF CANDIDATE SUPERHEATER TUBE ALLOYS, COATINGS, AND CLADDINGS

Research sponsored by the U.S. Department of Energy,
Fossil Energy
Advanced Research and Technology Development Materials Program

Report Prepared by
FOSTER WHEELER DEVELOPMENT CORPORATION
12 Peach Tree Hill Road
Livingston, New Jersey 07039

under

Subcontract SA-187-89

for

OAK RIDGE NATIONAL LABORATORY
Oak Ridge, Tennessee 37831
managed by
MARTIN MARIETTA ENERGY SYSTEMS, INC.
for the
U. S. Department of Energy
under Contract No. DE-AC05-840R21400

ABSTRACT

Fireside corrosion, caused by liquid alkali-iron trisulfates, has been an obstacle to higher steam temperatures and to efficient utilization of high-sulfur coals. Tests simulating the environment in the superheater bank of a pulverized-coal-fired boiler were conducted on several promising new alloys and claddings. Alloys were exposed to a variety of synthetic ash and simulated flue gas compositions at 650 and 700°C for times ranging up to 800 hours.

Included in the testing program were new high-chromium/high-nickel alloys, modified commercial alloys, lean stainless steels (modified Type 316) clad with high-chromium/high-nickel alloys, and intermetallic aluminides.

Thickness loss measurements indicated that resistance to attack improved with increasing chromium level. Silicon and aluminum were also helpful in resisting attack, while molybdenum was detrimental to the resistance of the alloys to attack. Three different attack modes were observed on the alloys tested. Alloys with low resistance to attack exhibited uniform wastage, while pitting was observed in more resistant alloys. In addition to surface fluxing by molten alkali-iron trisulfates, subsurface sulfur penetration and intergranular attack also occurred.

ACKNOWLEDGMENTS

I am indebted to Edward M. Davis, Istvan Dojcsanszky, and Robert Carrigan for their assistance in preparing the specimens, conducting the tests, and analyzing the exposed specimens. I thank Irwin Rehn, Greg Stanko, and Eugene Montrone for their guidance and invaluable technical advice. Finally, I wish to acknowledge Hayley Morton and William Marcinko for their patience in formatting and revising this document and Jean Rabe for editing.

Contents

Contents (Cont)

Tables

Figures

Figures (Cont)

Figures (Cont)

Figures (Cont)

Figures (Cont)

Section 1

INTRODUCTION

Liquid alkali-iron trisulfate attack has been a serious obstacle to raising steam temperatures above 538°C (1000°F) in boilers fired by coals with moderate to high sulfur and alkali contents. The reasons for evaluating new alloys to resist trisulfate attack include:

- Higher coal costs, making supercritical boilers economically attractive
- Diminishing reserves of low-sulfur coal, forcing utilities to burn the larger reserves of moderate- to high-sulfur coal.
- Single-alloy tubing, which can provide adequate corrosion resistance, may become prohibitively expensive as the cost of chromium increases and operating environments become more demanding. Claddings and new lower-chromium alloys could provide an economical alternative to more traditional high (single)-alloy tubes.

This research was sponsored by the U.S. Department of Energy, Fossil Energy AR&TD Materials Program, DOE/FE AA 15 10 10 0, Work Breakdown Structure Element FW-2. The objectives of this testing program were: to evaluate the resistance of several promising alloys to alkali-iron trisulfate (AIT) attack in various environments, to characterize the resultant corrosion morphologies, and to determine the corrosion mechanisms of these alloys. Alloys and claddings chosen for testing consisted of:

- Recently developed commercial alloys containing between 20- and 35-percent chromium
- Commercial alloys modified to improve creep strength and corrosion resistance (i.e., Type 316 Mod.)
- Lean stainless steels clad with high-chromium alloys
- Intermetallic aluminides.

Selected commercial alloys widely used in pulverized-coal-fired (PC-fired) boilers provided references against which the corrosion resistances of the new alloys could be gauged. Testing was conducted at 650 and 700°C with synthetic ashes containing 10 wt% and 75 wt% alkali sulfates under three different conditions--an ash containing 75 wt% alkali sulfates and a flue gas containing 0.25 vol% SO_2, an ash containing 10 wt% alkali sulfates and a flue gas containing 0.25 vol% SO_2, and an ash containing 10 wt% alkali sulfates and a flue gas containing 1.0 vol% SO_2. These conditions were designed to simulate the environment found in the superheater section of an advanced PC-fired boiler burning different grades of coal. The temperatures were chosen to be representative of the skin temperature of a tube under a layer of ash and to provide conditions corrosive enough to allow us to gather meaningful test data in a short time period. This work has been patterned after previous work by Rehn and Kihara [1-4]. Procedures and alloy selection in this program have been extensively verified in reports by Rehn [1-3].

Section 2

EXPERIMENTAL APPROACH AND TEST PLAN

2.1 SIMULATING BOILER CONDITIONS IN THE LABORATORY

To simulate conditions within a boiler for the purpose of corrosion testing, alloy coupons were coated with a synthetic coal ash, placed in a sealed retort, and heated to the testing temperature (650 or 700°C) while a simulated flue gas was passed through the retort and over the coupons.

2.1.1 Simulated Flue Gas Creation

Simulated flue gases were continuously blended from cylinder gases. Figure 2.1 schematically illustrates the gas train used to create the gas mixtures. Nitrogen, carbon dioxide, and air were metered through rotometers into a common manifold. After the gas mixture passed through a water bubbler, SO_2 was added to the gas stream, and the gas was sent into the experimental retorts. Tubing after the water bubbler was heated to prevent the condensation of sulfuric acid in the system.

Simulated flue gases were composed of 3.6 vol% O_2, 14.0 vol% CO_2, 10.0 vol% H_2O, and either 0.25 or 1.0 vol% SO_2, with the balance N_2. The O_2, CO_2, and SO_2 levels in the gas stream were determined by analyzing samples taken from the gas inlet of the retort.

2.1.2 Synthetic Fuel Ash Preparation

Three synthetic ashes were used in this program; their compositions are listed in Table 2.1. Ash Compositions 1 and 2 were used during the initial testing; however, Ash Composition 1 was too corrosive for the length of the planned tests. A less-corrosive ash, which would be more representative of ashes found in PC-fired boilers, was chosen for all later tests (Ash 3).

Table 2.1 Ash Compositions (wt%)

Ash 1	Ash 2	Ash 3
25 Fe_2O_3	90 Fe_2O_3	30 Fe_2O_3
37.5 Na_2SO_4	5 Na_2SO_4	5 Na_2SO_4
37.5 K_2SO_4	5 K_2SO_4	5 K_2SO_4
		30 Al_2O_3
		30 SiO_2

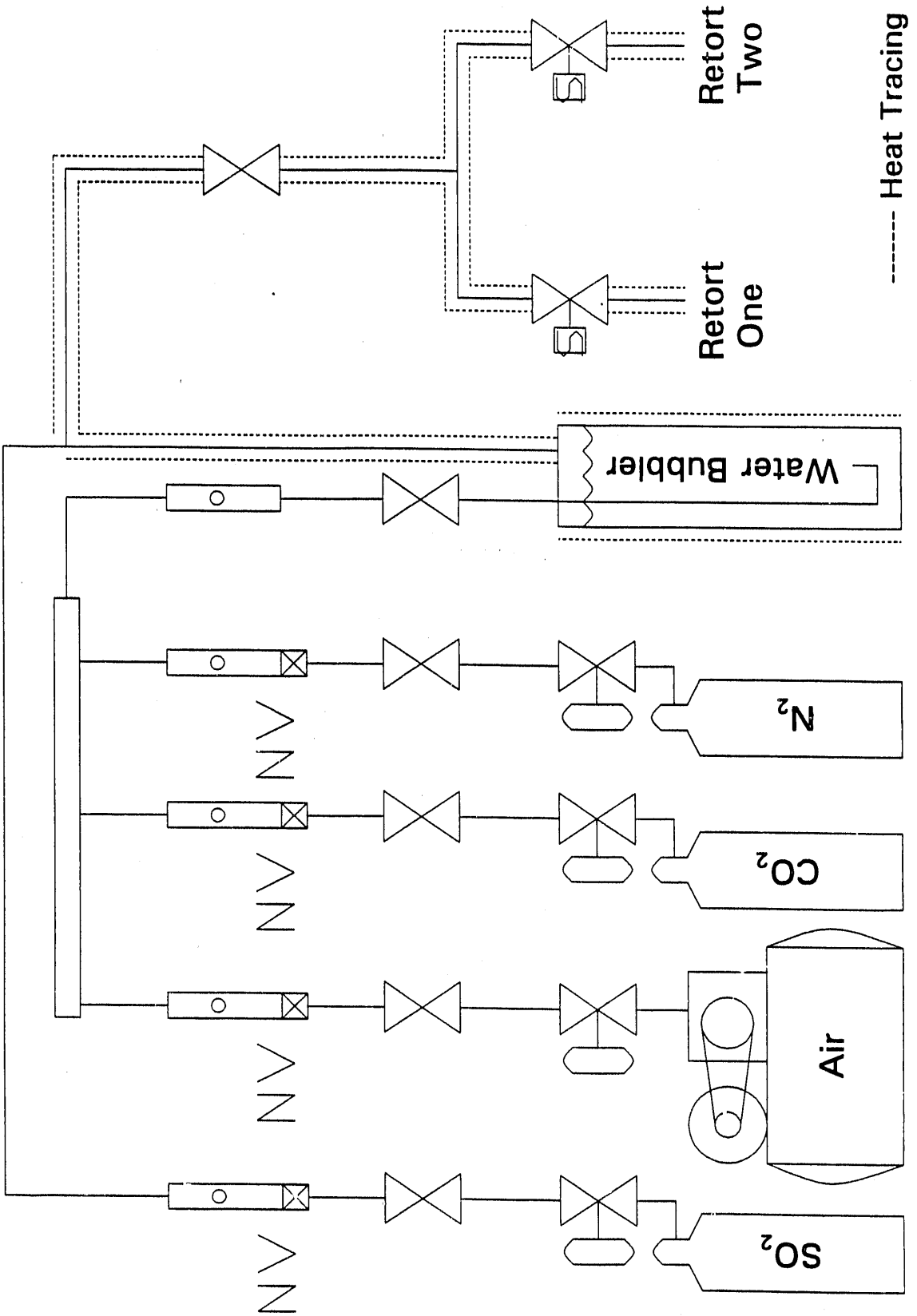

Figure 2.1 Gas Train Schematic

To prepare an ash, reagent-grade chemicals listed in Table 2.1 were ground in a ball mill and sieved through a 325-mesh screen. After screening, the powders were measured and blended to form a synthetic ash. The ash was milled for 24 hours to further grind and mix the component powders.

2.1.3 Furnace and Experimental Retort

The retorts for this project were similar to the retorts used in earlier fireside corrosion studies by Rehn [1]. Figure 2.2 illustrates a side view of a retort. Simulated flue gas was passed from the inlet, through iron turnings placed to catalyze SO_2 to SO_3, over the specimens, and out the exhaust tubes. Thermowells in the retorts monitored interior temperatures during the experiments.

2.2 MATERIALS SELECTION

Alloys and claddings that appeared to have promising resistance to AIT attack, along with alloys considered as industry standards, were selected for examination. The coupons for these tests were 1 in. x 2 in. Three or four coupons were placed in each tube of the retort. The alloys and claddings selected for testing, with their chemical compositions, are listed in Table 2.2.

2.3 OVERVIEW OF TESTING SEQUENCE

The experimental technique used in this project follows work conducted earlier by Rehn [1]. Coupons were stamped and weighed; their thicknesses were then measured. The top surface of the coupons was coated with a synthetic ash and they were exposed to simulated flue gas at elevated temperatures. After exposure the coupons were either evaluated, re-coated with synthetic ash, or steam cleaned and recoated with synthetic ash.

Three series of tests were conducted, each test exposure being run in parallel at both 650 and 700°C. Table 2.3 summarizes the exposure conditions for each series of tests. Test Series 1 was conducted for 100 and 200 hours with a high-sulfate ash in a gas containing 0.25 vol% SO_2. Test Series 2 was conducted for 100 and 800 hours with a low-sulfate ash in a gas containing 0.25 vol% SO_2. Test Series 3 was conducted for 100 and 800 hours with a low-sulfate ash in a gas containing 1.0 vol% SO_2.

To determine the effects of steam cleaning on corrosion rates, duplicate sets of coupons were tested for exposures longer than one 100-hour cycle. The ash layer on one set of coupons was replenished between exposures. The ash was steam cleaned from the second set of coupons, and the coupons were recoated with new ash between exposures.

2.3.1 Initial Characterization of Coupons

All alloys with the exception of CR35A were received in coupon form; Alloy CR35A was received in plate form and machined to size. Clad materials were analyzed by x-ray spectroscopy to determine which surface was the

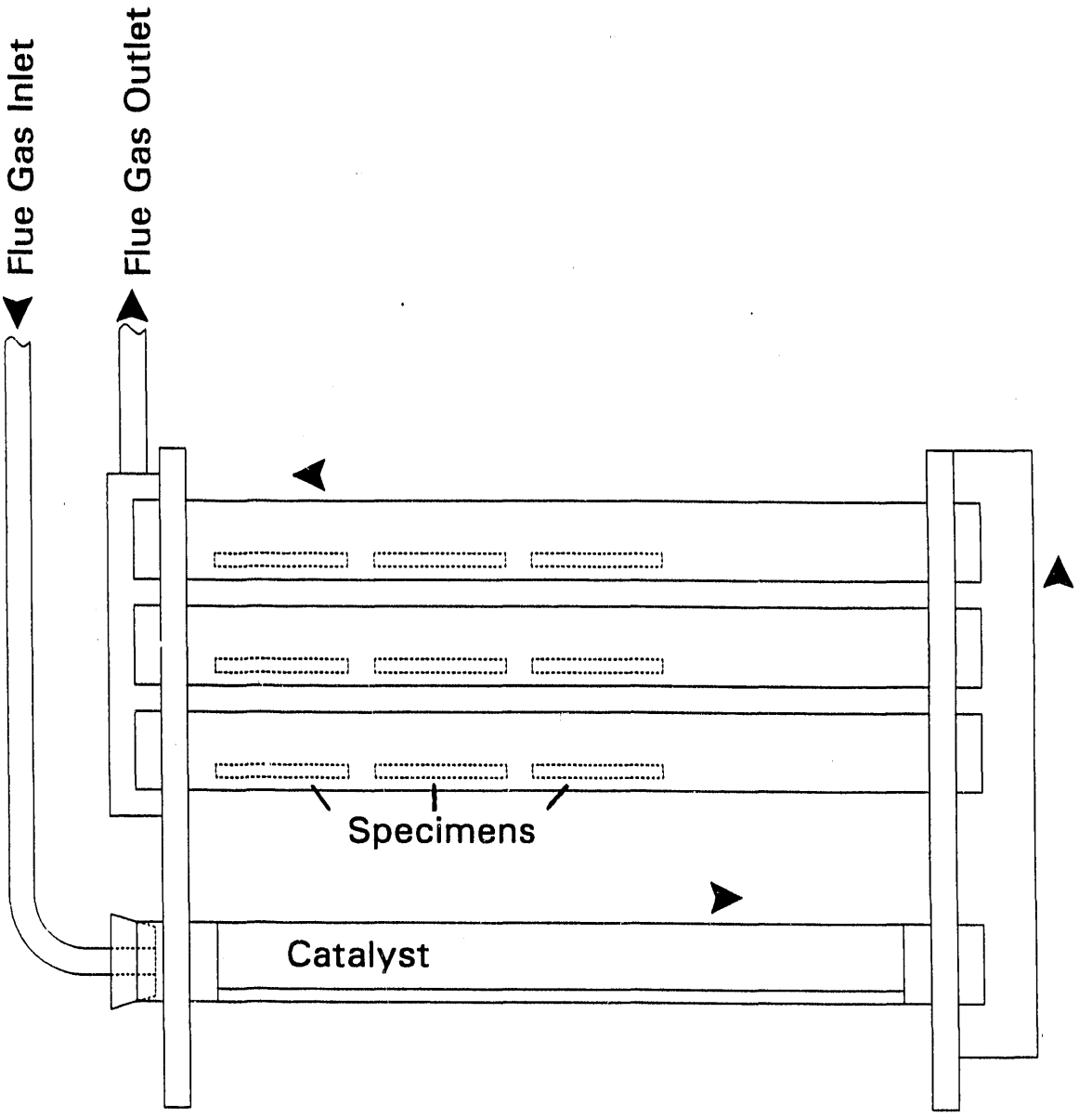

Figure 2.2 Furnace Experimental Retort

Table 2.2 Composition of Alloys Examined

Alloy	Fe	Ni	Cr	Mo	C	Si	Mn	Al	N	S	P	Other
Fe_3Al-2Cr	81.86		2.19					15.93				B 0.01
Fe_3Al-5Cr	77.5		5.6					15.9				
$(FeNi)_3Al$	11.7	70.1	7.2					11.0				
Modified 316	Bal	16.83	14.27	2.25	0.079	0.23	1.77	0.06	0.012	0.01	0.037	V 0.52, Nb 0.1, Ti 0.21
17-14 CuMo	Bal	14.08	16.37	1.95	0.078	0.72	0.88			0.005	0.023	Cu 3.34
Type 347*†	Bal	10.3	17.5		0.08	1.3	1.6			0.03	0.045	Nb 0.8
RA85H	Bal	15.26	18.50	0.06	0.24	3.90	0.50	0.700	0.10		0.015	Cu 0.39
Modified 800H	Bal	31.08	20.87	2.01	0.097	0.21	1.93	0.02	0.01	0.013	0.003	Nb 0.19, Ti 0.29, V 0.47
NF709*†	Bal	24.3	21.5	1.0-2.0	<0.2	0.7	<1.5		0.05-0.02	<0.01	<0.03	Nb 0.1 - 0.4
Haynes 556	Bal	22.1	21.55	2.83	0.1	0.4	0.95	0.13	0.16	0.002	0.006	Ta 0.68, Nb 0.07, W 2.45, B 0.01
HR3C†	Bal	20.45	24.95		0.06	0.42	1.28		0.23	0.0001	0.013	Nb 0.45
690/316	9.09	57.3	31.65	<0.05	0.048	0.26	0.17			0.002	<0.005	
690/800H	9.13	57.3	31.50	<0.05	0.049	0.26	0.17			0.002	<0.005	
690*	9.5	Bal	30.0		0.03							
CR35A†	17.7	43.8	37.3				0.2					
72 Clad Lean Stainess Steel§	0.27	55.89	43.73		0.01	0.07	0.03			0.001		
72 Clad 800H	0.55	55.3	43.00	0.067	0.041	0.15	0.025			0.001	0.006	
671 Clad Lean Stainess Steel§		Bal	48.5	<0.05	0.057	0.11	<0.10	<0.05	0.0095	0.003	0.002	Ti 0.46, Nb <0.05, Cu <0.05
671*		Bal	48.0		0.05							Ti 0.35
Sandvik 28†	Bal	31.19	26.94	3.36	0.011	0.15	0.67		0.045	0.003	0.014	Cu 1.00

*Typical. †Supplied by FWDC, all others supplied by ORNL. §Modified Type 316.

Table 2.3 Test Exposure Conditions

	Test 1	Test 2	Test 3
Testing Time			
100 hours	X	X	X
200 hours	X		
800 hours		X	X
Ash Composition			
Ash 1	X		
Ash 2	X		
Ash 3		X	X
Gas Composition			
Low SO_2	X	X	
High SO_2			X

cladding. Identifying markings were stamped on the coupons, the coupons were weighed, and their thickness was measured at each corner and at the center.

2.3.2 Preparing Coupons Before Exposure

The following was done to simulate a layer of coal ash on the test coupons: A binder of ethanol saturated with camphor was mixed with the synthetic coal ash to form a paste. This paste was spread over the top of the coupons to form a uniform layer of ash weighing approximately 1 g/in^2. (Rehn [1] found that a coating thinner than 40 mg/in^2 limited corrosive weight loss for a 100-hour testing period, while thicker coatings contained ample reactants for the entire testing period.) After coating, coupons were loaded into the retort; care was taken to ensure that the coupons were set in a horizontal position in the tubes of the retort.

2.3.3 Exposing Specimens to a Simulated Boiler Environment

After a retort was loaded, sealed, and lowered into a box furnace, a nitrogen purge was started, and the retort was brought to temperature. As the retort was heating, the camphor binder was driven off and carried out with the nitrogen. When the retort reached operating temperature, the nitrogen purge gas was stopped, and simulated flue gas was passed through the retort. At the end of the 100-hour exposure, the furnace was turned off to cool, and a nitrogen purge was started.

2.3.4 Post-Exposure Steam Cleaning and Recoating

After exposure the specimens were sorted into two groups. One group of specimens was recoated with fresh coal ash over the previous ash, while the second group of specimens was steam cleaned and recoated with fresh ash. The specimens were steam cleaned by holding them under a spray of saturated steam.

2.4.2 Weight Loss, Thickness Loss, and Pit Depth Measurements

All descaled specimens were weighed and measured for average and maximum thickness loss. Specimen weights were measured on a Sartorius 1202MP electronic scale; thicknesses were measured with Mitutoyo digital micrometers. Average thickness losses were determined by taking measurements at the corners and in the middle of a specimen before and after exposure to the simulated boiler environment, then subtracting the averaged preexposure measurements from the post-exposure measurements. Maximum thickness loss was determined by measuring the thinnest area of a specimen after exposure and subtracting it from the preexposure average.

2.4.3 Microscopic Examination and Chemical Analysis

To study the mechanisms of attack, selected specimens were sectioned and examined using optical and electron microscopy. Specimens to be examined were sectioned, mounted in Bakelite, ground (with water as a lubricant), and polished. After preparation the mounted specimens were examined with both an optical measurescope (to determine scale thickness and morphological features) and an EXEC Autoscan electron microscope with an EDAX 9800 energy dispersive x-ray unit (to examine fine features and to analyze chemical makeup).

Section 3

RESULTS OF FIRESIDE TESTING

This section summarizes all relevant weight and thickness loss data from the experimental portion of the program. Data are given primarily in graphic format to allow easily drawn comparisons between alloys. Corrosion rate data presented in this section are intended for comparing the corrosion resistance of various alloys--not as design data. Appendix A contains photographs of the exposed specimens that illustrate the morphology of attack.

Several cautions are appropriate when reviewing the graphs and tables presented in this section:

- Weight loss and thickness loss measurements on the pack cementation-coated specimens from Ohio State University are misleading. The specimens on which the corrosion-resistant outer layer was breached show anomalously high corrosion rates as a result of catastrophic corrosion of the inner core. Thus these coupons were evaluated "pass/fail", depending on whether the coating was breached.

- The 671 clad lean stainless steel coupons had a layer of lean stainless steel remaining on the underside of the coupons. This layer lost more metal as a result of gas phase attack and descaling than the 671 layer lost from AIT attack. The losses from the 671 layer were gauged visually.

- Greater-than-expected wastage rates of several highly alloyed coupons may have been caused by the descaling procedure. The highly alloyed specimens were coated with a hard black scale that defied all but the most severe descaling methods. Consequently, some base metal may have been removed from the specimens along with the scale.

- Several aluminide specimens suffered so much wastage that accurate weight loss and thickness loss measurements were no longer possible.

3.1 RESULTS OF THE 100- AND 200- HOUR HIGH-SULFATE 0.25 vol% SO_2 TESTS

The testing program was initially conducted using a highly aggressive synthetic coal ash (37.5 wt% Na_2SO_4, 37.5 wt% K_2SO_4, 25 wt% Fe_2O_3) to provide accelerated corrosion testing. Conditions were otherwise chosen to be representative of an advanced PC-fired boiler burning a medium-sulfur coal: A simulated flue gas composition of 0.25 vol% SO_2, 3.6 vol% O_2, 14.0 vol% CO_2, 10.0 vol% H_2O, Bal. N_2 and test temperatures of 650 and 700°C. Materials marked with an asterisk in the graphs were coated with a less-aggressive coal ash (5 wt% Na_2SO_4, 5 wt% K_2SO_4, 90 wt% Fe_2O_3) as a comparison.

Two 100-hour exposures were conducted, with ash replenishment between exposures. Testing was stopped after the second 100-hour exposure because there were unacceptably high corrosion losses; the corrosion rates of several specimens were so high that complete penetration of the specimens was projected by the end of the third or fourth exposure.

3.1.1 Weight Loss*†

Weight loss data for specimens exposed at 650°C are shown in Figure 3.1. Data for specimens exposed at 700°C are shown in Figure 3.2. All data have been normalized to mg lost/cm^2/100 hours.

3.1.2 Thickness Losses*†

Data for average thickness losses are shown in Figures 3.3 and 3.4; maximum thickness loss data are shown in Figures 3.5 and 3.6. All data have been normalized to mils lost/100 hours.

*Specimens are shown left to right in order of increasing chromium content.
†LSS (lean stainless steel) is Type 316 mod.

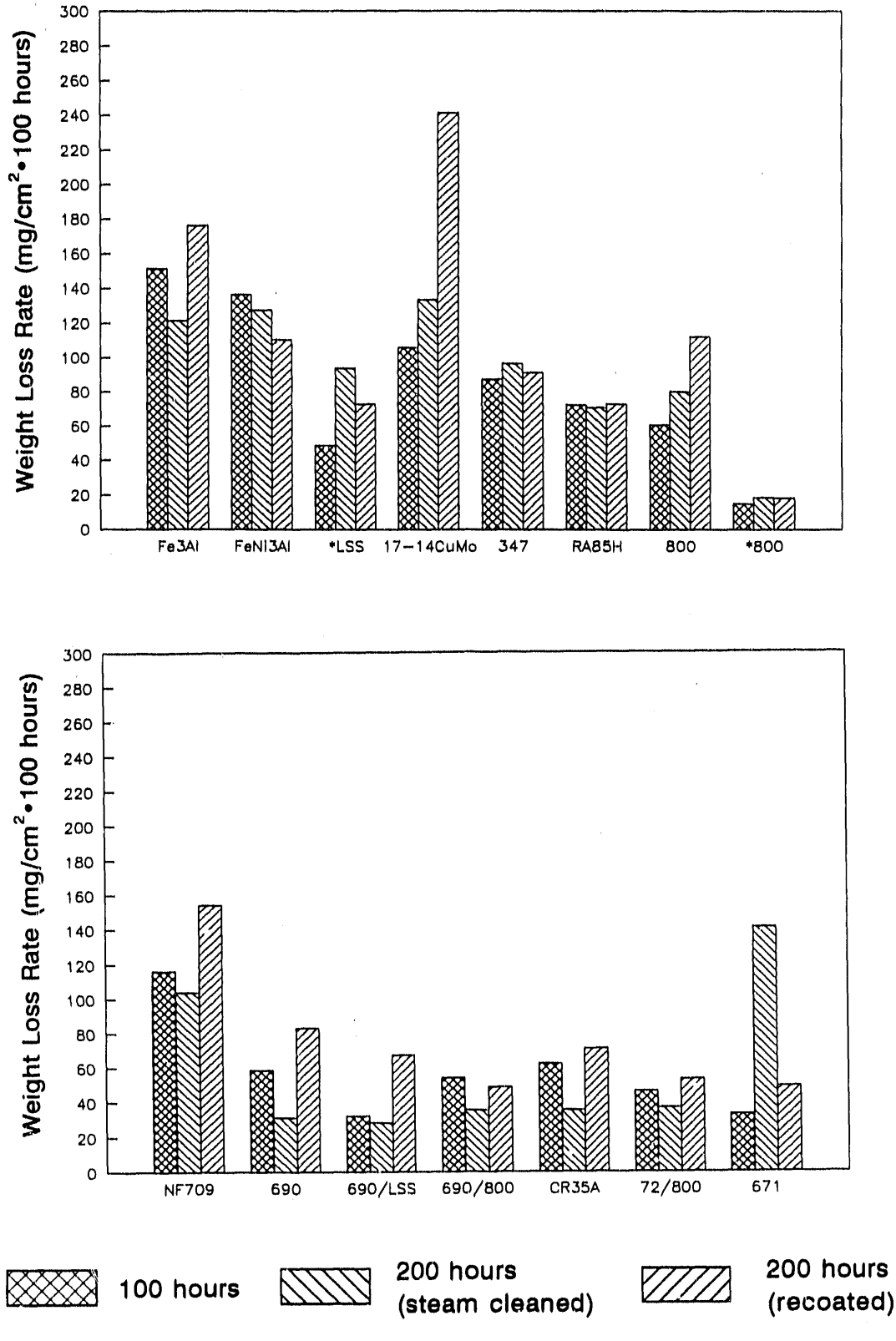

Figure 3.1 Normalized Weight Loss Rates for Alloys Coated With a 75 wt% Alkali Sulfate Ash and Exposed at 650°C to a 0.25 vol% SO_2 Flue Gas

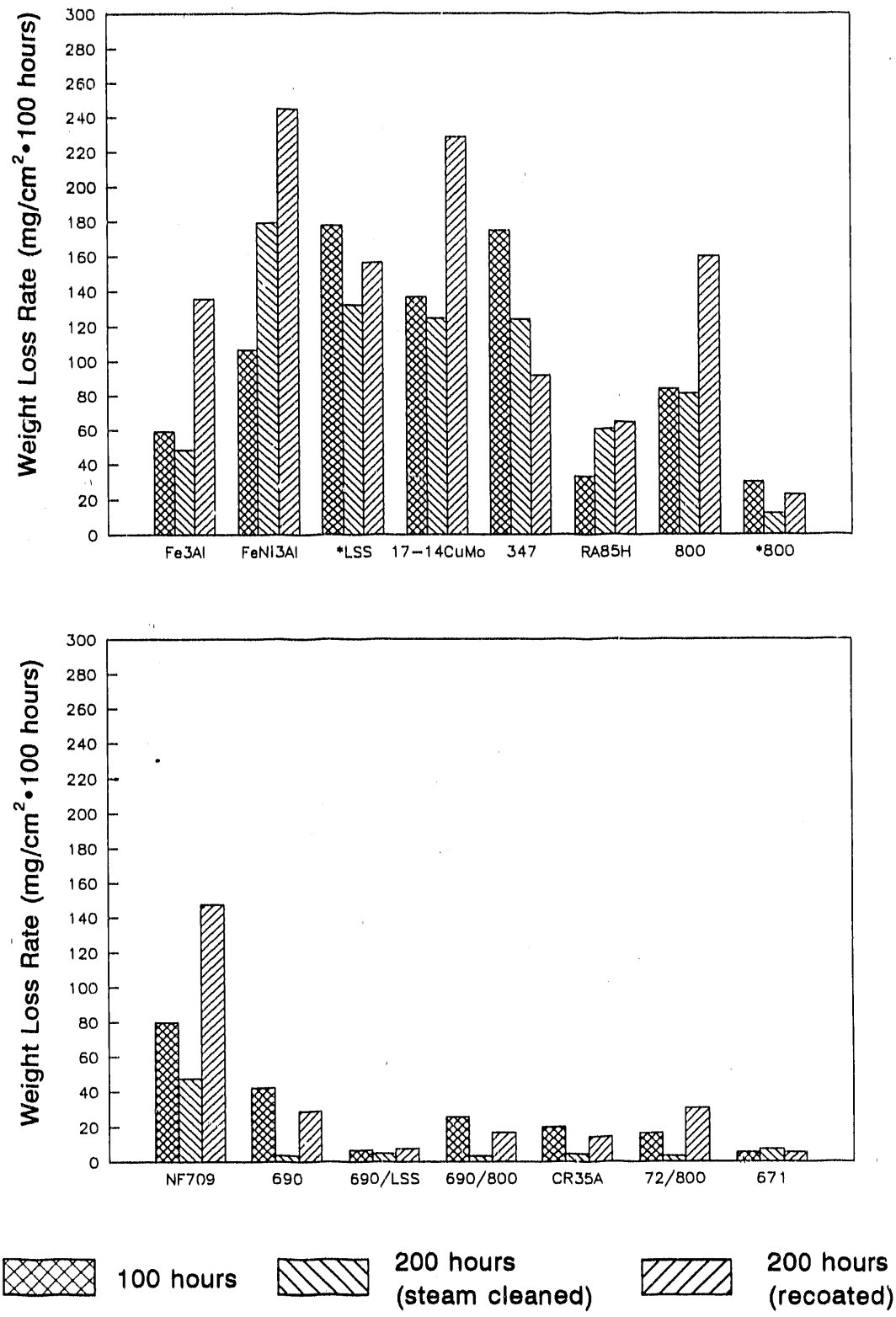

Figure 3.2 Normalized Weight Loss Rates for Alloys Coated With a 75 wt% Alkali Sulfate Ash and Exposed at 700°C to a 0.25 vol% SO_2 Flue Gas

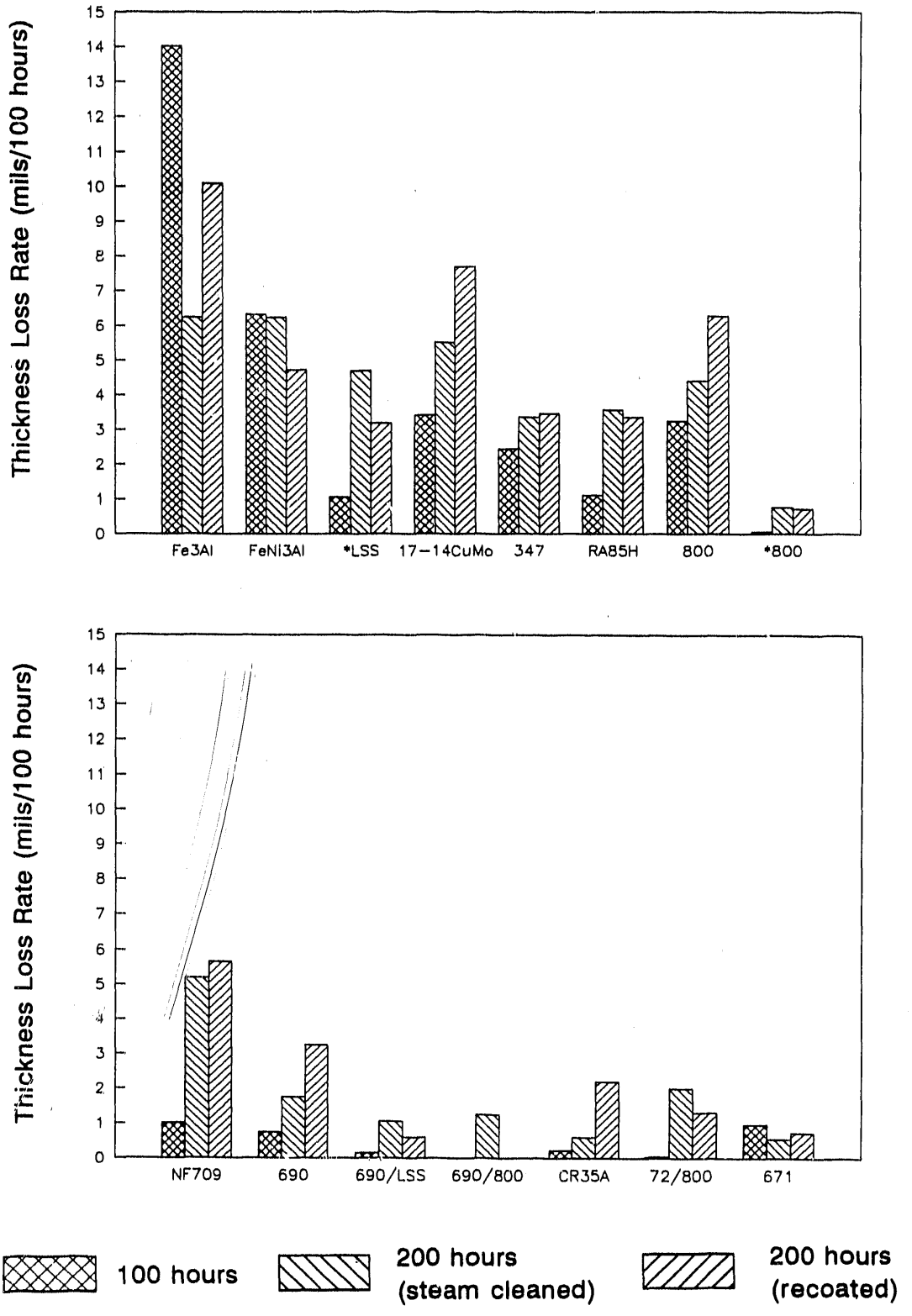

Figure 3.3 Normalized Thickness Loss Rates for Alloys Coated With a 75 wt% Alkali Sulfate Ash and Exposed at 650°C to a 0.25 vol% SO_2 Flue Gas

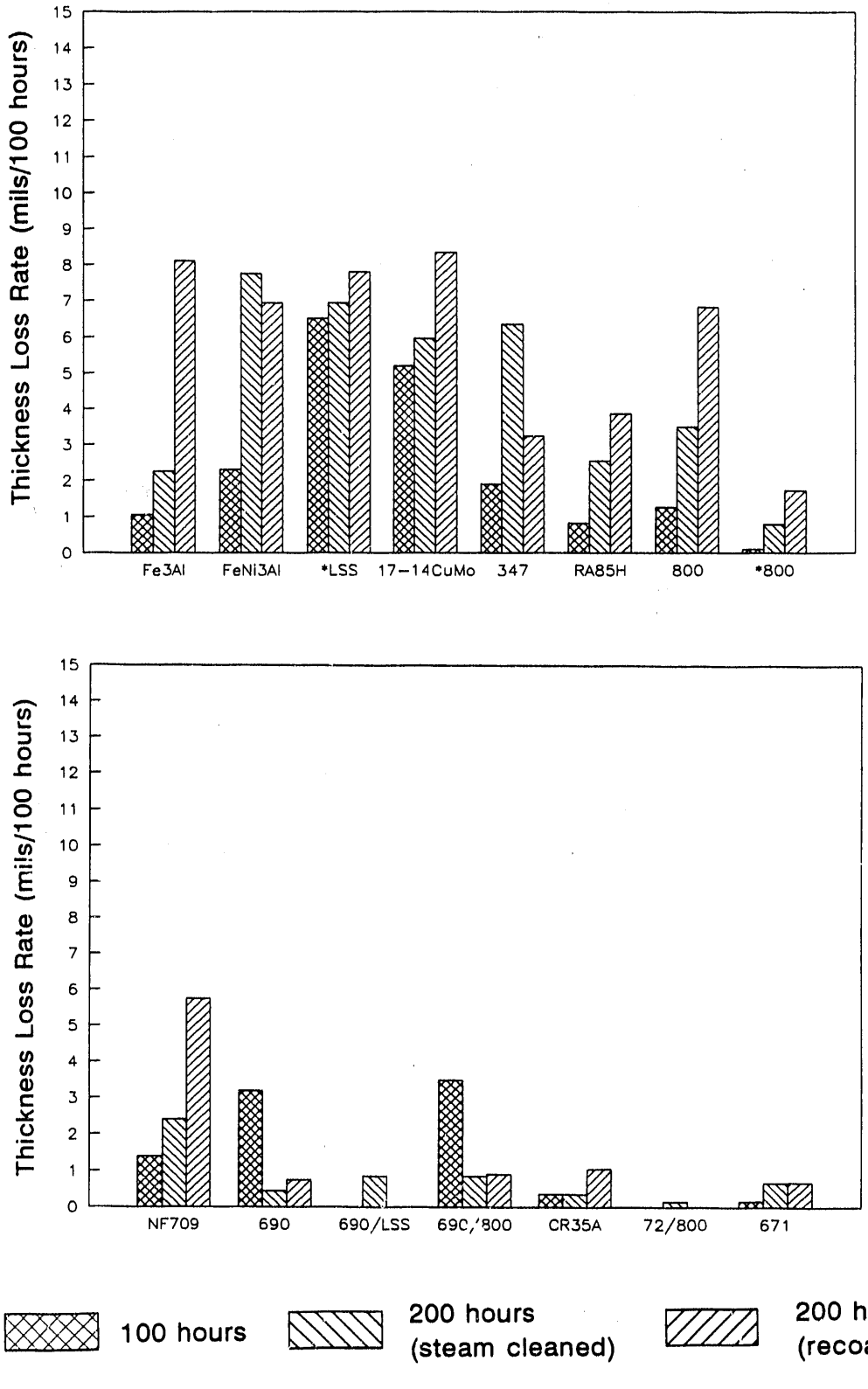

Figure 3.4 Normalized Thickness Loss Rates for Alloys Coated With a 75 wt% Alkali Sulfate Ash and Exposed at 700°C to a 0.25 vol% SO_2 Flue Gas

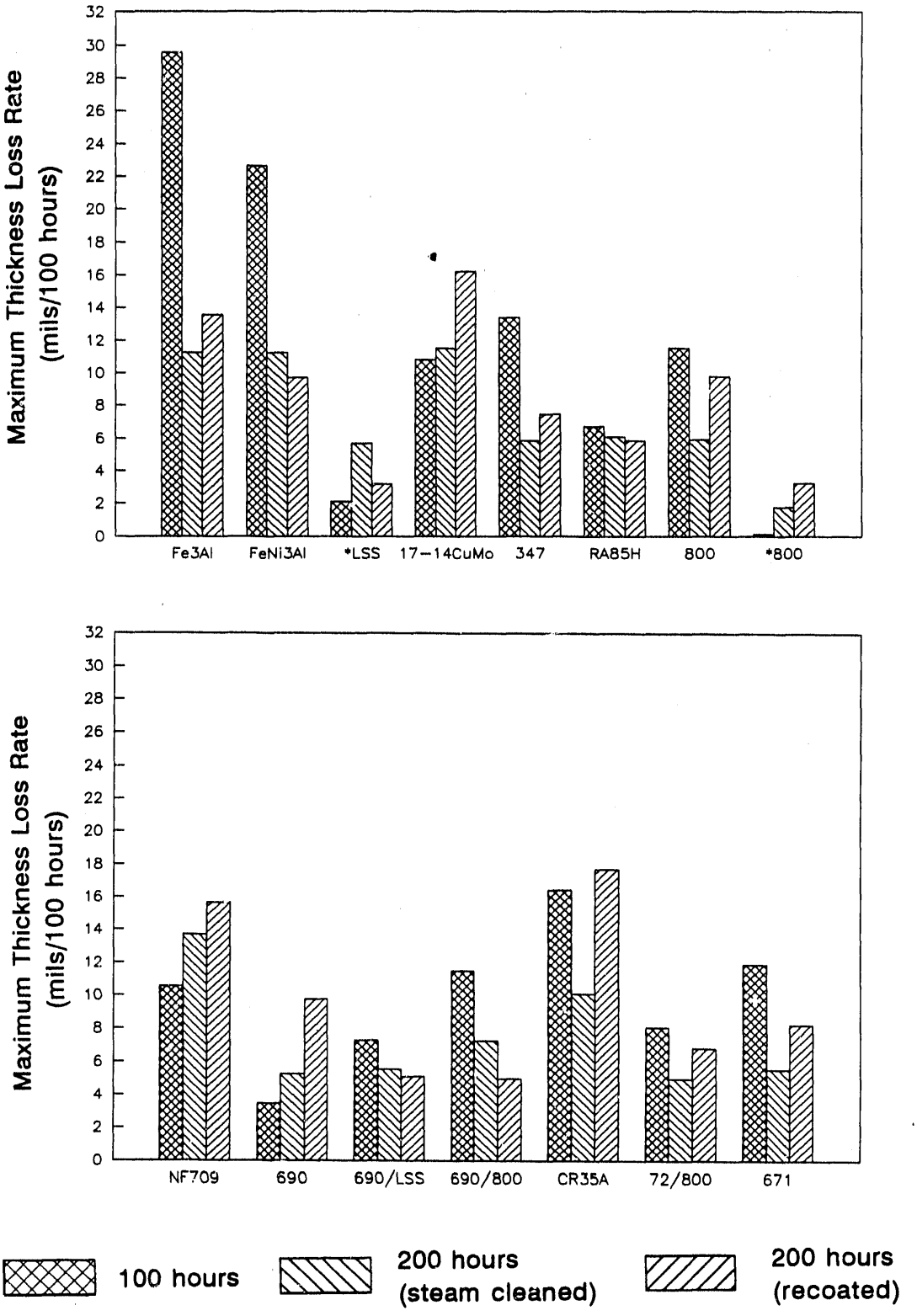

Figure 3.5 Normalized Maximum Thickness Loss Rates for Alloys Coated With a 75 wt% Alkali Sulfate Ash and Exposed at 650°C to a 0.25 vol% SO_2 Flue Gas

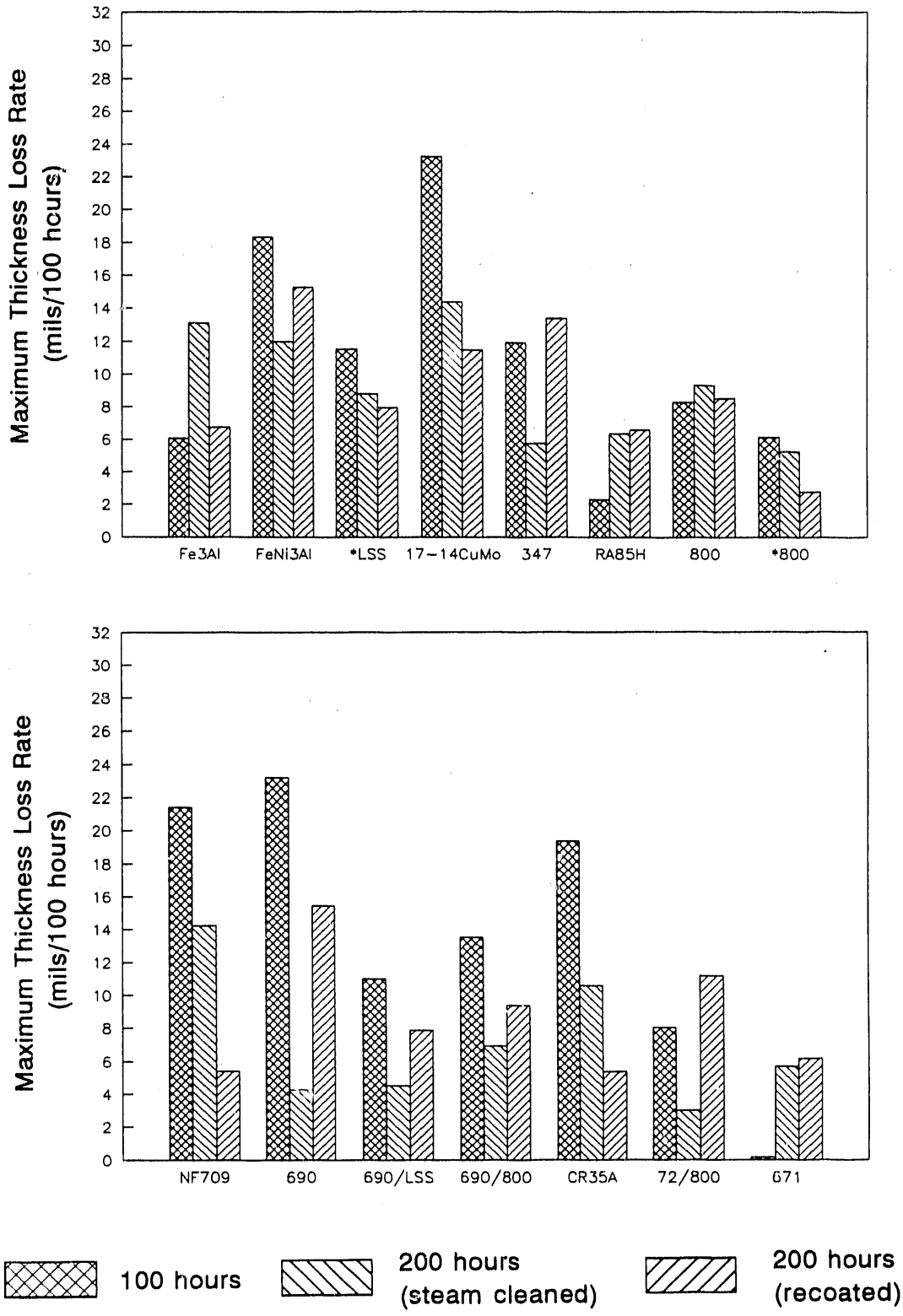

Figure 3.6 Normalized Maximum Thickness Loss Rates for Alloys Coated With a 75 wt% Alkali Sulfate Ash and Exposed at 700°C to a 0.25 vol% SO_2 Flue Gas

3.2 RESULTS OF THE 100- AND 800-HOUR LOW-SULFATE 0.25 vol% SO_2 TESTS

A second set of tests was conducted with a synthetic coal ash similar in composition to ashes found in PC-fired boilers (5 wt% Na_2SO_4, 5 wt% K_2SO_4, 30 wt% Fe_2O_3, 30 wt% Al_2O_3, 30 wt% SiO_2). The simulated flue gas (composition: 0.25 vol% SO_2, 3.6 vol% O_2, 14.0 vol% CO_2, 10.0 vol% H_2O, Bal. N_2) is representative of flue gases found in PC-fired boilers burning medium-sulfur coals.

3.2.1 Weight Loss*

Weight loss data are shown in Figures 3.7 and 3.8. All data have been normalized to mg lost/cm^2/100 hours.

3.2.2 Thickness Losses*

Data for average thickness losses are shown in Figures 3.9 and 3.10; maximum thickness loss data are shown in Figures 3.11 and 3.12. All data have been normalized to mils lost/100 hours.

*Specimens are listed in order of increasing chromium content.

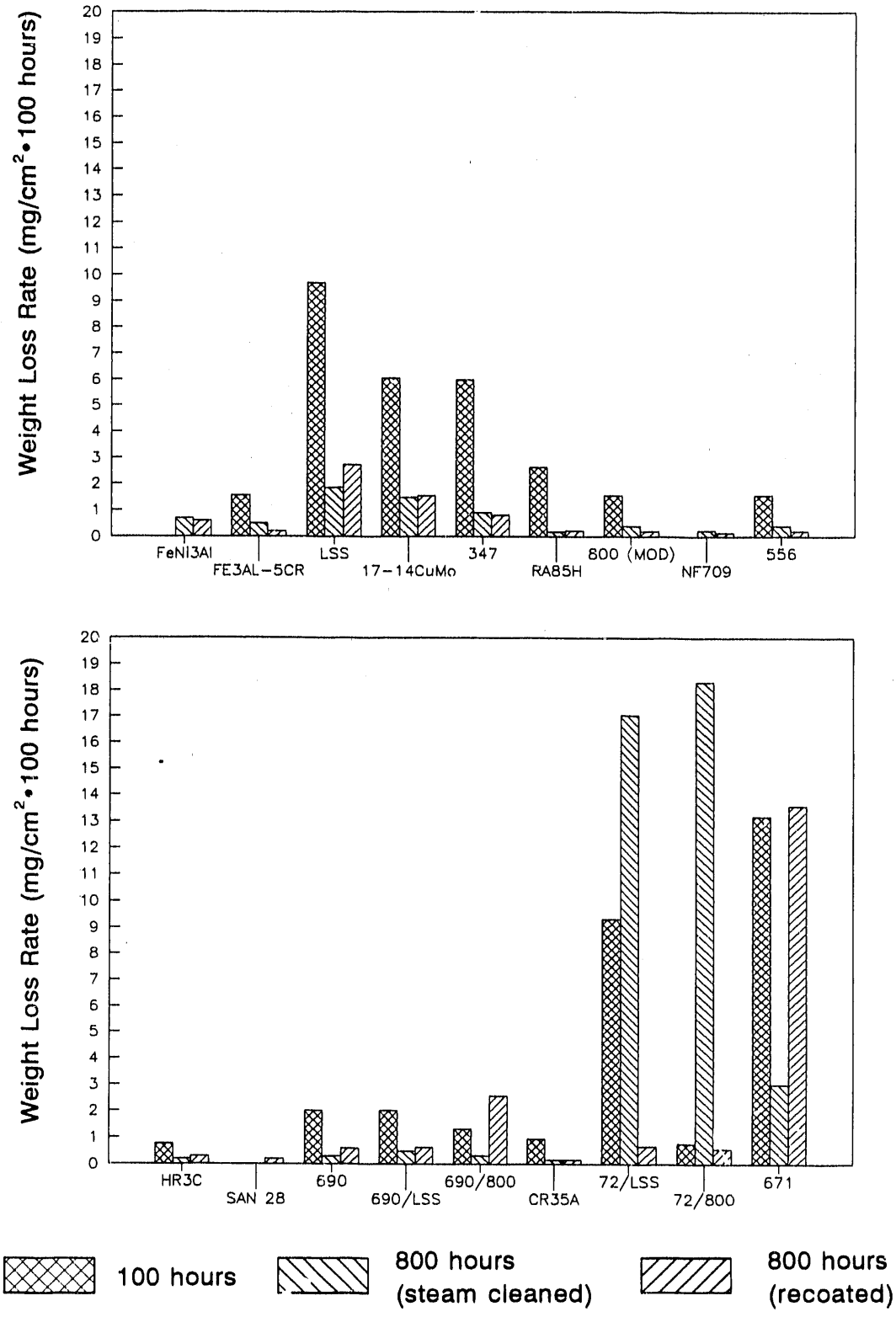

Figure 3.7 Normalized Weight Loss Rates for Alloys Coated With a 10 wt% Alkali Sulfate Ash and Exposed at 650°C to a 0.25 vol% SO_2 Flue Gas

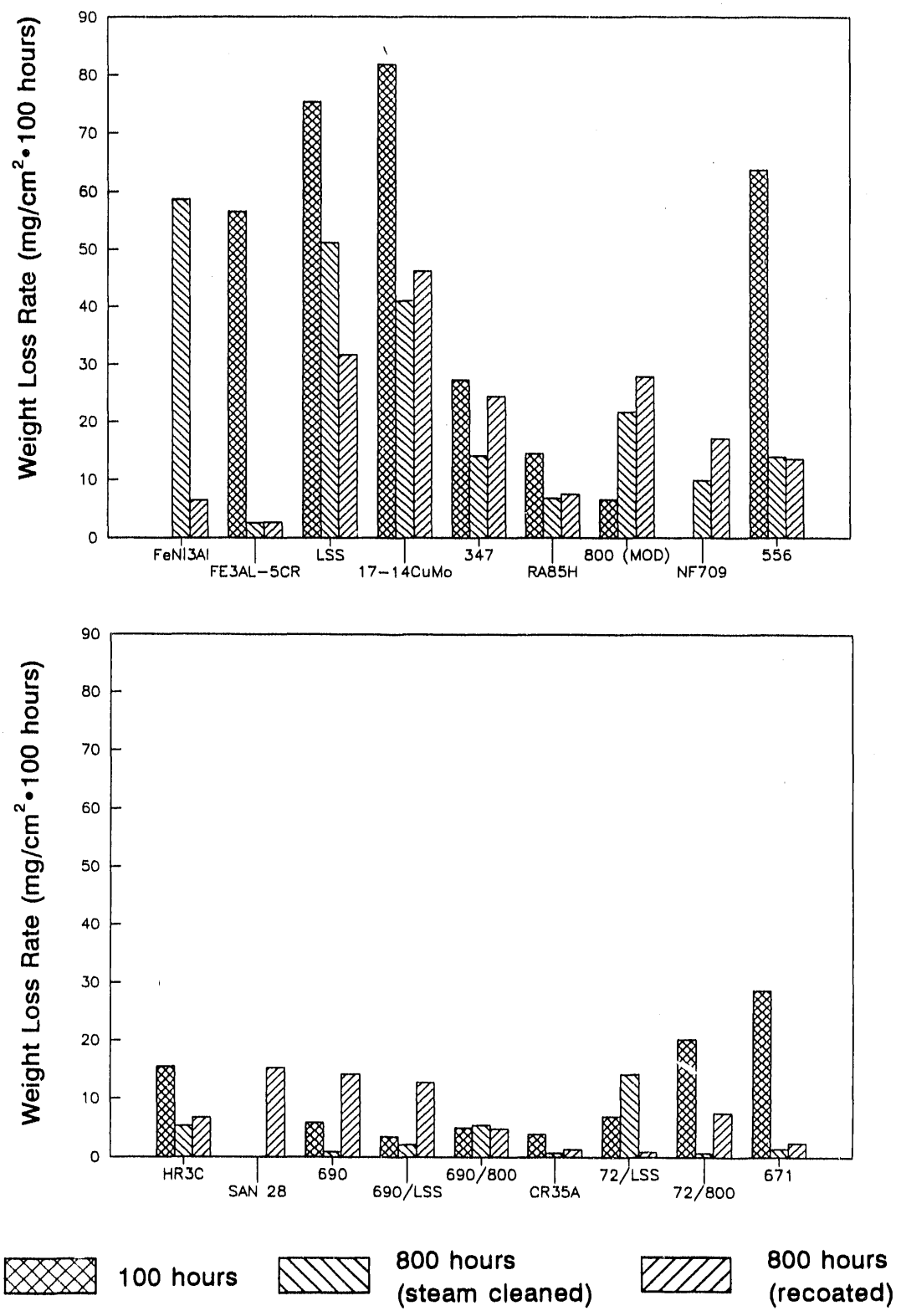

Figure 3.8 Normalized Weight Loss Rates for Alloys Coated With a 10 wt% Alkali Sulfate Ash and Exposed at 700°C to a 0.25 vol% SO_2 Flue Gas

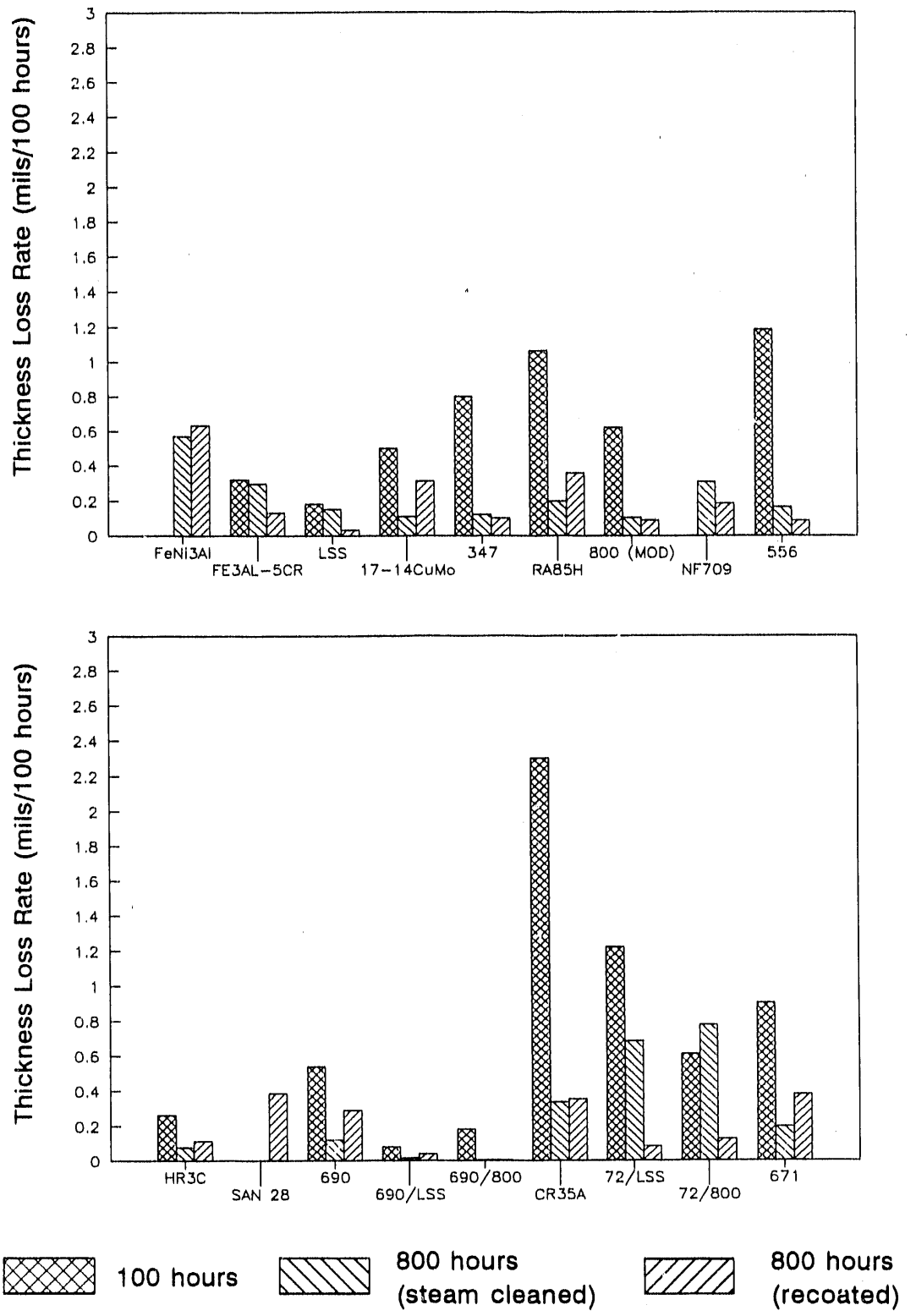

Figure 3.9 Normalized Thickness Loss Rates for Alloys Coated With a 10 wt% Alkali Sulfate Ash and Exposed at 650°C to a 0.25 vol% SO_2 Flue Gas

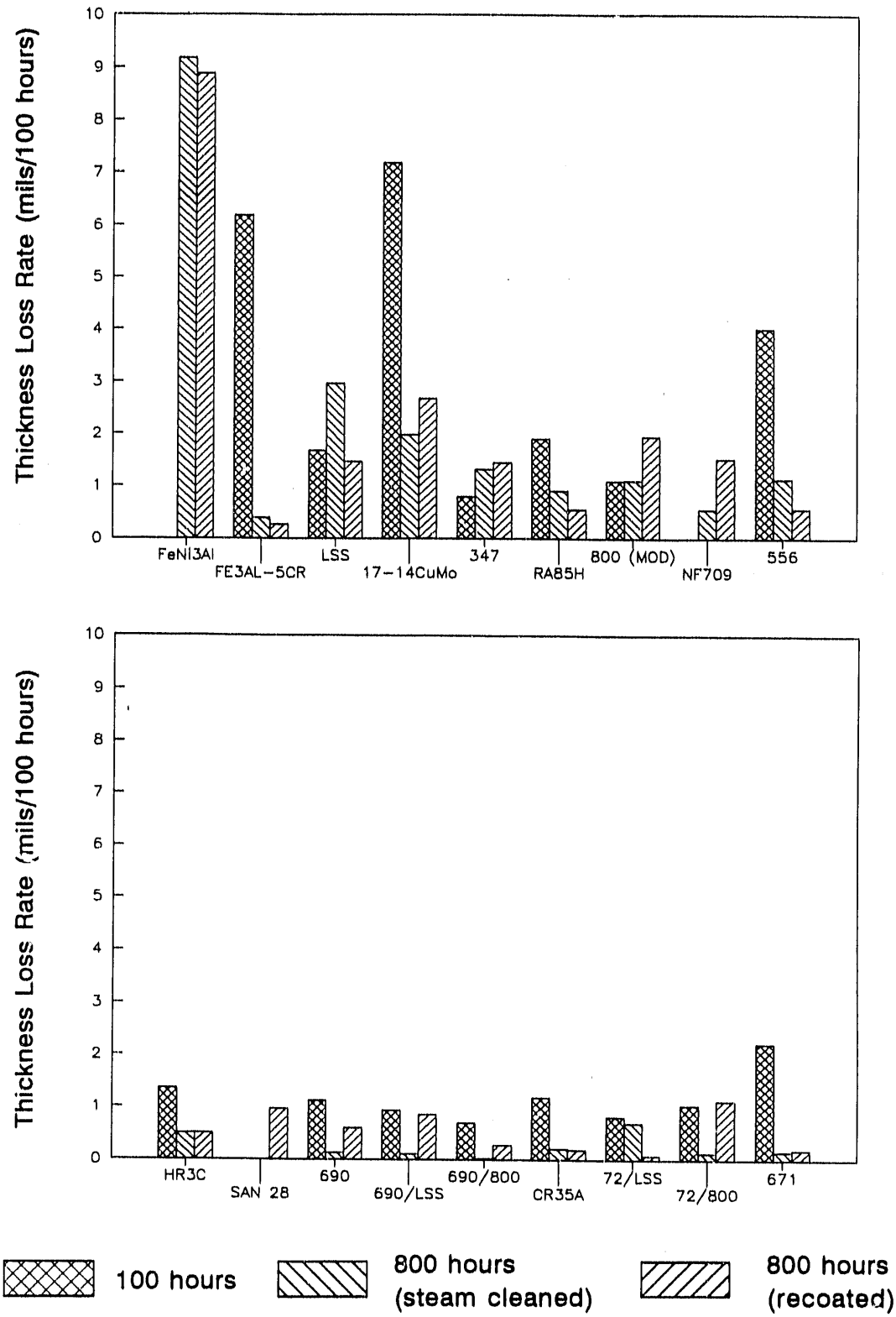

Figure 3.10 Normalized Thickness Loss Rates for Alloys Coated With a 10 wt% Alkali Sulfate Ash and Exposed at 700°C to a 0.25 vol% SO_2 Flue Gas

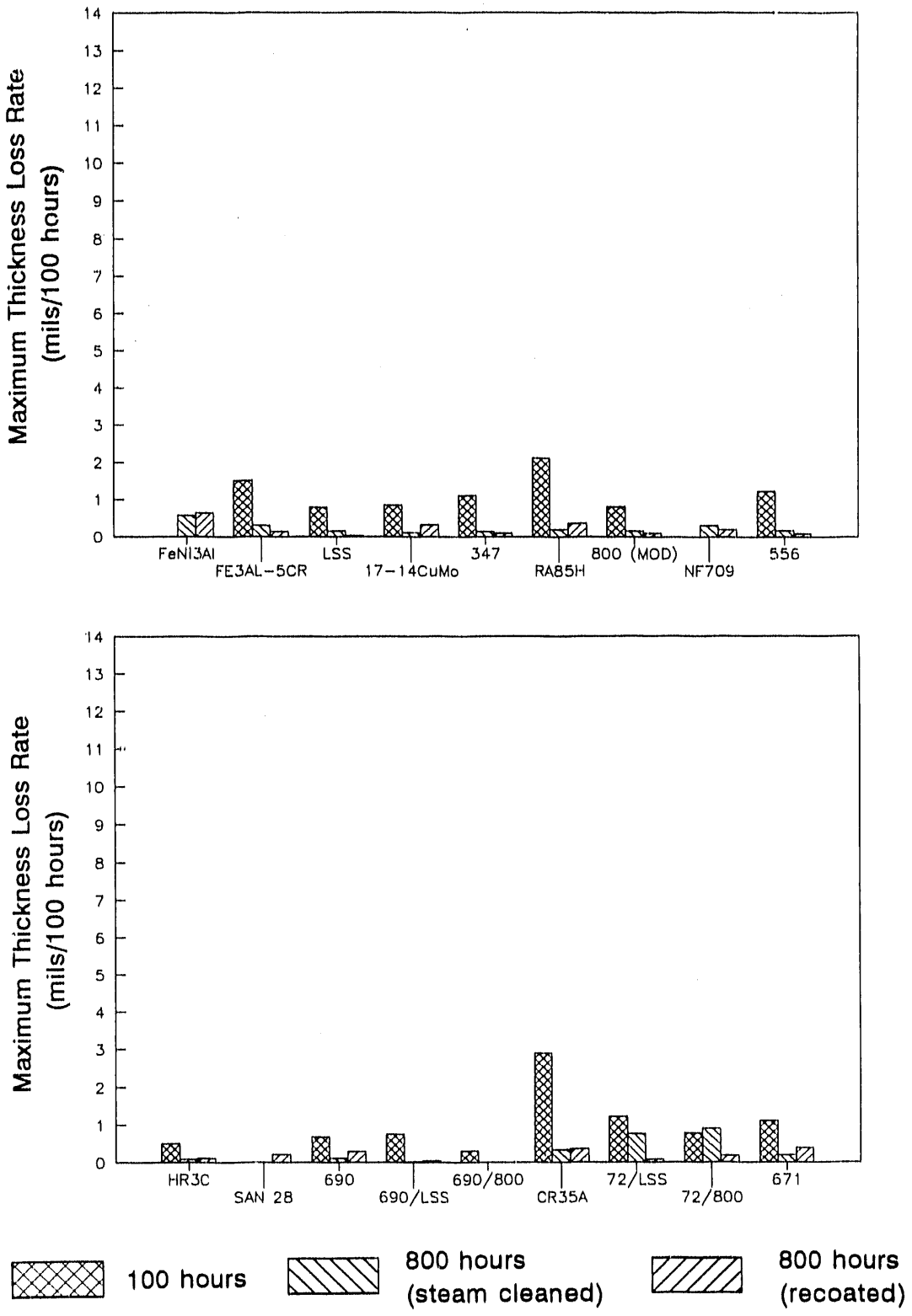

Figure 3.11 Normalized Maximum Thickness Loss Rates for Alloys Coated With a 10 wt% Alkali Sulfate Ash and Exposed at 650°C to a 0.25 vol% SO_2 Flue Gas

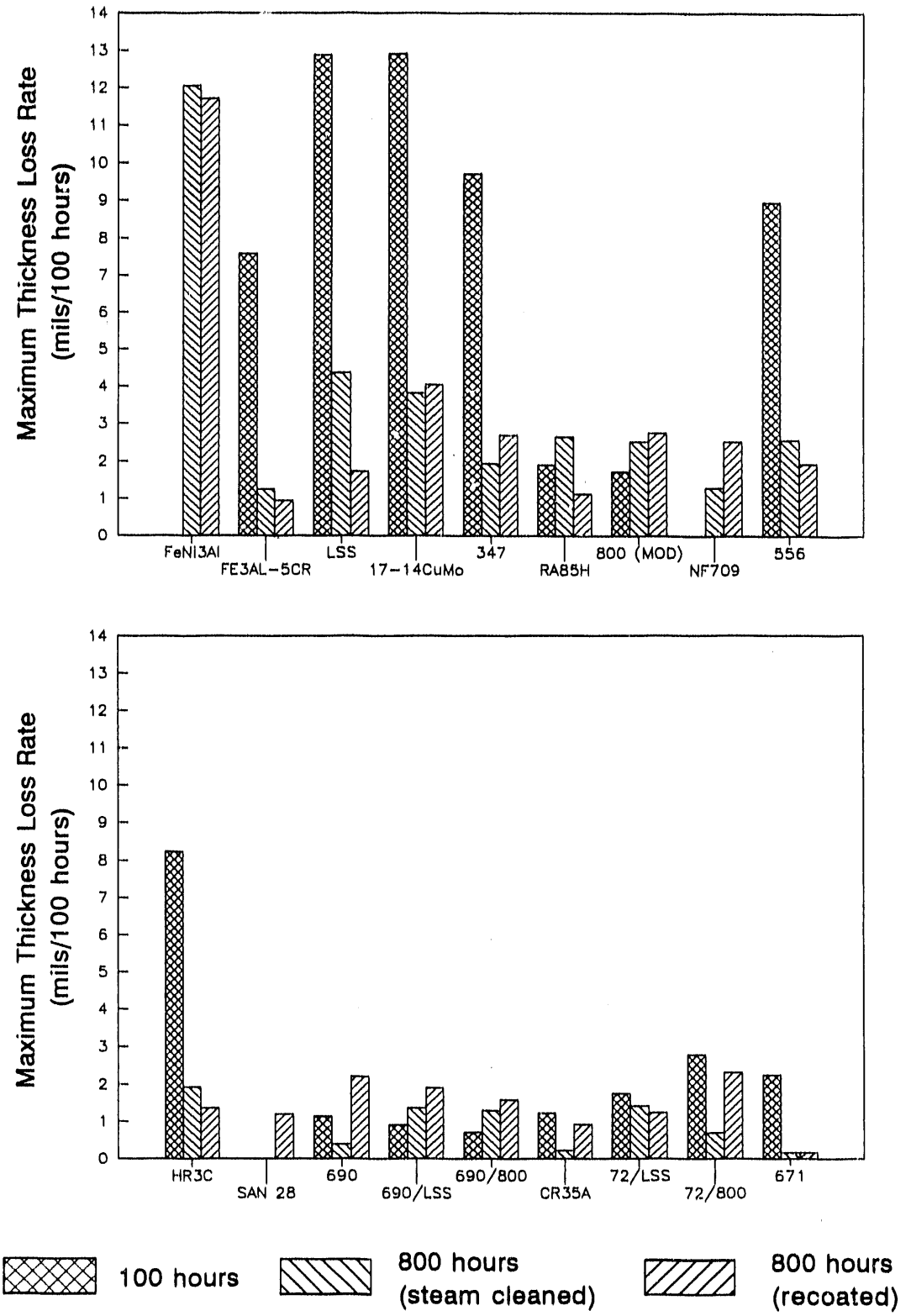

Figure 3.12 Normalized Maximum Thickness Loss Rates for Alloys Coated With a 10 wt% Alkali Sulfate Ash and Exposed at 700°C to a 0.25 vol% SO_2 Flue Gas

3.3 RESULTS OF THE 100- AND 800-HOUR LOW-SULFATE 1.0 vol% SO_2 TESTS

Tests were conducted with a synthetic coal ash similar in composition to ashes found in PC-fired boilers (5 wt% Na_2SO_4, 5 wt% K_2SO_4, 30 wt% Fe_2O_3, 30 wt% Al_2O_3, 30 wt% SiO_2). The simulated flue gas (composition: 1.0 vol% SO_2, 3.6 vol% O_2, 14.0 vol% CO_2, 10.0 vol% H_2O, Bal. N_2) is representative of flue gases found in PC-fired boilers burning high-sulfur coals.

3.3.1 Weight Loss*

Weight loss data are shown in Figures 3.13 and 3.14. All data have been normalized to mg lost/cm^2/100 hours.

3.3.2 Thickness Losses*

Data for average thickness losses are shown in Figures 3.15 and 3.16; maximum thickness loss data are shown in Figures 3.17 and 3.18. All data have been normalized to mils lost/100 hours.

*Specimens are listed in order of increasing chromium content.

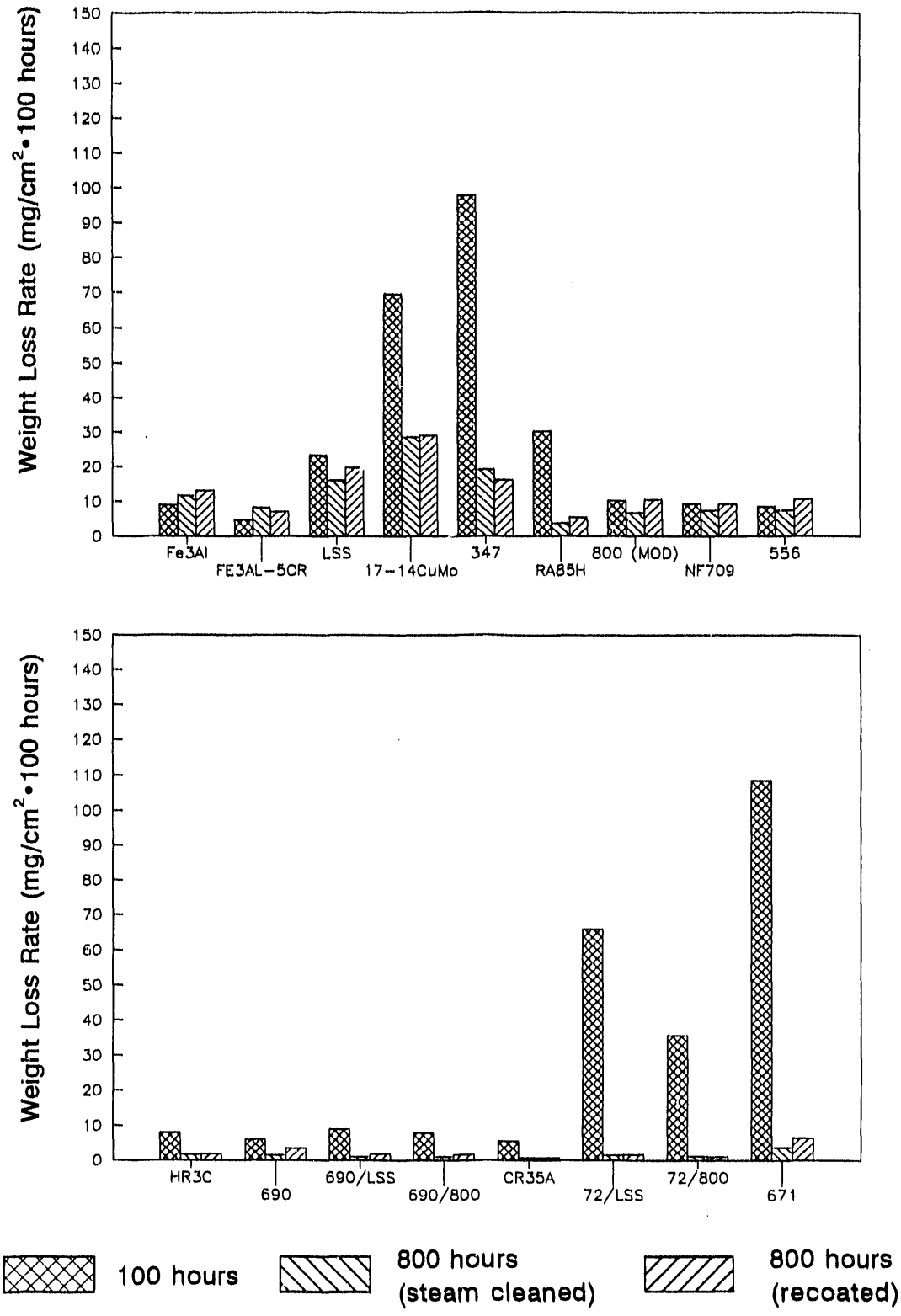

Figure 3.13 Normalized Weight Loss Rates for Alloys Coated With an Ash Containing 10 wt% Alkali Sulfates and Exposed at 650°C to a Flue Gas Containing 1.0 vol% SO_2

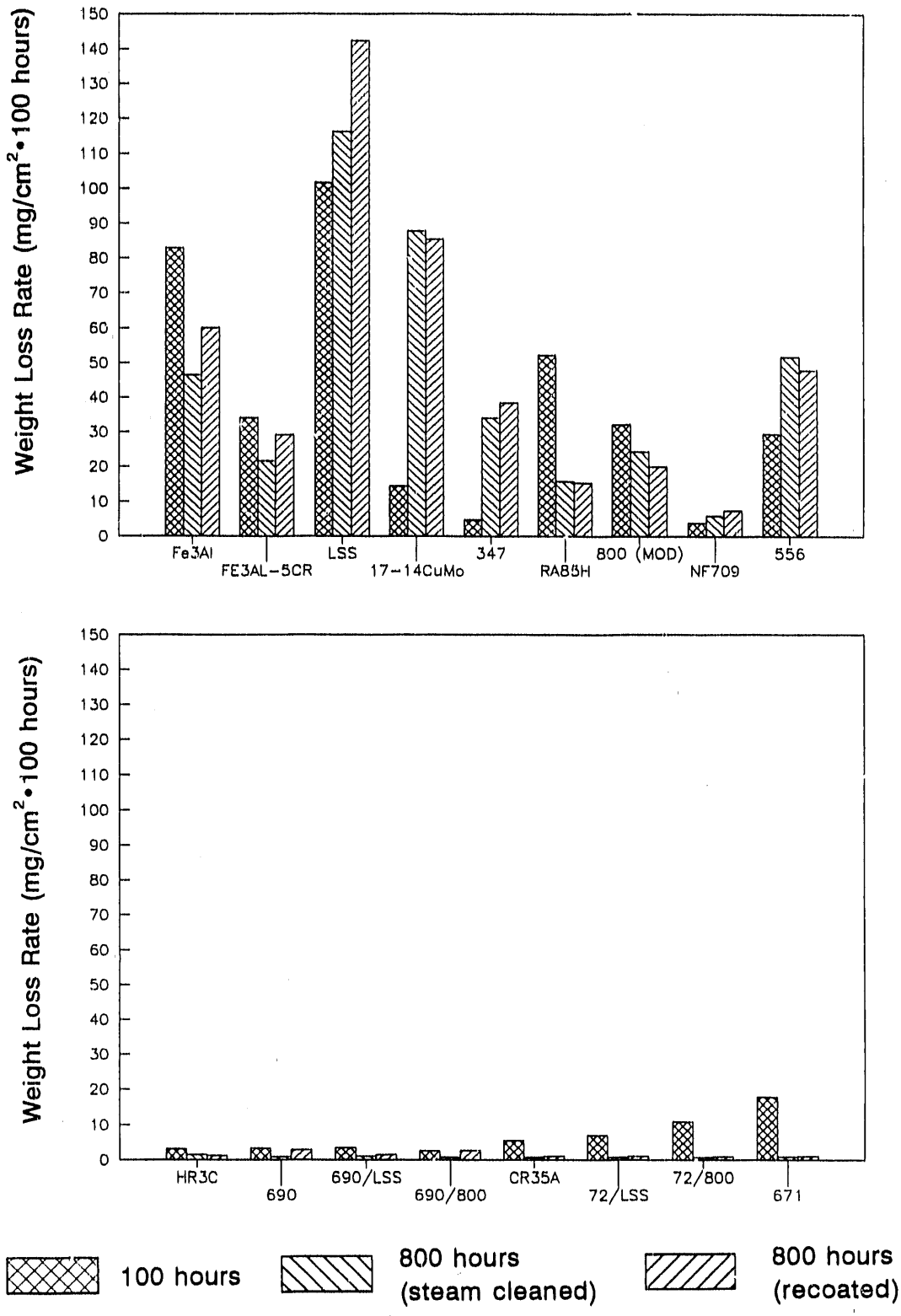

Figure 3.14 Normalized Weight Loss Rates for Alloys Coated With an Ash Containing 10 wt% Alkali Sulfates and Exposed at 700°C to a Flue Gas Containing 1.0 vol% SO_2

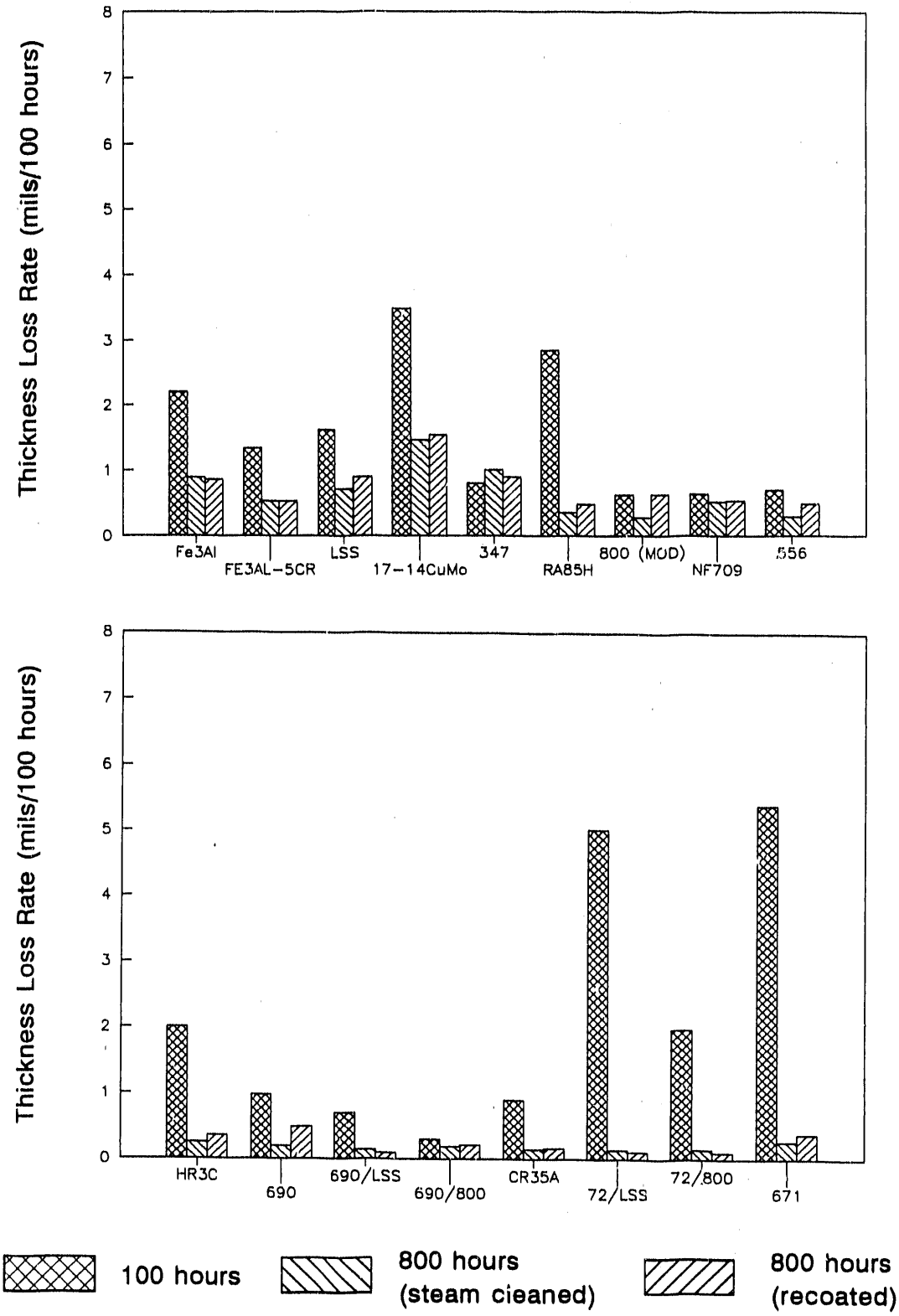

Figure 3.15 Normalized Thickness Loss Rates for Alloys Coated With an Ash Containing 10 wt% Alkali Sulfates and Exposed at 650°C to a Flue Gas Containing 1.0 vol% SO_2

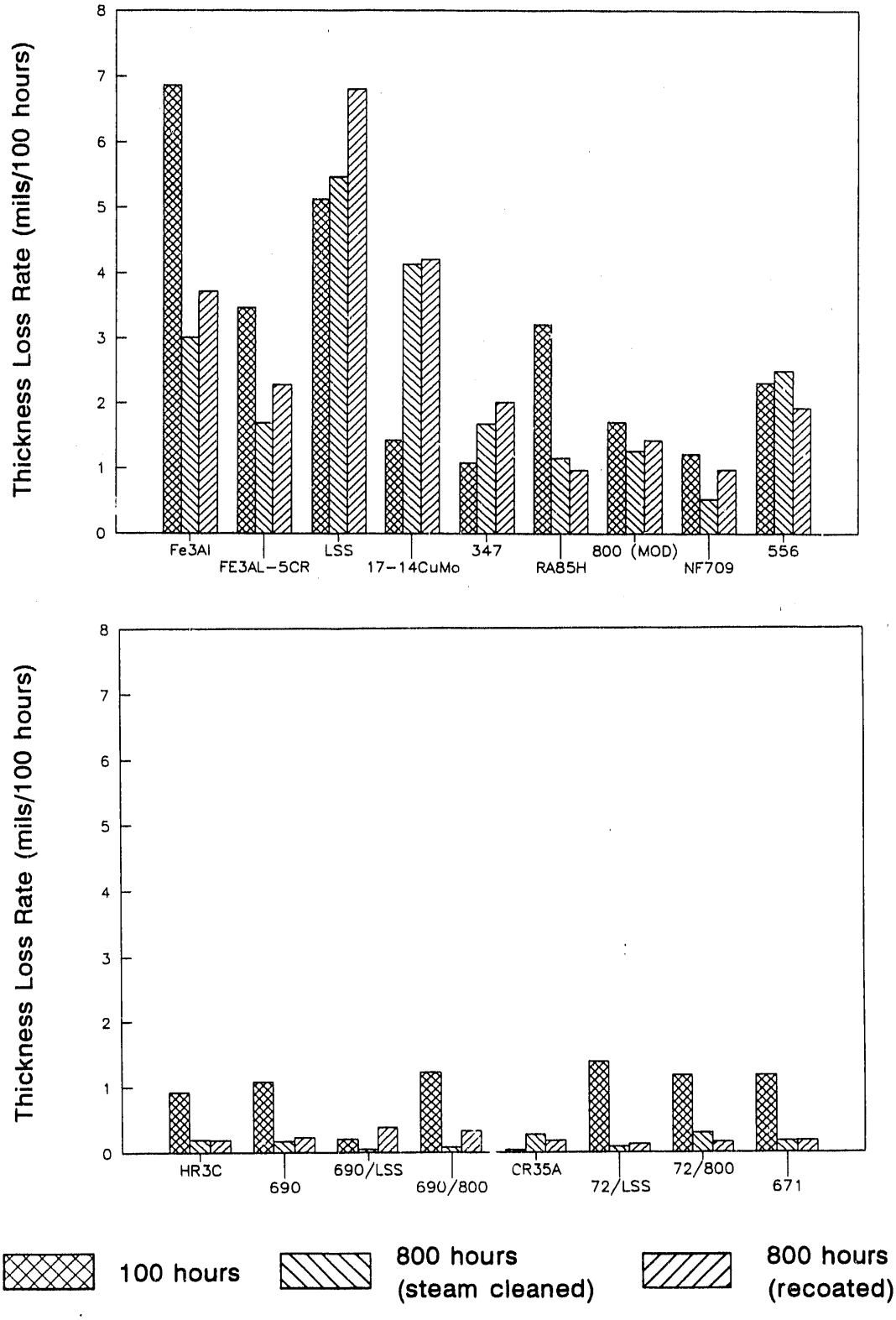

Figure 3.16 Normalized Thickness Loss Rates for Alloys Coated With an Ash Containing 10 wt% Alkali Sulfates and Exposed at 700°C to a Flue Gas Containing 1.0 vol% SO_2

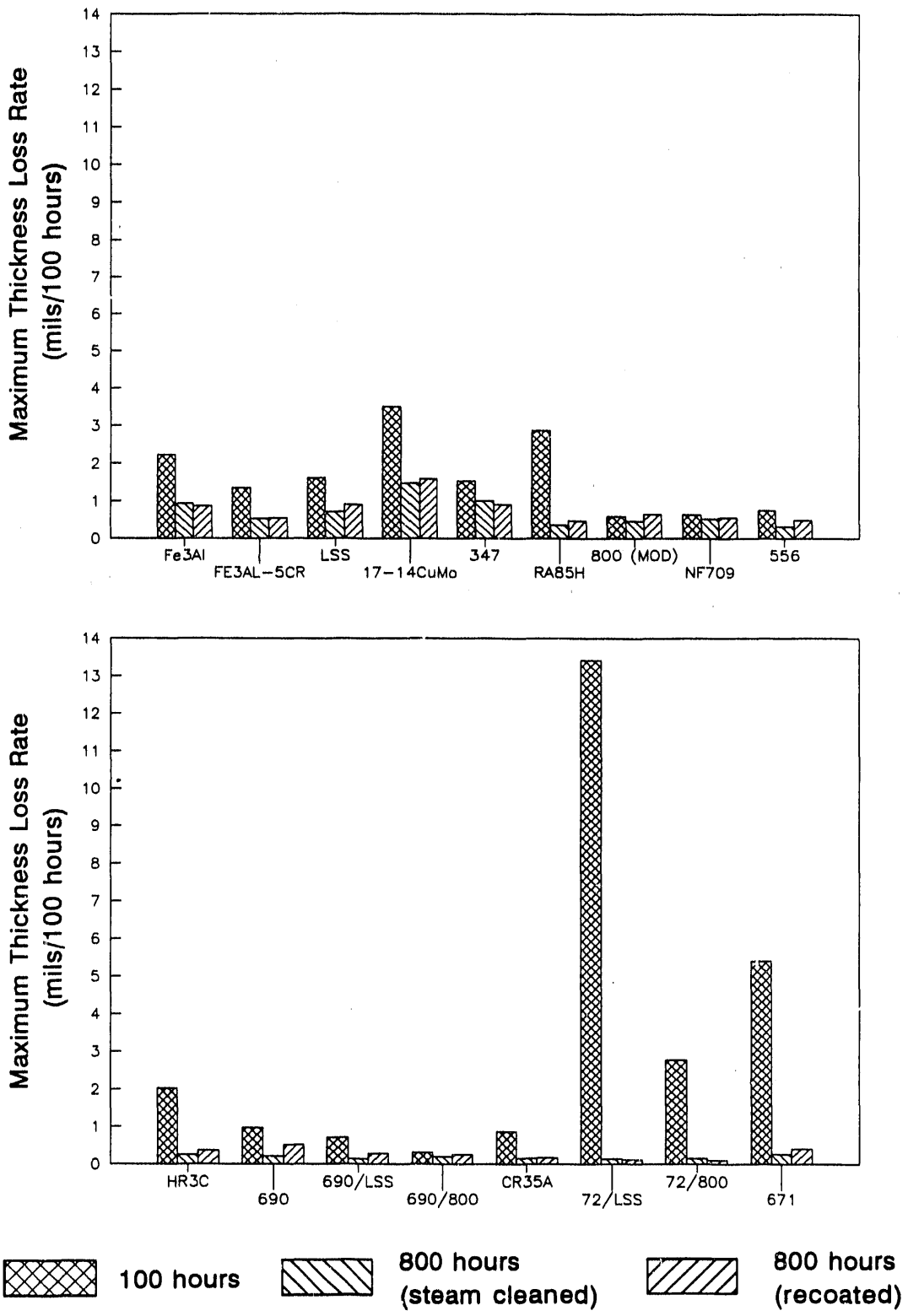

Figure 3.17 Normalized Maximum Thickness Loss Rates for Alloys Coated With an Ash Containing 10 wt% Alkali Sulfates and Exposed at 650°C to a Flue Gas Containing 1.0 vol% SO_2

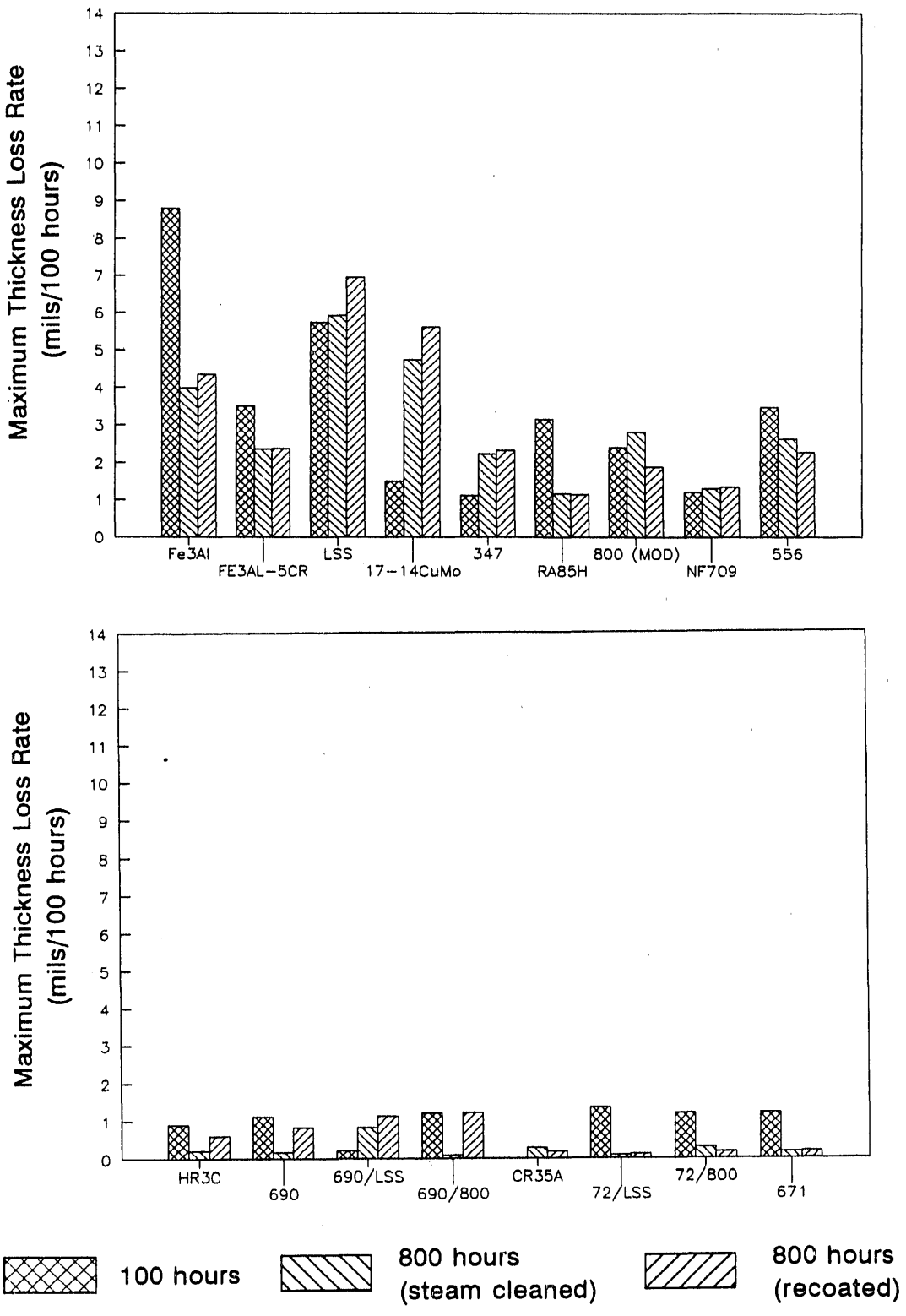

Figure 3.18 Normalized Maximum Thickness Loss Rates for Alloys Coated With an Ash Containing 10 wt% Alkali Sulfates and Exposed at 700°C to a Flue Gas Containing 1.0 vol% SO_2

3.4 EVALUATION OF CHROMIZED SPECIMENS

The chromized specimens evaluated in this project consisted of a low-alloy core coated with a high-chromium/high-silicon layer. These specimens were not evaluated by weight and thickness loss measurements, but by visual observations of the integrity of the coating. Table 3.1 summarizes the condition of the chromized specimens after exposure to various environments.

Table 3.1 Visual Evaluations of Chromized Specimens Exposed to Various Simulated Boiler Environments

Environment	Condition
High-Sulfate Ash, 0.25 vol% SO_2 in Flue Gas	
650°C, 100 hours	Coating Breached
650°C, 200 hours steam cleaned	Coating Breached
650°C, 200 hours recoated	Coating Breached
700°C, 100 hours	Coating Breached
700°C, 200 hours steam cleaned	Coating Breached
700°C, 200 hours recoated	Coating Breached
Low-Sulfate Ash, 0.25 vol% SO_2 in Flue Gas	
650°C, 100 hours	Coating Intact
650°C, 800 hours steam cleaned	Coating Intact
650°C, 800 hours recoated	Coating Intact
700°C, 100 hours	Coating Intact
700°C, 800 hours steam cleaned	Coating Breached
700°C, 800 hours recoated	Coating Breached

3.5 EVALUATION OF LEAN STAINLESS STEEL CLAD WITH TYPE 671

The specimens of lean stainless steel clad with Type 671 that we received contained a thin backing layer of lean stainless steel. Because machining off the backing layer was impractical, the specimens were exposed in the same conditions they were received. Unfortunately, the lean stainless steel backing suffered greater losses as a result of gas-phase attack and descaling than the Type 671 layer did by coal-ash attack. Because of the high losses of the backing, the specimens were evaluated visually. Table 3.2 lists the condition of the Type 671 layer after exposure to various environments.

Table 3.2 Visual Evaluations of Lean Stainless Steel Clad With Type 671 to Various Simulated Boiler Environments

Environment	Condition
High-Sulfate Ash, 0.25 vol% SO_2 in Flue Gas	
650°C, 100 hours	Light Pitting
650°C, 200 hours steam cleaned	Pitting
650°C, 200 hours recoated	Pitting
700°C, 100 hours	Minor Surface Attack
700°C, 200 hours steam cleaned	Minor Surface Attack
700°C, 200 hours recoated	No Corrosion
Low-Sulfate Ash, 0.25 vol% SO_2 in Flue Gas	
650°C, 100 hours	No Corrosion
650°C, 800 hours steam cleaned	No Corrosion
650°C, 800 hours recoated	Minor Surface Attack
700°C, 100 hours	No Corrosion
700°C, 800 hours steam cleaned	Minor Surface Attack
700°C, 800 hours recoated	Minor Surface Attack
Low-Sulfate Ash, 1.0 vol% SO_2 in Flue Gas	
700°C, 100 hours	Minor Surface Attack
700°C, 800 hours steam cleaned	Minor Surface Attack
700°C, 800 hours recoated	Minor Surface Attack

Section 4

EFFECTS OF ENVIRONMENTAL VARIABLES AND COMPOSITION ON RESISTANCE OF MATERIALS TO ALKALI-IRON TRISULFATE ATTACK

4.1 EFFECTS OF CHROMIUM ON ALLOY RESISTANCE

Past studies by Rehn [1-3] and Kihara and Wolowodiuk [4] have shown the strong influence of chromium content in an alloy on the corrosion resistance of that alloy to trisulfate attack. Figure 4.1 presents the relative corrosion rates of the alloys tested in relationship to their chromium content. The trend shown confirms the results previously mentioned: the corrosion resistance of an alloy increases as chromium content rises. Figures 4.2 through 4.4 show subsets of the plot in Figure 4.1. Figures 4.2, 4.3, and 4.4 respectively show the corrosion rates for alloys exposed to 0.25 vol% SO_2 while coated with coal ash containing 10 wt% alkali sulfates (the mildest environment), alloys exposed to 1.0 vol% SO_2 while coated with coal ash containing 10 wt% alkali sulfates (a moderate environment), and alloys exposed to 0.25 vol% SO_2 while coated with coal ash containing 75 wt% alkali sulfates (the harshest environment). As Figures 4.2 and 4.3 illustrate, the alloys containing chromium above 25 wt% (approximately) exhibited rather low corrosion rates in environments simulating conditions inside a boiler firing moderate-to high-sulfur coals. Even when subjected to a synthetic ash much higher in trisulfate content than would ever be found in a boiler, alloys with a chromium content greater than 25 wt% performed much better than the alloys with chromium contents less than 25 wt%. Among the alloying elements evaluated in this study, none was as effective as chromium in providing hot corrosion resistance.

4.2 EFFECTS OF OTHER ALLOYING ELEMENTS ON ALLOY RESISTANCE

Elements other than chromium have both beneficially and detrimentally affected the corrosion resistance of an alloy to AIT. In a laboratory study by Rehn [1], AL-6X, containing 6-percent molybdenum, had less resistance to AIT attack than similar alloys without molybdenum (IN-840 or Type 310). Kihara and Wolowodiuk noted greater wastage rates on Inconel 617 than on alloys with similar chromium contents [4]. They attributed this greater wastage to the high molybdenum content of Inconel 617 (8.5 percent). Figure 4.5 illustrates the comparative corrosion rates of six stainless steels in four different environments. The alloys shown range in chromium content from 14 to 30 wt%. Alloys containing 1 to 4 wt% molybdenum are marked with an asterisk. These alloys display less resistance to corrosion than alloys with comparable chromium contents (Type 347, RA85H, HR3C), validating the previous work.

A clear consensus was not reached in previous studies on the effects that aluminum and silicon have on the corrosion resistance of an alloy. Both silicon and aluminum were found by Rehn to be beneficial in reducing corrosion of alloys exposed to 100 percent AIT [1]. Rehn developed a high-silicon/high-aluminum alloy, Alloy 4C, (20% Cr, 20% Ni, 2.5% Si, 2.0% Al), which

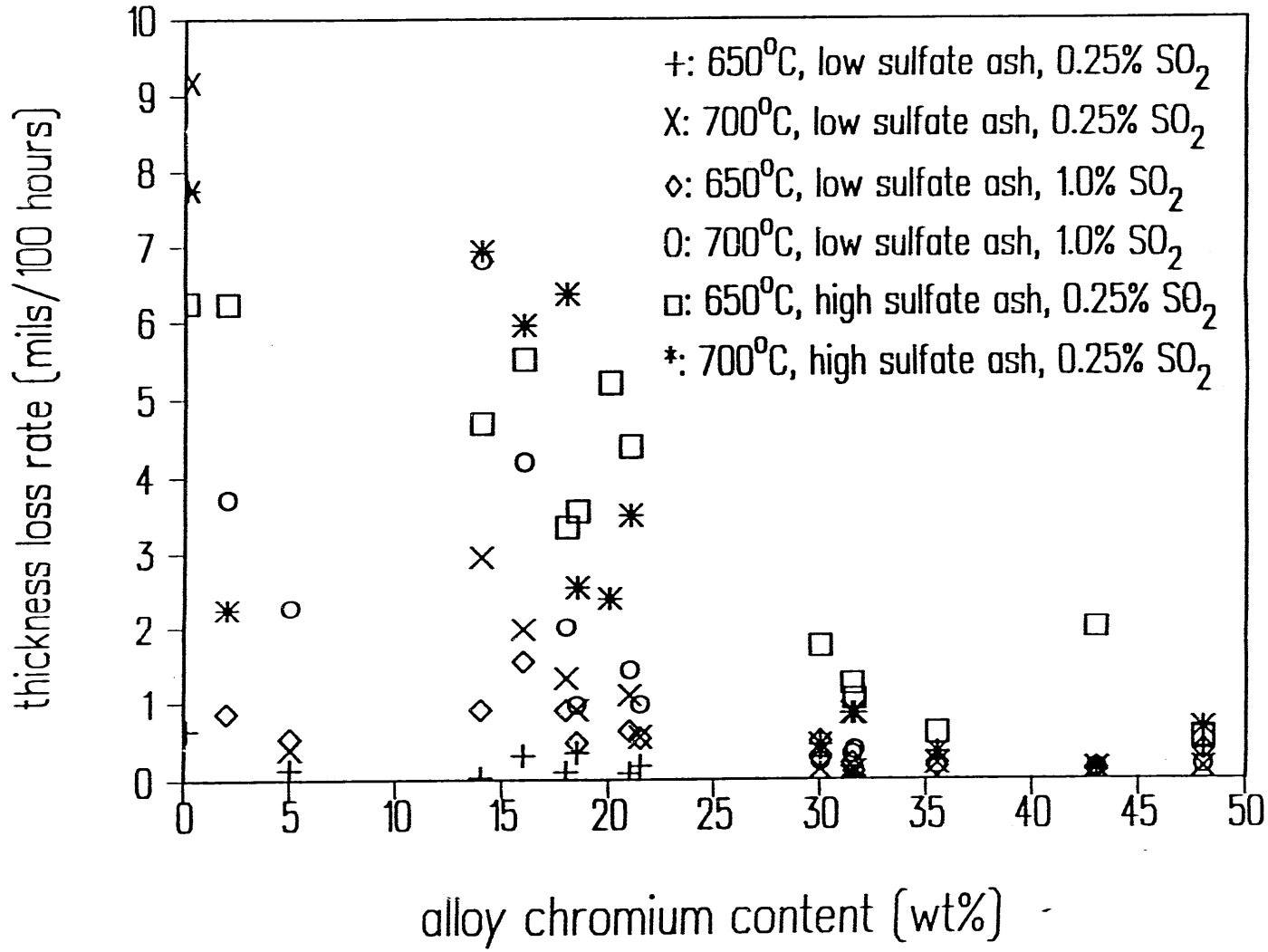

Figure 4.1 Average Thickness Loss Rate of Alloy Compared With Chromium Content of Alloy (Plot contains data for all alloys exposed under every environment tested in program.)

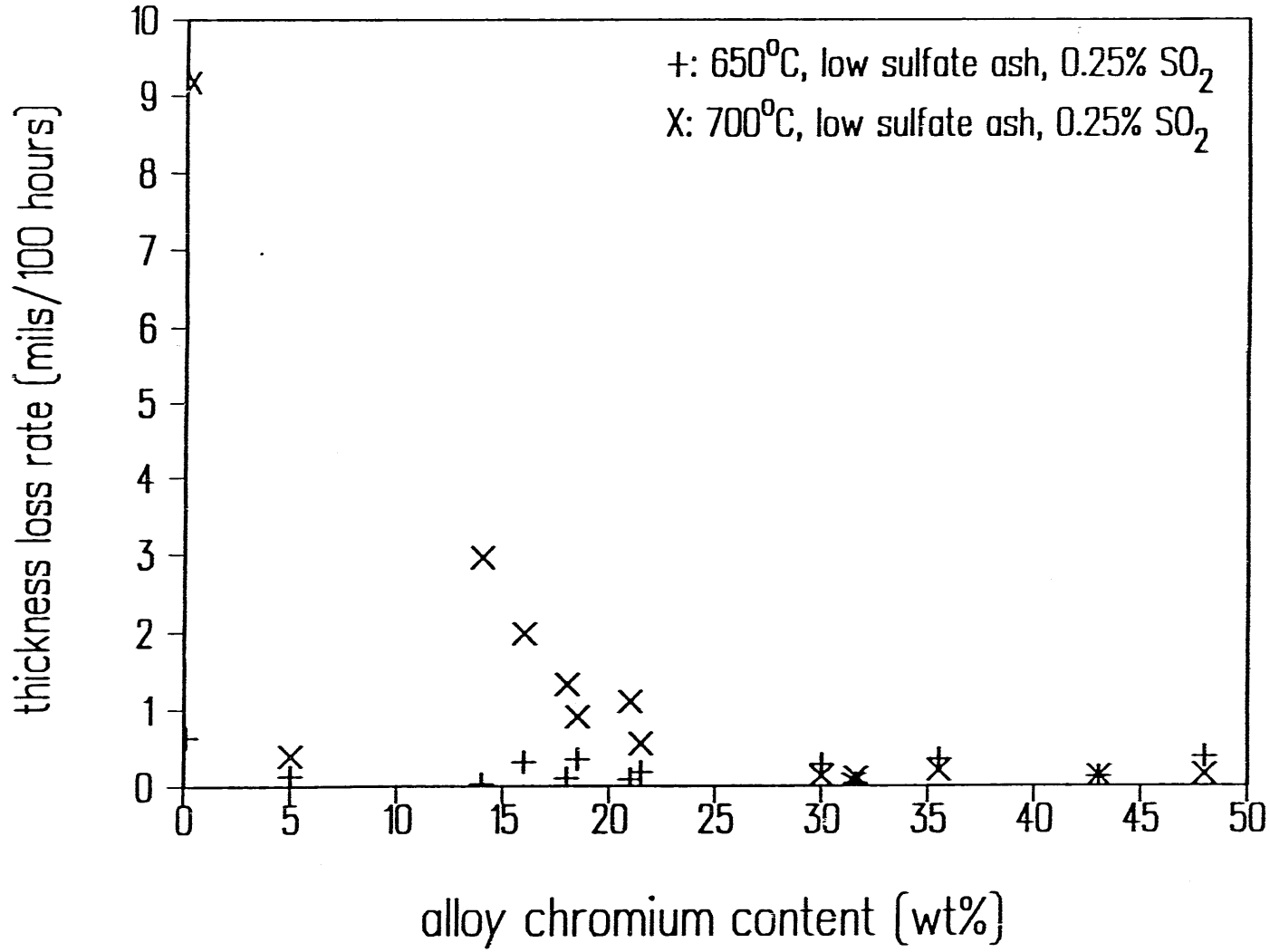

Figure 4.2 Average Thickness Loss Rate of Alloy Compared With Chromium Content of Alloy (Plot contains data for alloys exposed to flue gas containing 0.25 vol% SO_2 and coated with ash containing 10 wt% alkali sulfates.)

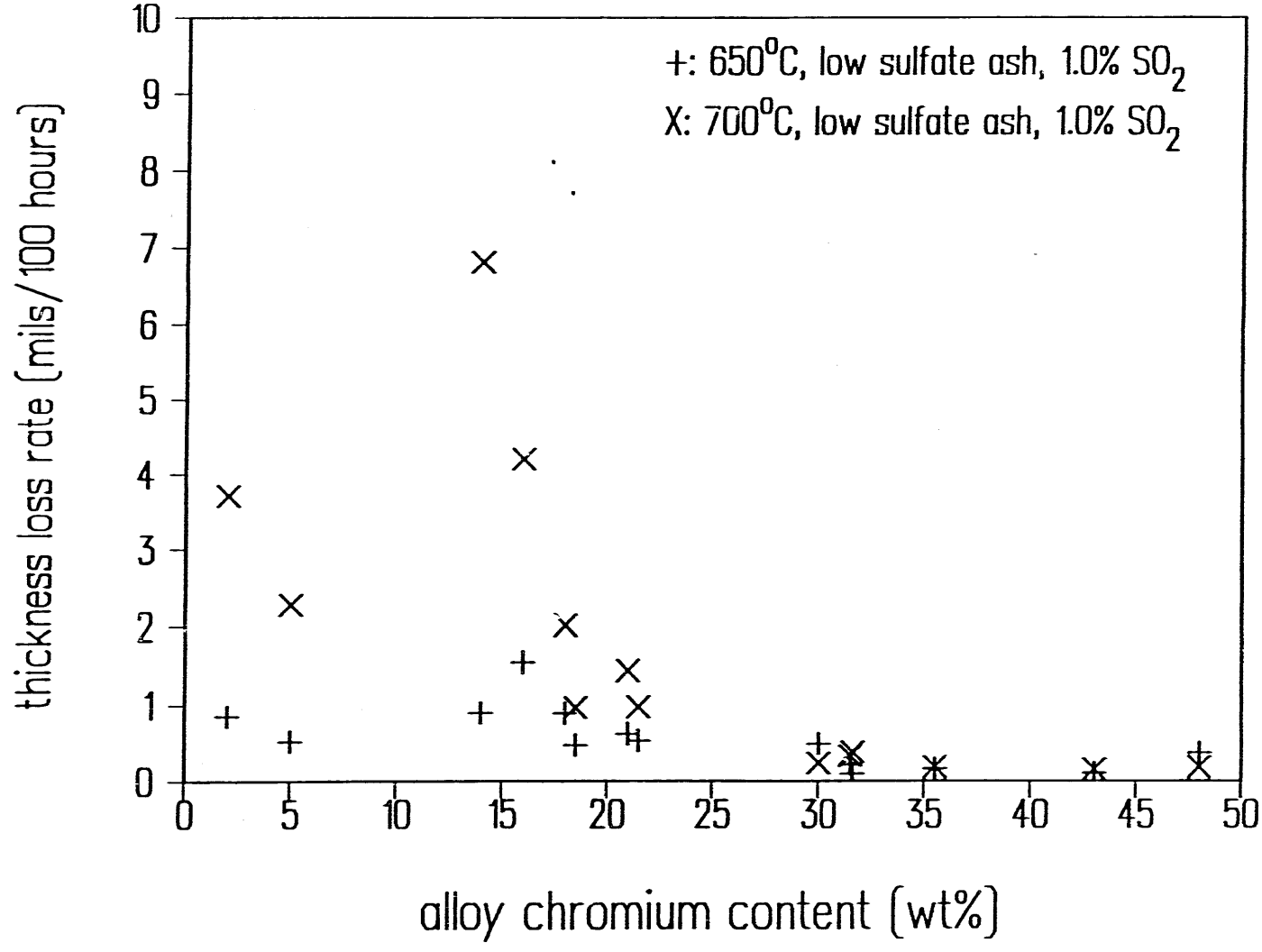

Figure 4.3 Average Thickness Loss Rate of Alloy Compared With Chromium Content of Alloy (Plot contains data for alloys exposed to flue gas containing 1.0 vol% SO_2 and coated with ash containing 10 wt% alkali sulfates.)

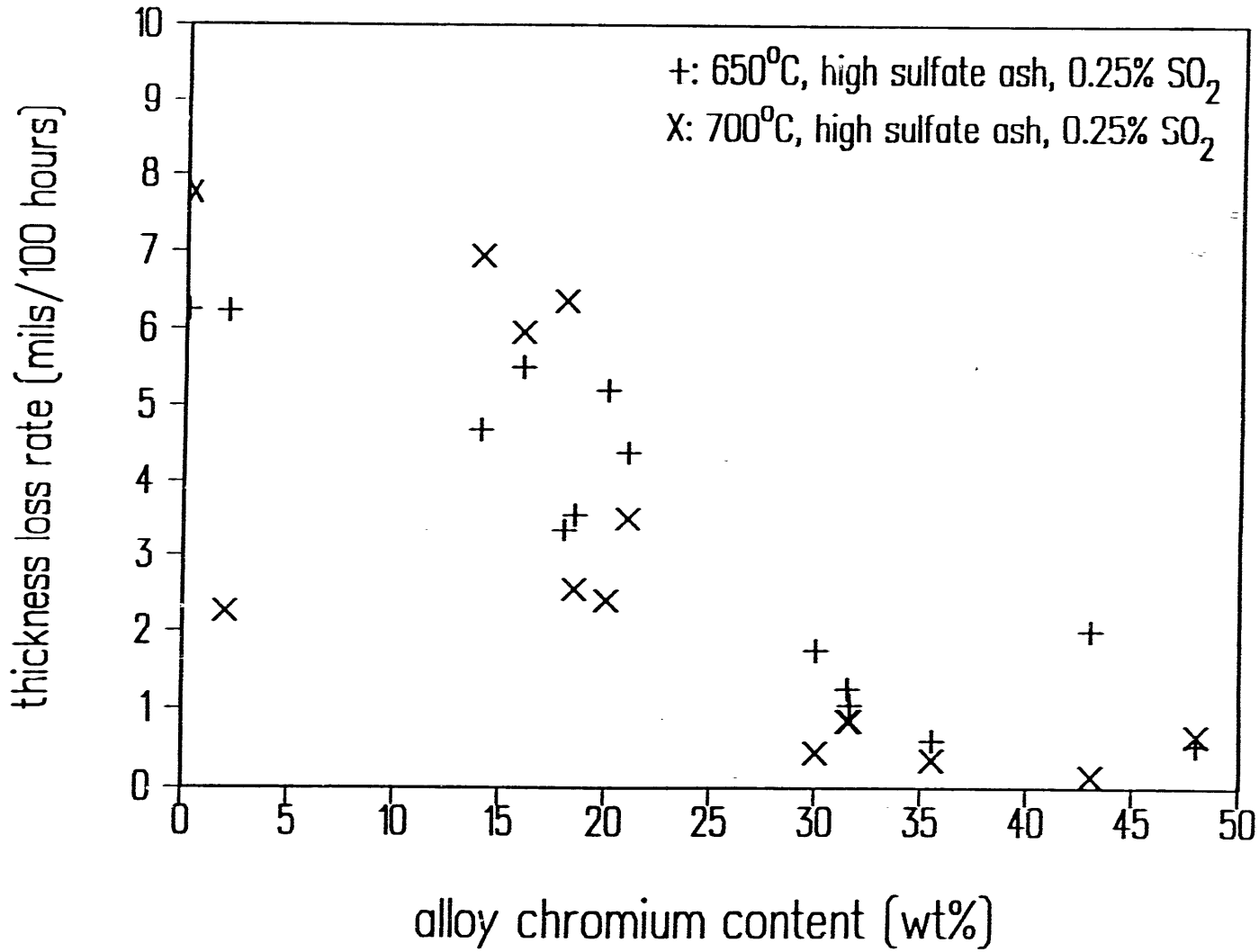

Figure 4.4 Average Thickness Loss Rate of Alloy Compared With Chromium Content of Alloy (Plot contains data for alloys exposed to flue gas containing 0.25 vol% SO_2 and coated with ash containing 75 wt% alkali sulfates.)

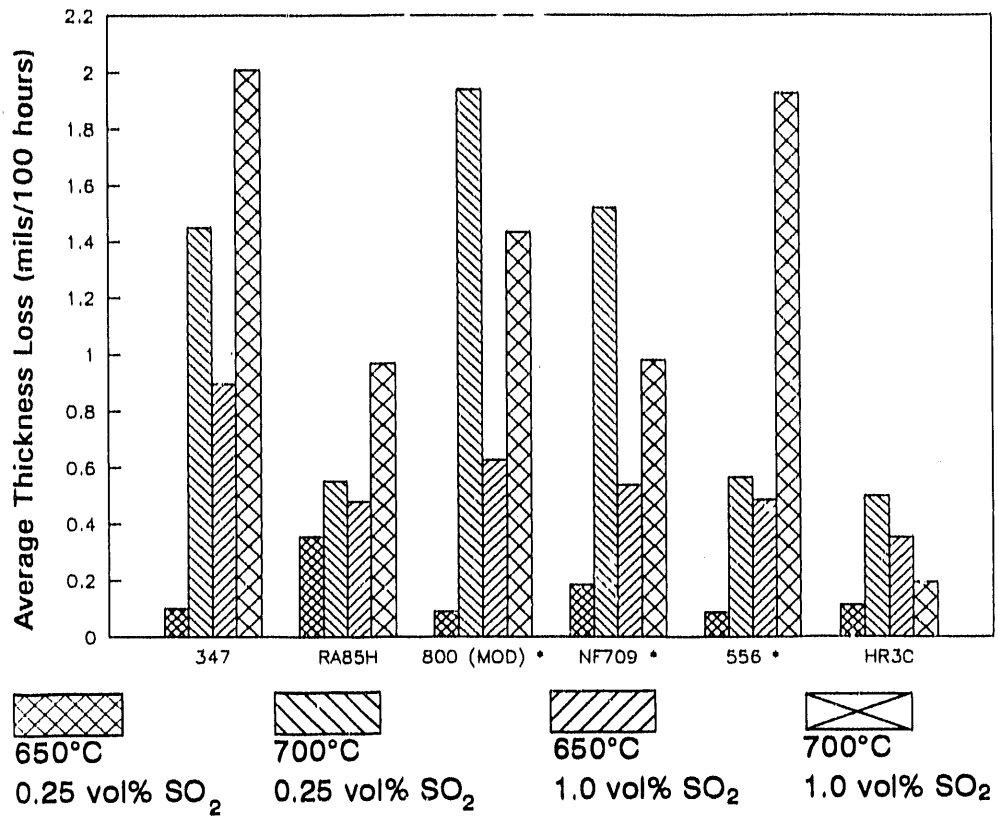

Figure 4.5 Average Thickness Loss Rate of Alloys Containing 14- to 30-Percent Chromium (Alloys marked with an asterisk contain between 1 and 4 percent molybdenum.)

showed markedly better corrosion resistance in 100 percent AIT than alloys of similar chromium and nickel contents. In a later work, Alloy 4C and high-silicon high-aluminum commercial alloys were exposed, using ashes containing between 2.5% and 10% alkali sulfates. In these tests silicon and aluminum had no noticeable beneficial effects [4].

As shown in Figure 4.5, RA85H, a high-silicon high-aluminum alloy with a chromium content between that found in Type 347 and the modified 800H displays twice the corrosion resistance of the former and three times the corrosion resistance of the latter, a finding that would seem to validate Rehn's work.

4.3 CLAD ALLOYS

Figure 4.6 illustrates the comparative corrosion resistance of base metals and cladding of the same nominal composition. The cladding performed as well as the base metals within the range of scatter for these tests. Two exceptions are the 690 clad Type 316 exposed to 0.25 vol% SO_2 at 700°C and the 72-clad 800 exposed to 0.25 vol% SO_2 at 700°C. The reasons for the lowered corrosion resistance of these specimens are discussed in Section 4.8.

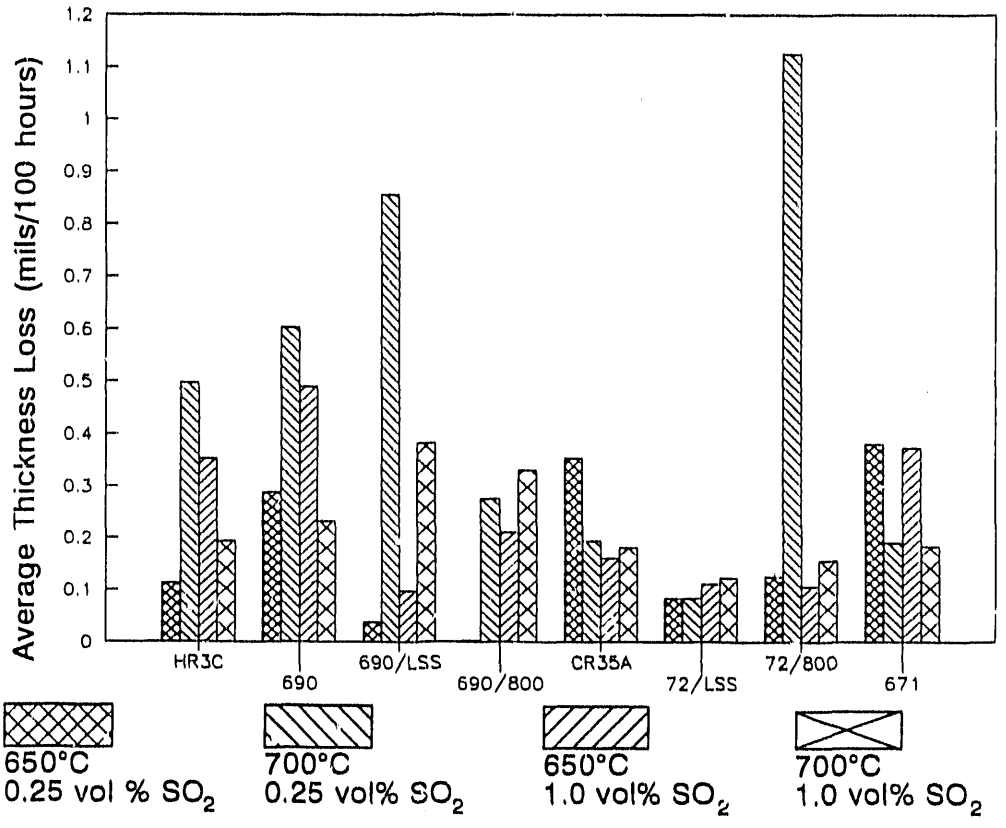

Figure 4.6 Average Thickness Loss Rates of Various Monolithic Alloys and Claudings Coated With Ash Containing 10 wt% Alkali Sulfates and Exposed for 800 Hours

4.4 ALUMINIDE ALLOYS

Corrosion losses of the aluminide alloys and two stainless steels are shown in Figure 4.7. Aluminide alloy development projects were undertaken concurrently with this test program, consequently improved alloys unavailable at the beginning of the program were incorporated in later stages.

Iron nickel aluminide specimens performed poorly in all environments. At 700°C, when exposed to a flue gas containing 1.0 vol% SO_2 the iron-nickel aluminide suffered catastrophic wastage. Most of the specimen was completely converted to scale. The morphology of attack on the iron-nickel aluminides appears to be primarily oxidation and sulfidation rather than liquid salt attack. In contrast to the iron-nickel aluminide, the iron aluminides did not suffer catastrophic wastage. Both aluminides were subjected to approximately the same degree of attack as the low-chromium stainless steels, with the iron aluminide containing 5 wt% chromium generally suffering less wastage than the iron aluminide containing 2 wt% chromium.

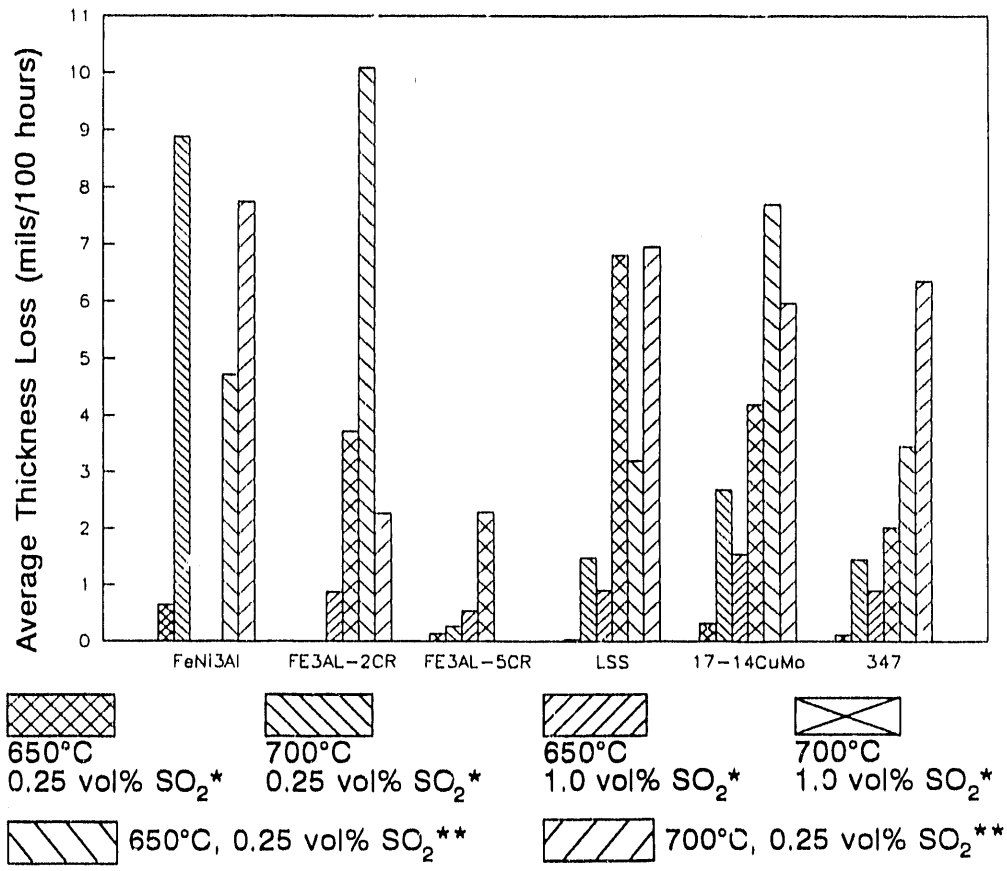

Figure 4.7 Average Thickness Loss Rates of Three Intermetallic Aluminides and Two Stainless Steels Exposed to a Variety of Environments (* = Low Sulfate Ash, ** = High Sulfate Ash)

4.5 INFLUENCE OF ENVIRONMENT ON WASTAGE RATES

The effects of temperature, SO_2 concentration in the flue gas, sulfate content of the ash, exposure time, and steam cleaning between exposures on the corrosion rates of various alloys are discussed in the following paragraphs. To prevent confusion and "information overload," only the corrosion rates of a representative selection of alloys in selected environments are given.

Figures 4.8 through 4.10 present the effects of temperature on the average thickness loss rates of alloys. Figures 4.8 and 4.9 show the corrosion rates of alloys coated with a coal ash containing 10 wt% alkali sulfate and exposed to a flue gases containing 0.25 and 1.0 vol% SO_2 respectively. Figure 4.10 illustrates the corrosion rates of alloys coated with a coal ash containing 75 wt% alkali sulfates while exposed to a flue gas containing 0.25 vol% SO_2.

The alloys coated with the low-sulfate ash and exposed to 0.25 vol% SO_2 (Figure 4.8) show minimal wastage at 650°C, indicating that liquid AITs may have had difficulty forming because of the lower SO_2 level. Specimens exposed at 700°C can be divided into two groups--alloys exhibiting wastage rates similar to those exposed at 650°C and alloys suffering much greater wastage at 700°C than at 650°C. A possible explanation for this behavior is that the alloys with high wastage rates promote the formation of a liquid phase. Several of the alloys exhibiting high wastage rates contained a

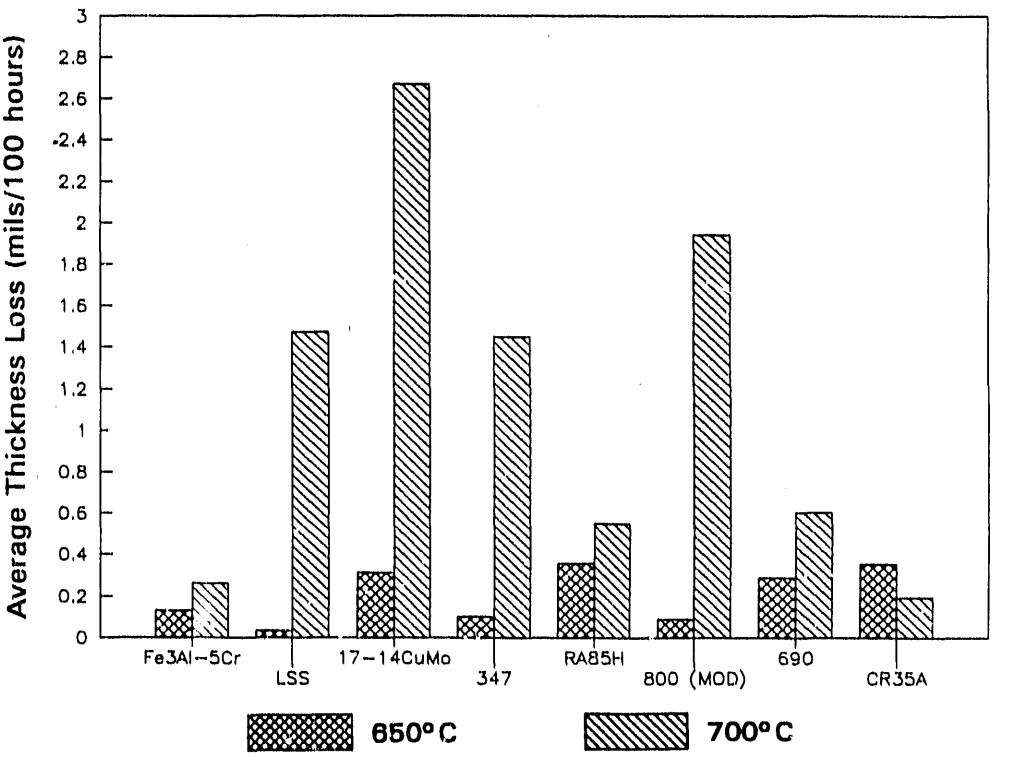

Figure 4.8 Average Thickness Loss Rates of Representative Alloys Coated With Ash Containing 10 wt% Alkali Sulfates and Exposed at 650 and 700°C for 800 Hours to Flue Gas Containing 0.25 vol% SO_2

substantial amount of molybdenum, which had been found by Rehn to promote AIT attack [1].

Lower-chromium alloys exposed to a flue gas containing 1.0 vol% SO_2 while coated with the lower-sulfate coal ash (Figure 4.9) suffered greater wastage rates at 700°C than at 650°C, while the higher-chromium alloys (690 and CR35A) exhibited approximately the same corrosion rates at 650°C as at 700°C. Note also that the corrosion rates of the alloys drop as the chromium content of the alloy increases, illustrating the beneficial effect of chromium.

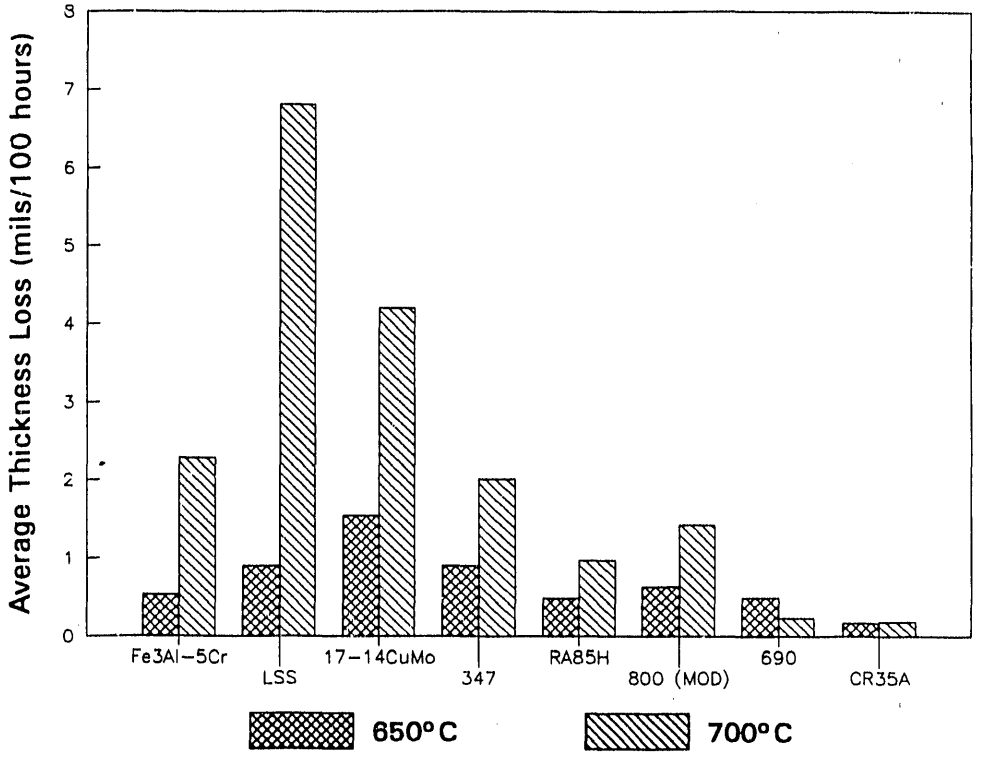

Figure 4.9 Average Thickness Loss Rates of Representative Alloys Coated With Ash Containing 10 wt% Alkali Sulfates and Exposed at 650 and 700°C for 800 Hours to Flue Gas Containing 1.0 vol% SO_2

The alloys coated with a 75 wt% alkali sulfate coal ash while exposed to 0.25 vol% SO_2 flue gas (Figure 4.10) did not display a consistent temperature dependence. The two higher-chromium alloys (690 and CR35A) suffered greater corrosion losses at 650°C than at 700°C, a dependence found in previous studies by Kihara [4] and Rehn [1].

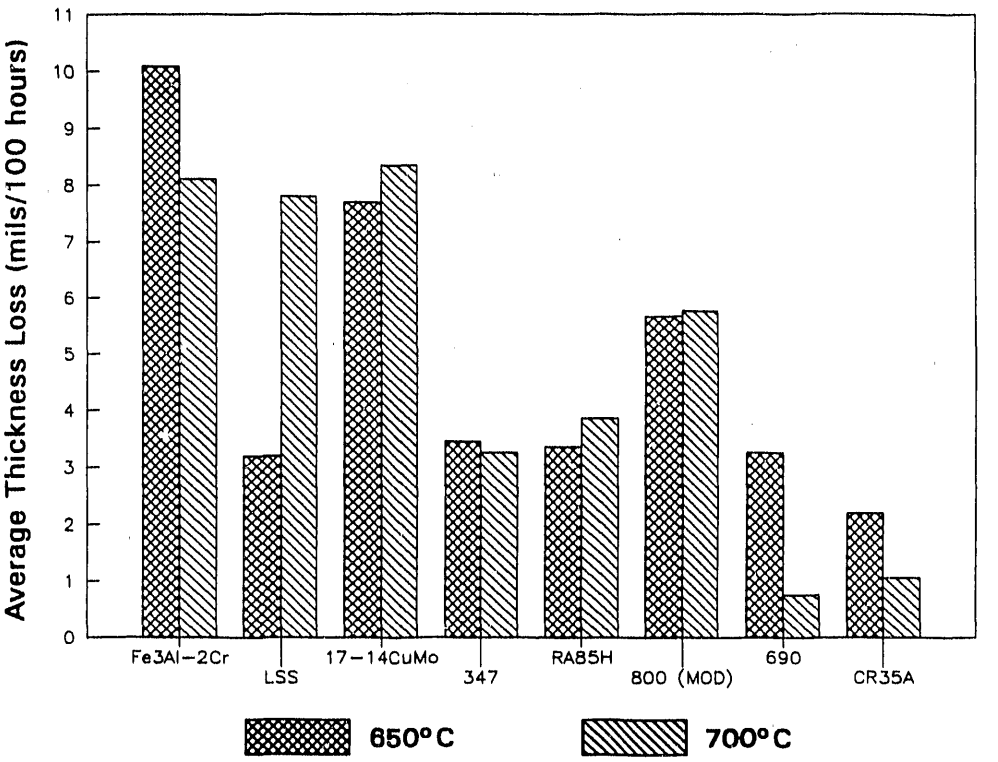

Figure 4.10 Average Thickness Loss Rates of Representative Alloys Coated With Ash Containing 75 wt% Alkali Sulfates and Exposed at 650 and 700°C for 200 Hours to Flue Gas Containing 0.25 vol% SO_2

The effects of increased SO_2 in the flue gas and a higher sulfate concentration in the coal ash are illustrated in Figures 4.11 through 4.14. Figures 4.11 and 4.12 display the effects of SO_2 concentration on the corrosion rates of alloys coated with 10 wt% sulfate coal ash and exposed for eight 100-hour cycles at 650 and 700°C respectively, with ash replenishment between cycles. Figures 4.13 and 4.14 show the effects of an increased sulfate concentration in the coal ash on the corrosion rates of alloys exposed to flue gas containing 0.25 vol% SO_2 and for 100 hours at 650 and 700°C respectively. An increase in both the SO_2 concentration in the flue gas and the sulfate concentration in the coal ash would be expected to produce a more aggressive environment. As shown in the figures, an increase in either the SO_2 level or the sulfate concentration will raise the corrosion rate.

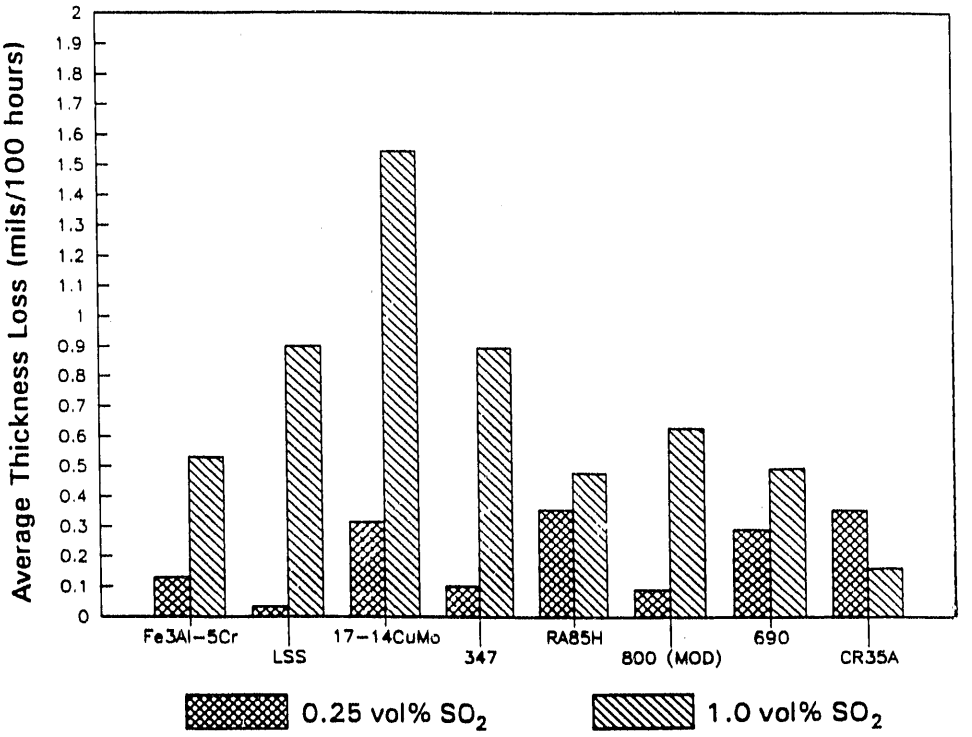

Figure 4.11 Average Thickness Loss Rates of Representative Alloys Coated With Ash Containing 10 wt% Alkali Sulfates and Exposed at 650°C for 800 Hours to Flue Gas Containing Either 0.25 or 1.0 vol% SO_2

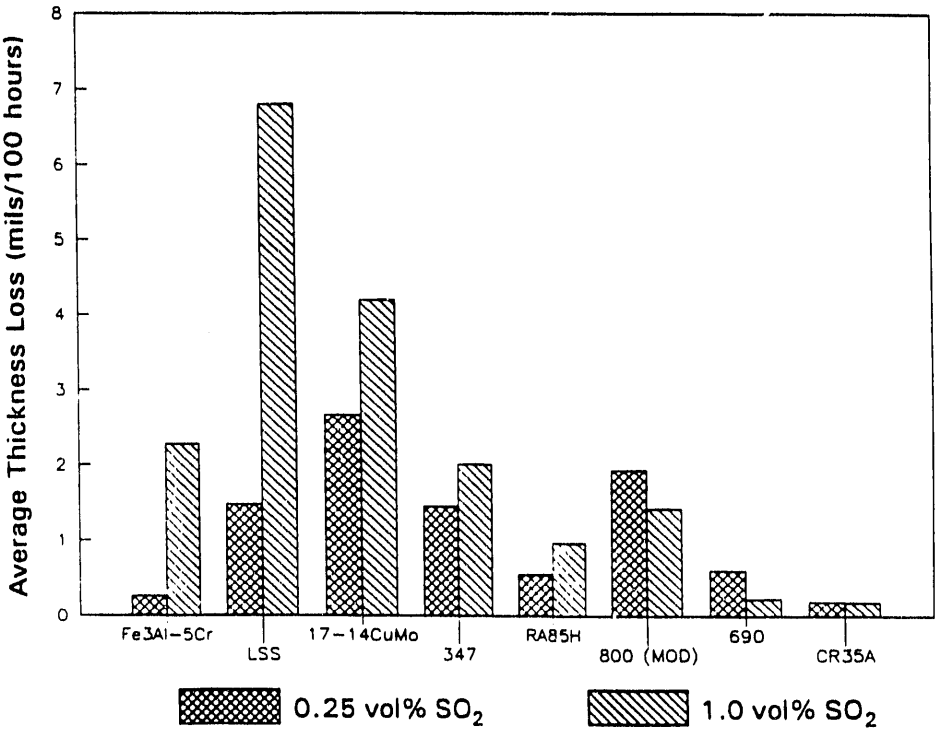

Figure 4.12 Average Thickness Loss Rates of Representative Alloys Coated With Ash Containing 10 wt% Alkali Sulfates and Exposed at 700°C for 800 Hours to Flue Gas Containing Either 0.25 or 1.0 vol% SO_2

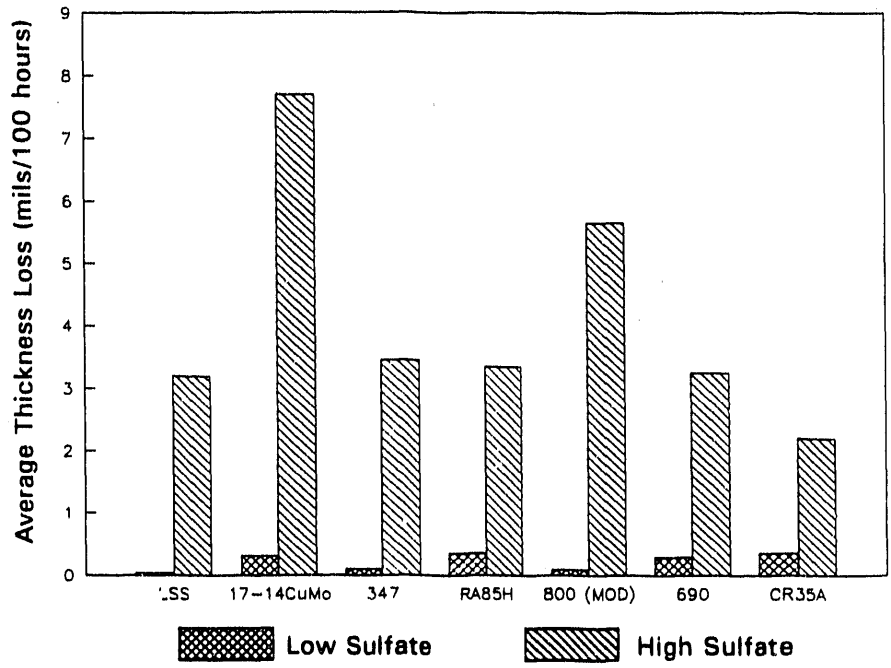

Figure 4.13 **Average Thickness Loss Rates of Representative Alloys Coated With Ash Containing Either 10 or 75 wt% Alkali Sulfates and Exposed at 650°C for 200 or 800 Hours Respectively to Flue Gas Containing 0.25 vol% SO_2**

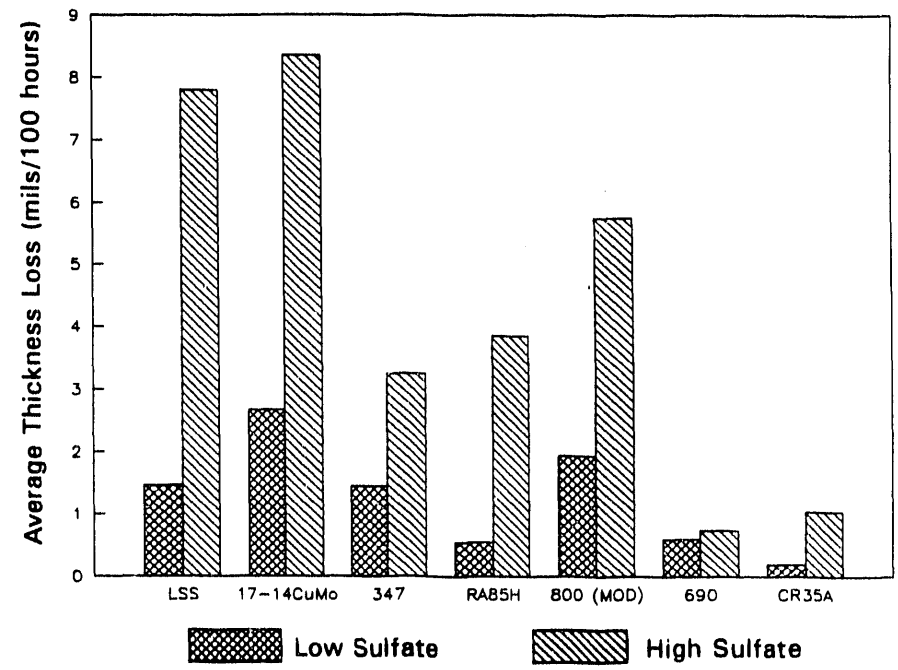

Figure 4.14 **Average Thickness Loss Rates of Representative Alloys Coated With Ash Containing Either 10 or 75 wt% Alkali Sulfates and Exposed at 700°C for 200 or 800 Hours Respectively to Flue Gas Containing 0.25 vol% SO_2**

The corrosion rate of an alloy after different lengths of exposure time can be used to determine whether passivation is taking place or whether breakaway corrosion is occurring. Figures 4.15 through 4.18 illustrate how the corrosion rates of various alloys change with exposure time in different environments.

Figures 4.19 through 4.22 present corrosion rates of specimens steam-cleaned between exposures and specimens where fresh ash was added between exposures. Summaries of the losses incurred under various conditions are shown in Figures 4.23 through 4.25. No pattern runs through all combinations of alloys and exposure conditions; however, several trends do exist. The corrosion rate increases with exposure time for alloys coated with high-sulfate ash (Figures 4.15, 4.16, and 4.23), indicating that either breakaway corrosion is taking place or there was a long induction time for AIT to form initially. The alloys coated with low-sulfate ash generally showed decreasing corrosion rates with time, indicating that a passive layer had formed. However, the coupons coated the lower sulfate ash and exposed to 1.0 vol% SO_2 at 700°C show conflicting trends between alloys. This conflicting behavior may indicate that alloys exposed to this set of conditions are on the border between passivity and breakaway corrosion.

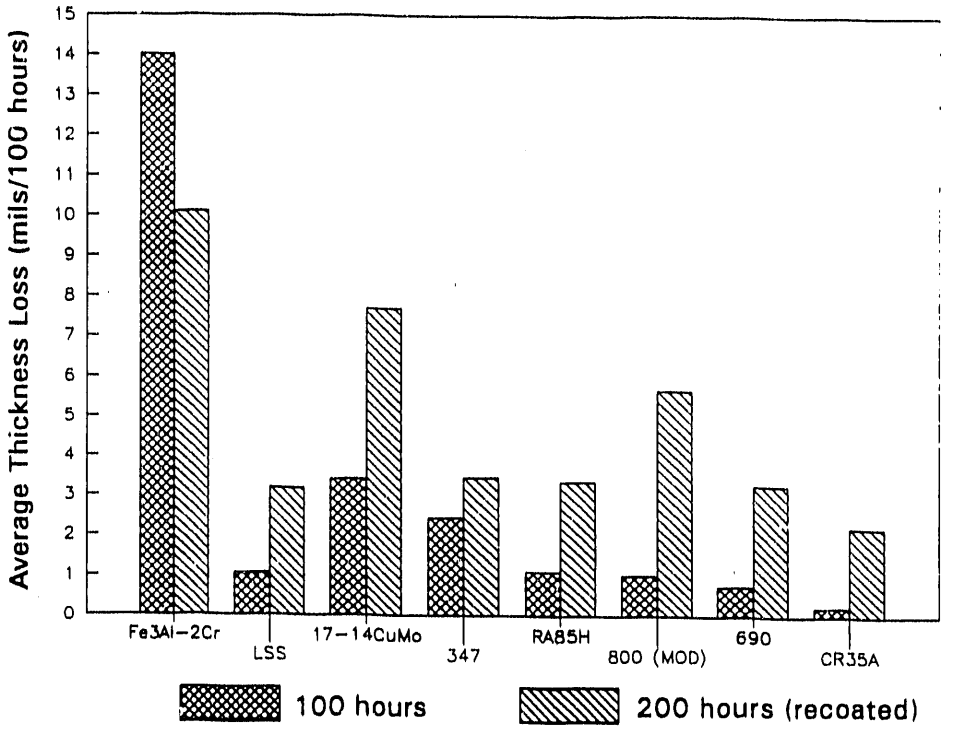

Figure 4.15 Average Thickness Loss Rates of Representative Alloys Coated With Ash Containing 75 wt% Alkali Sulfates and Exposed at 650°C for Either 100 or 200 Hours to Flue Gas Containing 0.25 vol% SO_2

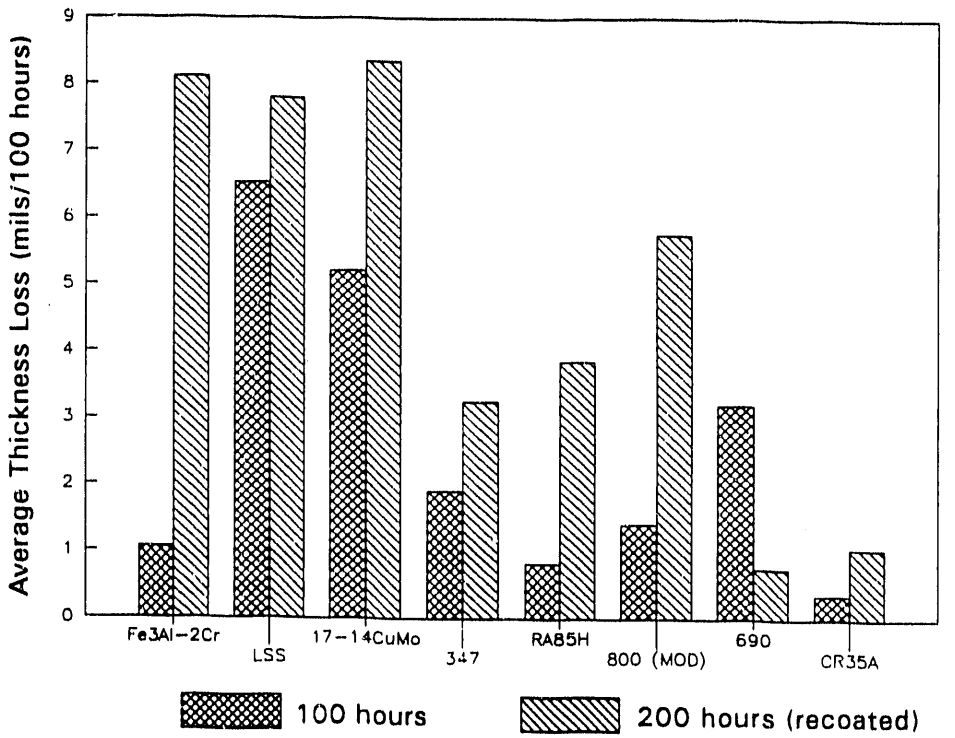

Figure 4.16 Average Thickness Loss Rates of Representative Alloys Coated With Ash Containing 75 wt% Alkali Sulfates and Exposed at 700°C for Either 100 or 200 Hours to Flue Gas Containing 0.25 vol% SO_2

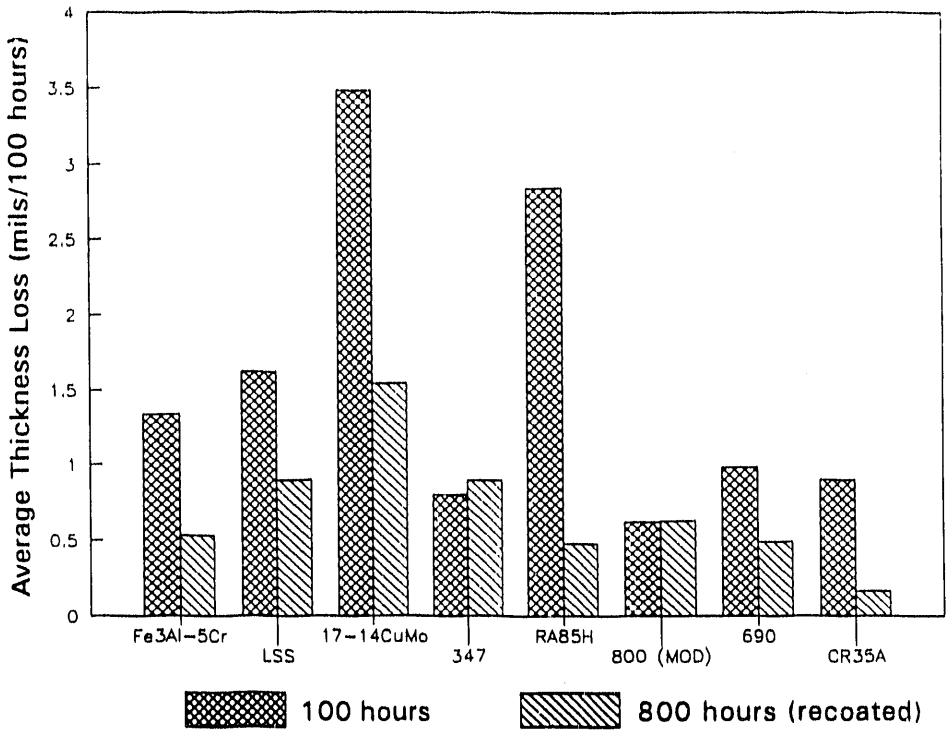

Figure 4.17 Average Thickness Loss Rates of Representative Alloys Coated With Ash Containing 10 wt% Alkali Sulfates and Exposed at 650°C for Either 100 or 800 Hours to Flue Gas Containing 1.0 vol% SO_2

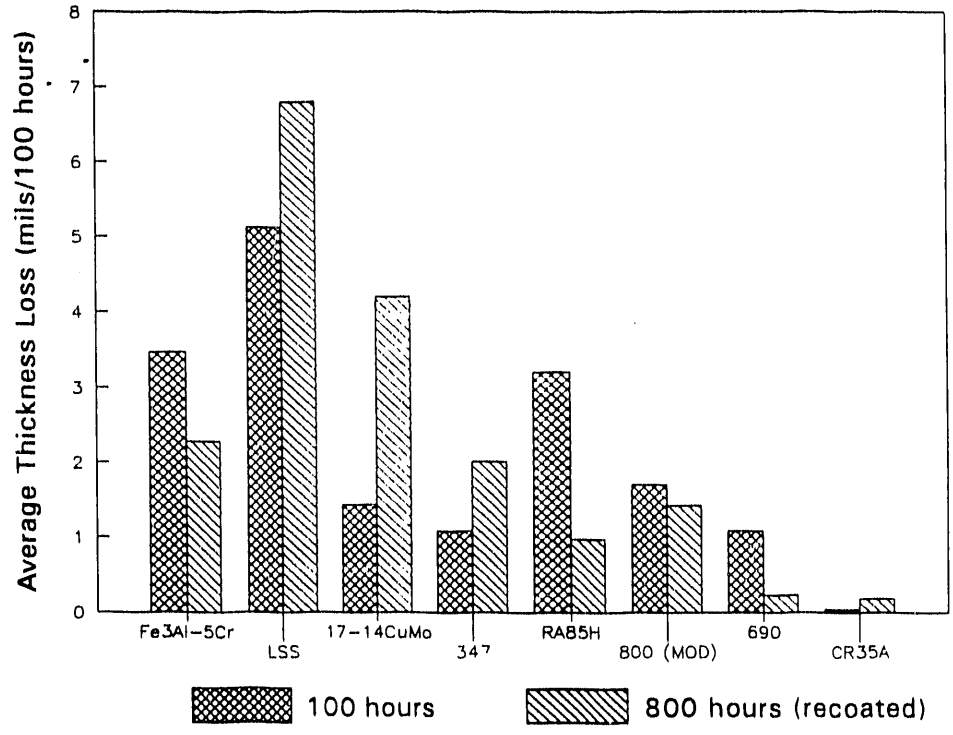

Figure 4.18 Average Thickness Loss Rates of Representative Alloys Coated With Ash Containing 10 wt% Alkali Sulfates and Exposed at 700°C for Either 100 or 800 Hours to Flue Gas Containing 1.0 vol% SO_2

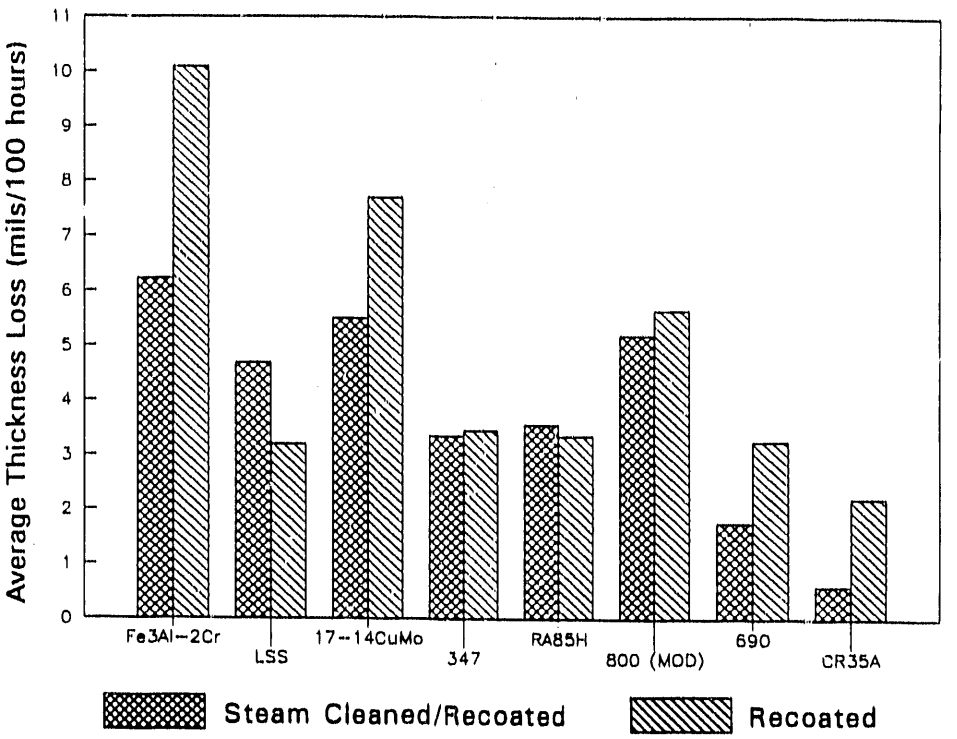

Figure 4.19 Average Thickness Loss Rates of Representative Alloys Coated With Ash Containing 75 wt% Alkali Sulfates and Exposed at 650°C for 200 Hours to Flue Gas Containing 0.25 vol% SO_2

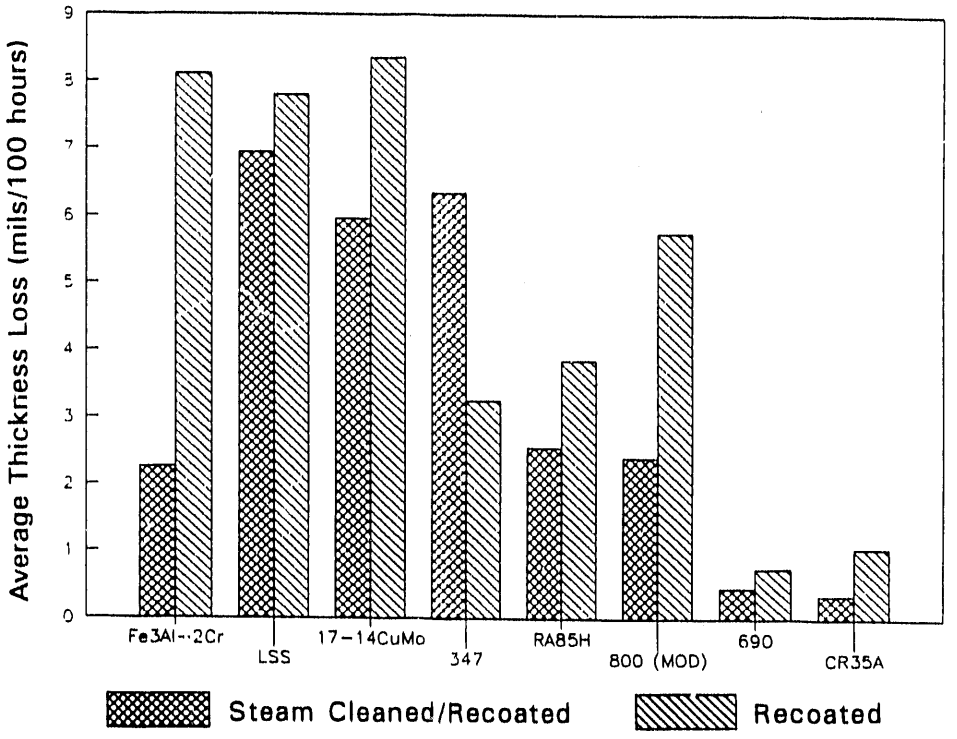

Figure 4.20 Average Thickness Loss Rates of Representative Alloys Coated With Ash Containing 75 wt% Alkali Sulfates and Exposed at 700°C for 200 Hours to Flue Gas Containing 0.25 vol% SO_2

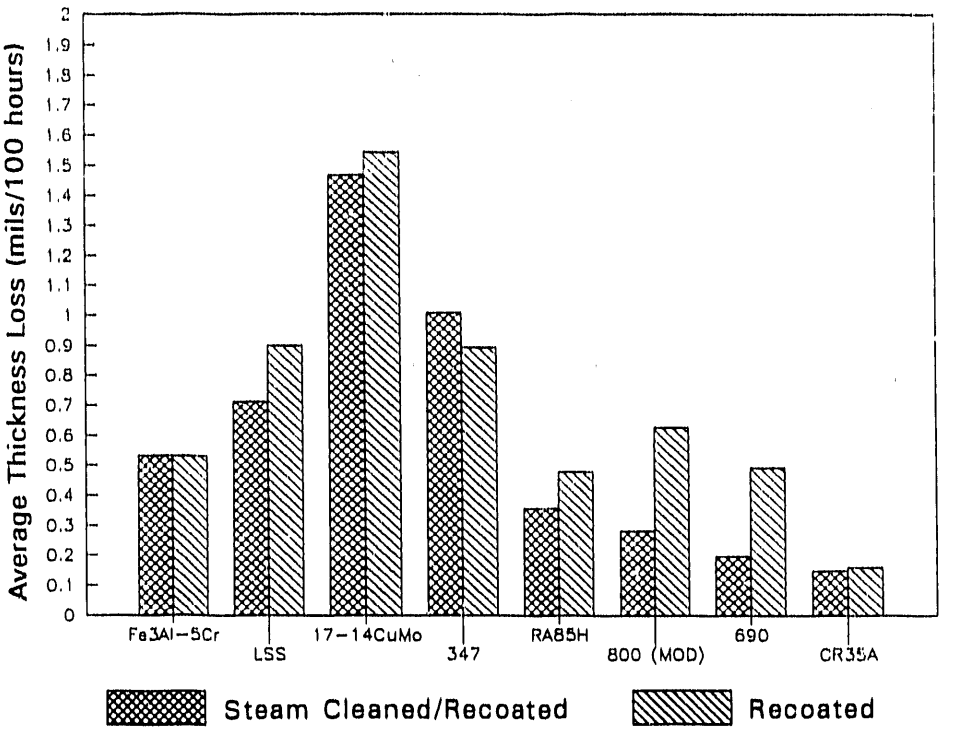

Figure 4.21 Average Thickness Loss Rates of Representative Alloys Coated With Ash Containing 10 wt% Alkali Sulfates and Exposed at 650°C for 800 Hours to Flue Gas Containing 1.0 vol% SO_2

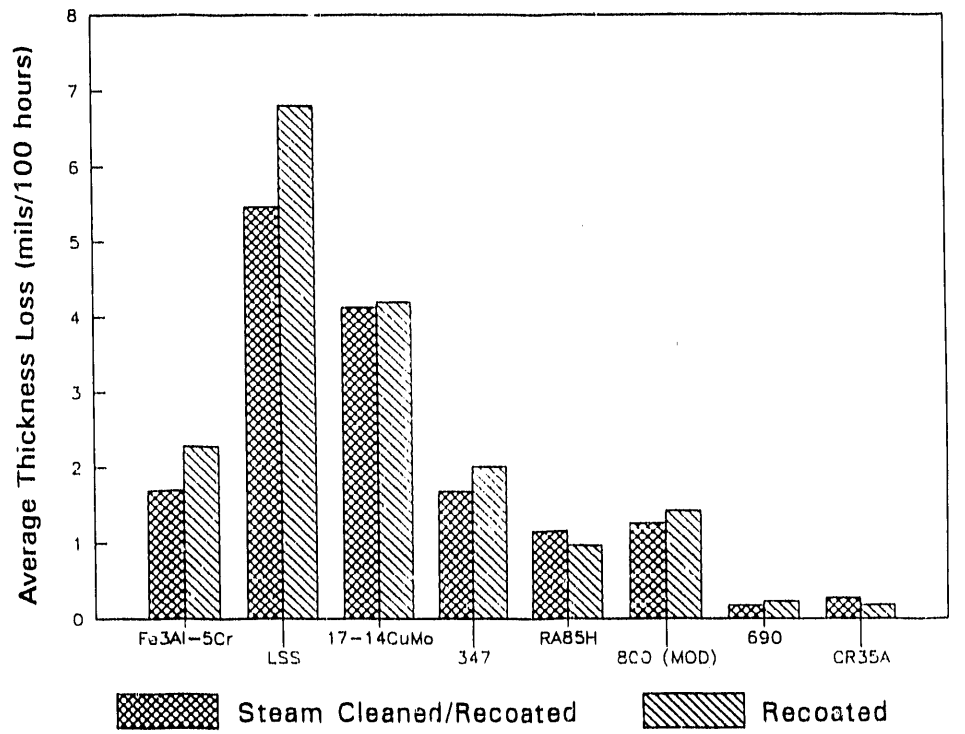

Figure 4.22 Average Thickness Loss Rates of Representative Alloys Coated With Ash Containing 10 wt% Alkali Sulfates and Exposed at 700°C for 800 Hours to Flue Gas Containing 1.0 vol% SO_2

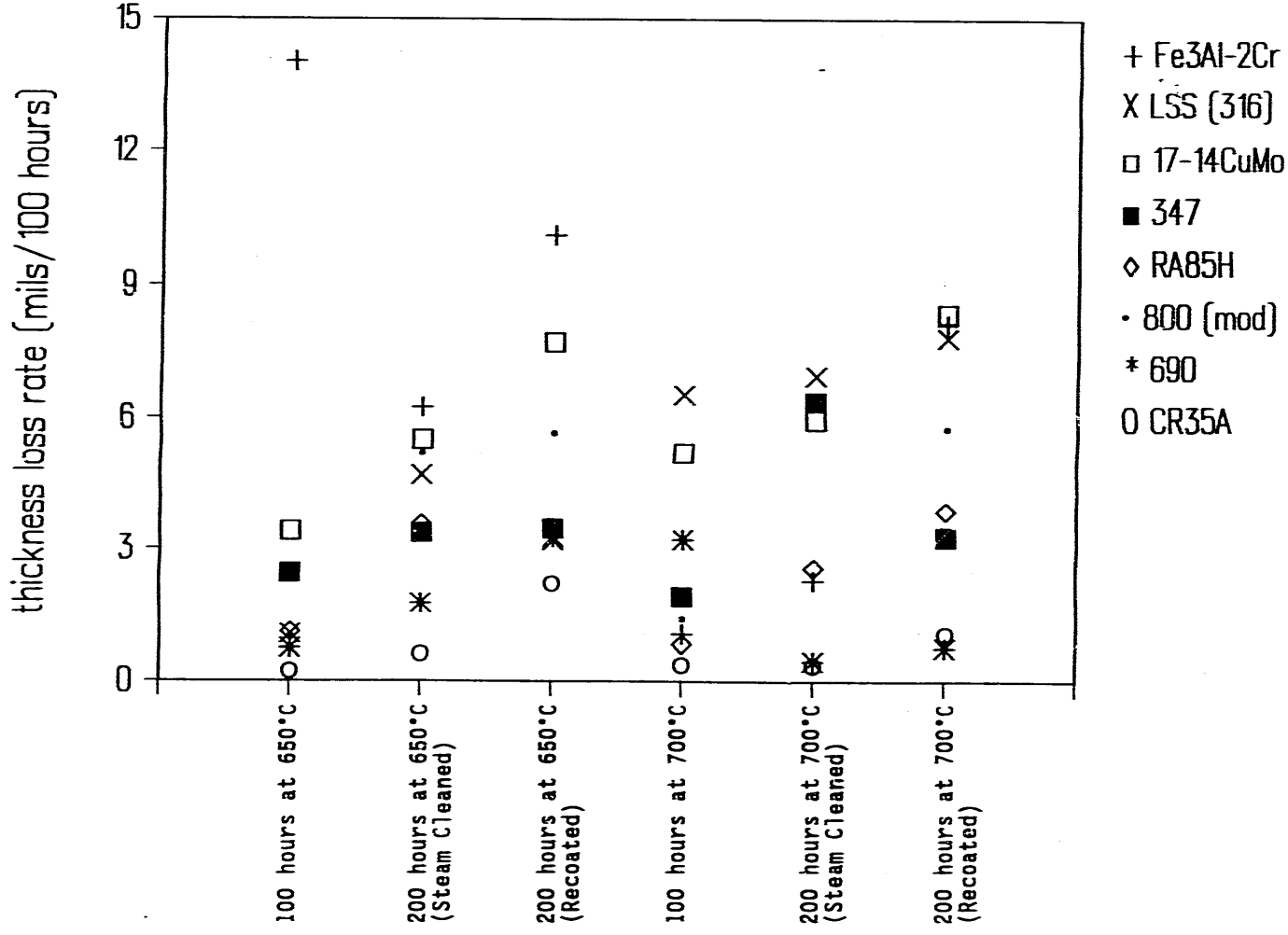

Figure 4.23 Summary of Average Thickness Loss Rates for Representative Alloys Coated With Ash Containing 75 wt% Alkali Sulfates and Exposed to Flue Gas Containing 0.25 vol% SO_2

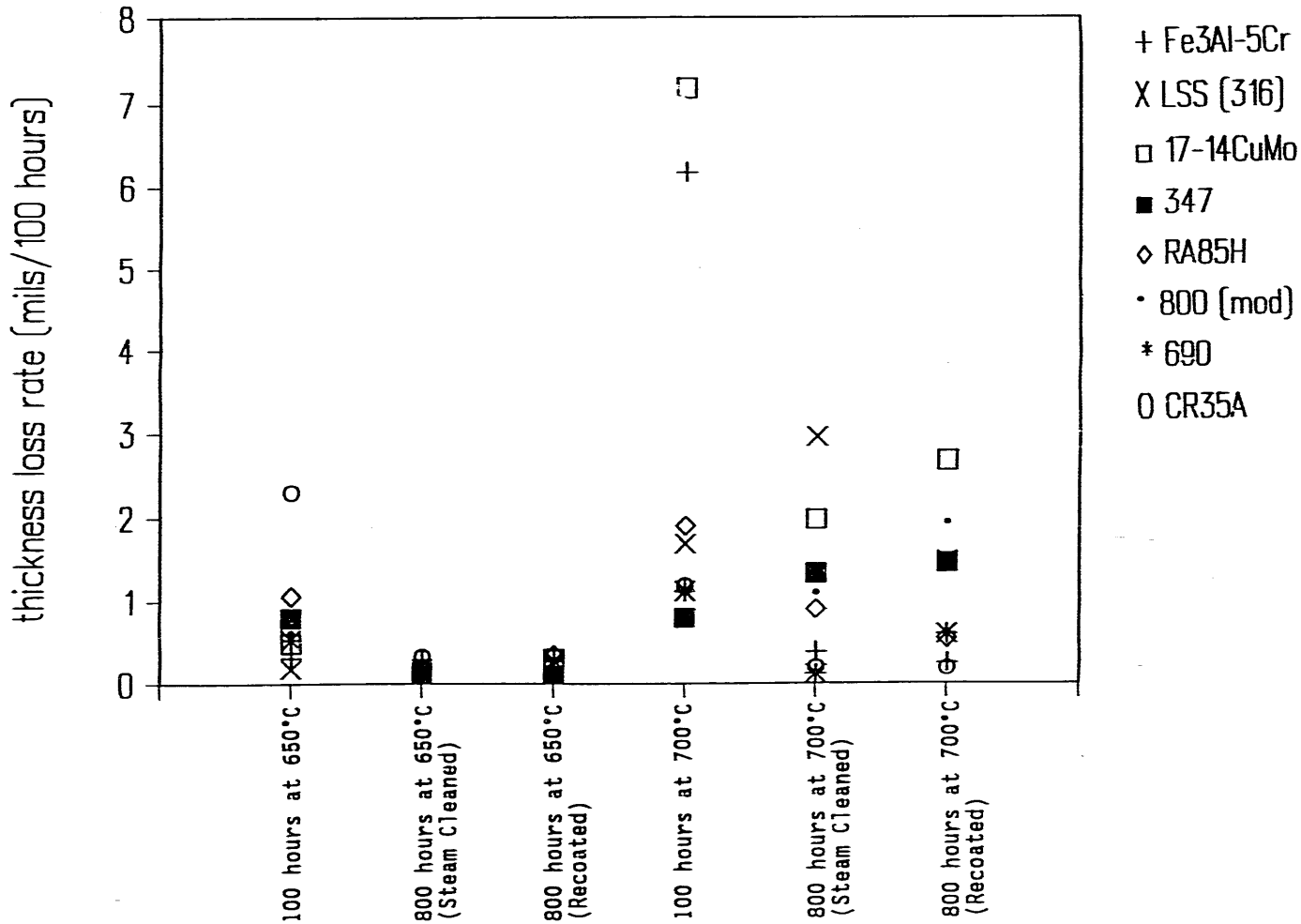

Figure 4.24 Summary of Average Thickness Loss Rates for Representative Alloys Coated With Ash Containing 10 wt% Alkali Sulfates and Exposed to Flue Gas Containing 0.25 vol% SO_2

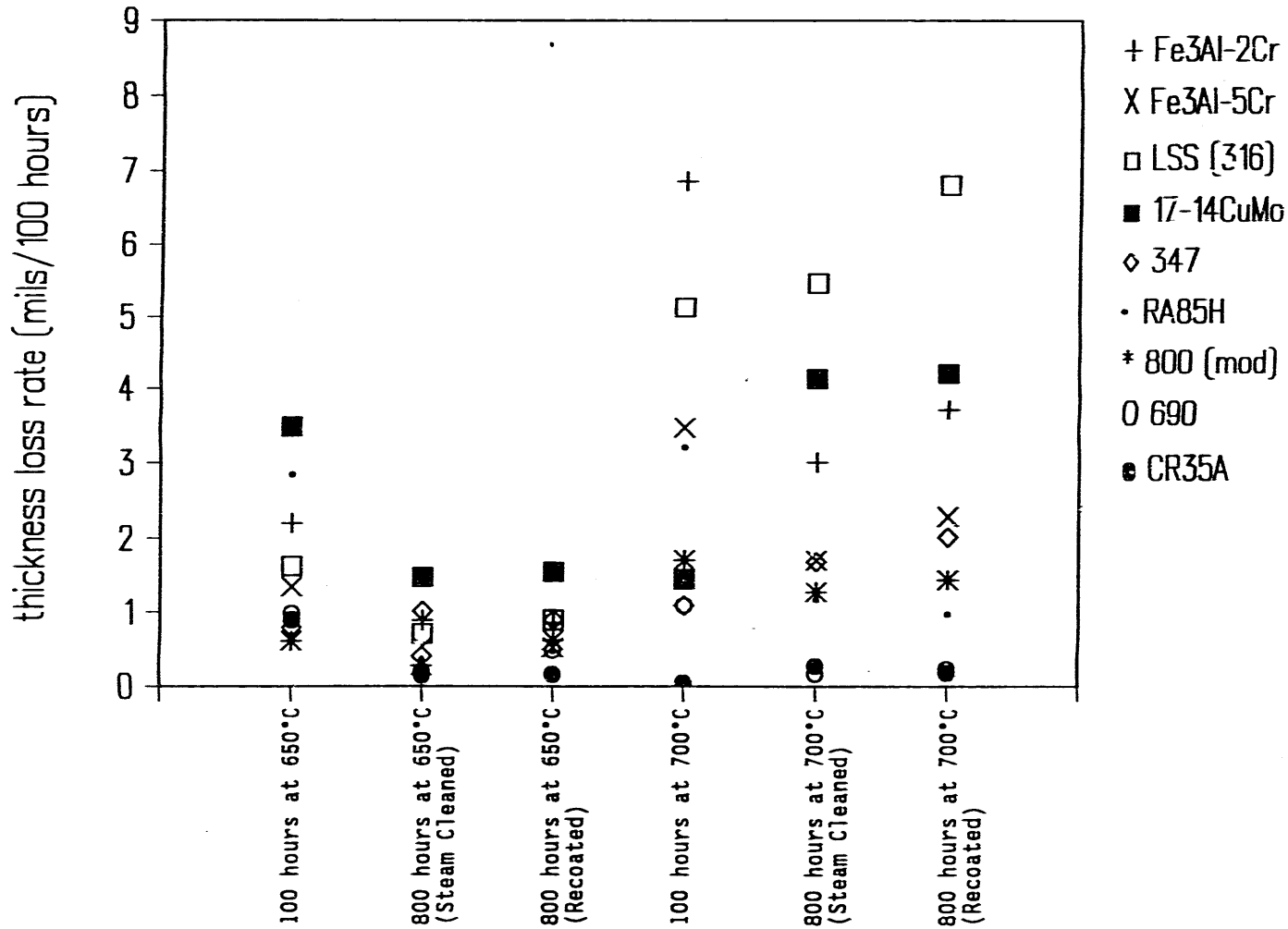

Figure 4.25 Summary of Average Thickness Loss Rates for Representative Alloys Coated With Ash Containing 10 wt% Alkali Sulfates and Exposed to Flue Gas Containing 1.0 vol% SO_2

4.6 MACROSCOPIC EXAMINATION OF EXPOSED SPECIMENS

Photomacrographs of selected specimens are shown in Figure 4.26. These specimens exhibit the range of corrosion morphologies found during testing. The severity of attack on these coupons ranges from surface blemishes and discoloration, through isolated pits and patches of corrosion, to uniform wastage. A complete photographic record of exposed specimens is presented in Appendix A. The specimens coated with an ash comprising of 75 wt% sulfates and exposed to a flue gas containing 0.25 vol% SO_2 displayed the following corrosion morphologies:

- The modified Type 316 specimen exhibited uniform wastage over its entire surface; small scalloped depressions gave the surface a pebbled appearance.
- The 690 specimen suffered deep, trench-like pits between sections completely free from corrosion. The trenches appeared to be made of numerous small, interlocked pits.
- Corrosion on the iron aluminide specimen left a rough mottled surface.
- The alloys containing chromium for corrosion protection primarily had a corrosion morphology consisting of regular, shallow, scalloped pits, while the aluminide specimens tended to corrode in uneven, roughened patches.

Specimens exposed to a flue gas containing 0.25 vol% SO_2 while coated with an ash containing 10 wt% alkali sulfates showed a much lesser degree of corrosion than the specimens coated with a 75 wt% alkali sulfate ash. In this rather mild environment, all specimens exhibited surface blemishes and isolated pits only. Increasing the SO_2 in the flue gas from 0.25 to 1.0 vol%, while keeping a coal ash containing 10 wt% alkali sulfates, moderately increased the wastage rates of the specimens. In each case the corrosion morphologies found are similar to those caused by exposure to a flue gas containing 0.25 vol% SO_2 while coated with an ash containing 75 wt% alkali sulfates.

- The 690 specimen showed a heavy blemish and the beginnings of the trench-like pitting morphology found in the specimen exposed to a coal ash containing 75 wt% alkali sulfates.
- The modified Type 316 specimen suffered uniform corrosion.
- The iron aluminide showed a slightly roughened surface.

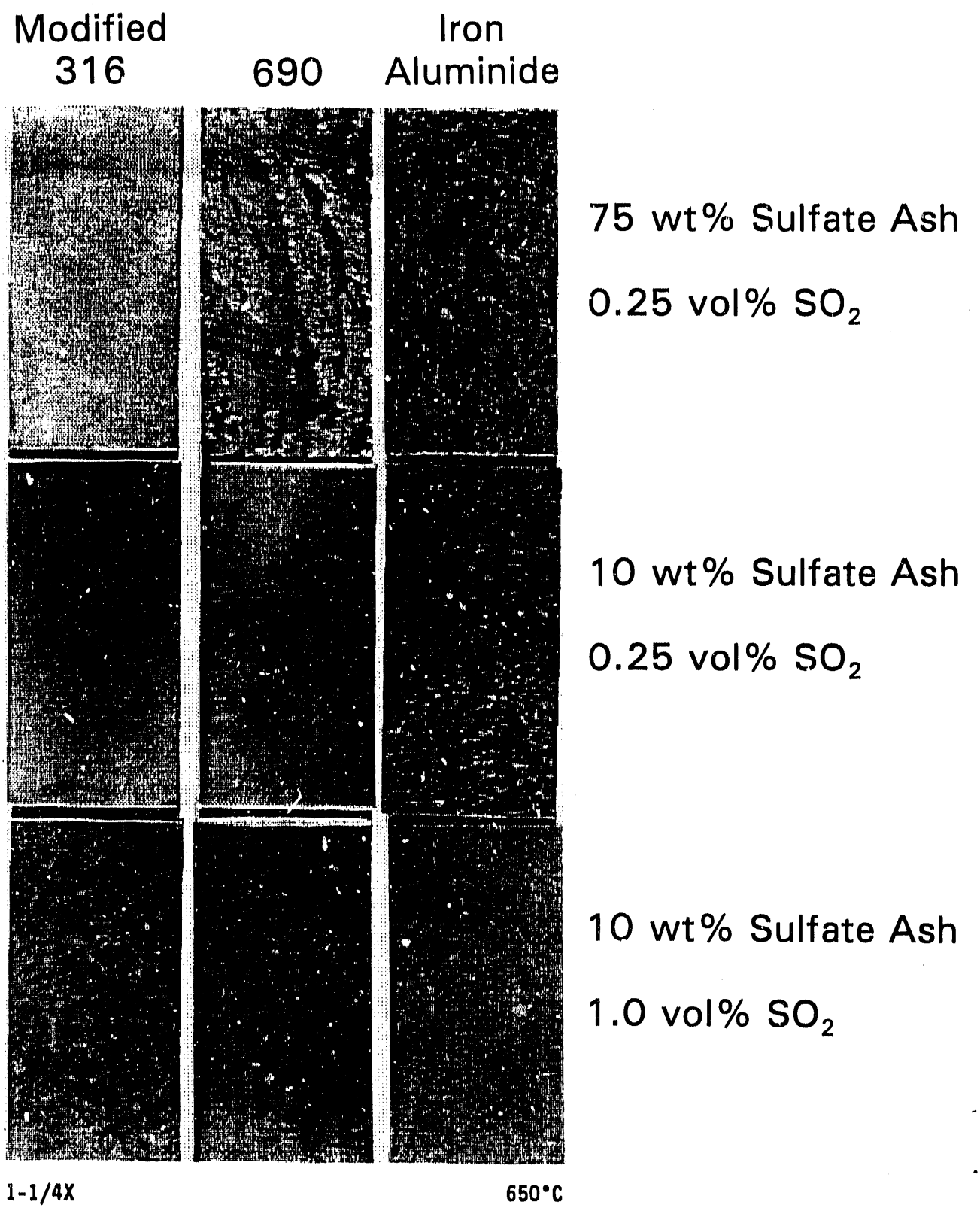

Figure 4.26 Representative Specimens After Exposure to Various Environments

4.7 MICROSCOPIC ANALYSIS OF COUPONS AND CORROSION PRODUCTS

After exposure, the morphology of selected coupons and samples of ash and scale were examined using optical and electron microscopy. The chemical composition of various samples was also evaluated by an electron microscope equipped with a energy dispersive x-ray analysis unit. This unit allowed qualitative chemical determination of elements with an atomic weight ≥ 11 (the atomic weight of sodium).

Representative photographs, SEM images, and x-ray maps of the corroded specimens are presented in Figures 4.27 through 4.43. Specimens displayed in Figures 4.27 through 4.30, 4.32, and 4.33 were not cleaned after exposure. These specimens were coated with a 10 wt% alkali sulfate coal ash and exposed to flue gas containing 1.0 vol% SO_2 at 700°C for 200 hours. A 690 specimen exposed for 800 hours to this same environment is shown in Figures 4.34 and 4.35. Figures 4.27 and 4.28 show an iron aluminide alloyed with 2 wt% chromium. This alloy was exposed to flue gas containing 0.25 vol% SO_2 at 700°C for 200 hours while coated with an ash containing 75 wt% alkali sulfates. Finally (for comparison), Figures 4.39 and 4.40 show a sample of Type 310 Nb exposed for 16,000 hours in a PC-fired boiler.

A section through a corroded 17-14 CuMo coupon at 700°C is shown in Figures 4.27 and 4.28. The corroding surface in Figure 4.27 shows a smooth interface between metal and ash, with no indications of subsurface enrichment, intergranular attack, or the formation of subsurface sulfides and oxides. To confirm this, the maps of chemical concentration in Figure 4.28 do not show any depletion or enrichment of the primary alloying elements or any subsurface concentrations of sulfur. An interesting feature of the ash is the regions of

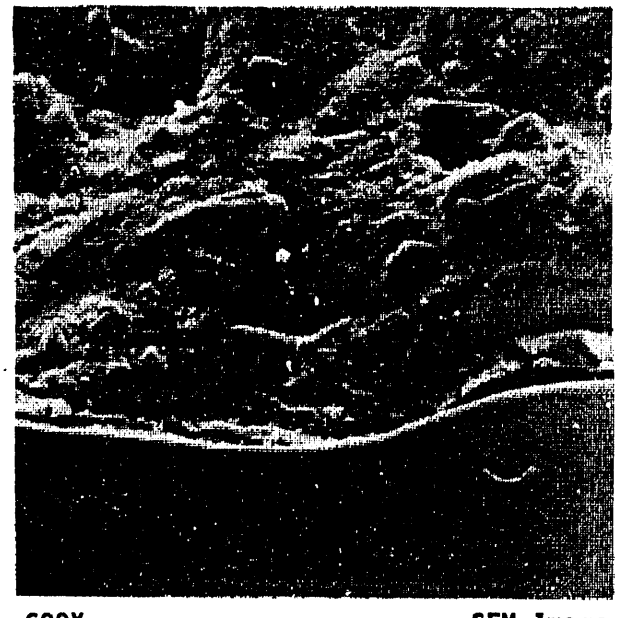

600X SEM Image

Figure 4.27 Corroded Surface of a 17-14 CuMo Specimen Coated With Ash Containing 10 wt% Alkali Sulfates After Exposure for 200 Hours at 700°C to Flue Gas Containing 1.0 vol% SO_2. (Top area of image shows ash coating; bottom area is specimen.)

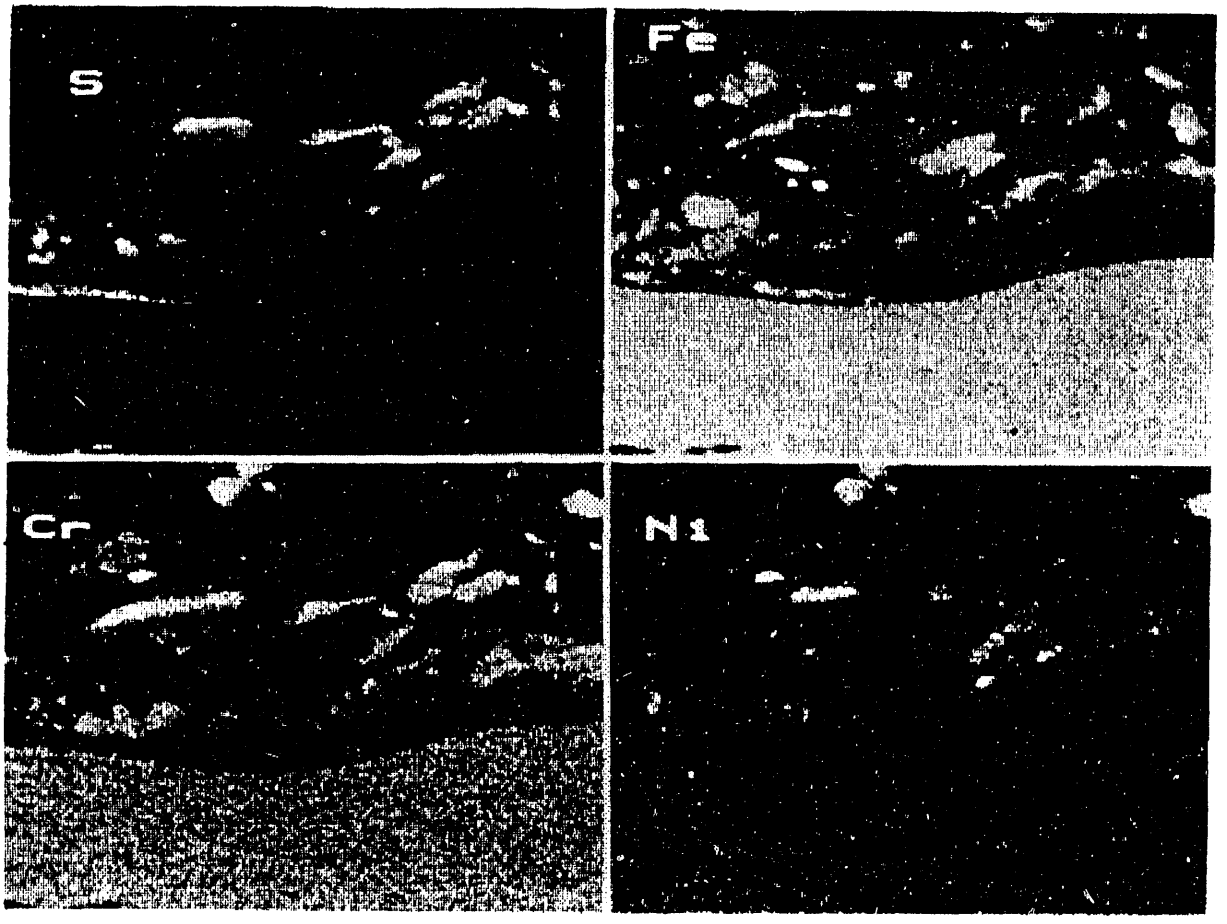

600X

Relative Concentration of Element

Figure 4.28 X-Ray Map of Corroded Surface of 17-14 CuMo Specimen Coated With Ash Containing 10 wt% Alkali Sulfates After Exposure for 200 Hours at 700°C to Flue Gas Containing 1.0 vol% SO_2

high sulfur and either high nickel or high chromium. These may be pockets of chromium and nickel sulfide which have precipitated in the ash layer. The chromium level in this alloy was apparently too low to form a protective barrier against molten AIT attack, and the alloy was simply fluxed away with no subsurface interactions. Examination of specimens exposed for 800 hours did not show any significant differences in microstructure from the specimen just described, supporting the hypothesis that this alloy did not contain enough chromium to passivate.

Figures 4.29 and 4.30 show a cross-section of RA85H coated with ash after exposure for 200 hours at 700°C. As shown in Figure 4.29, the corroded surface is jagged, with intergranular attack and subsurface penetration taking place. Chromium appears to have been depleted from the alloy to form a chromium-rich layer along grain boundaries and at the interface, where it formed sulfides and oxides. Near the interface, where chromium depletion has taken place, nickel has been selectively enriched. In several locations high concentrations of nickel and sulfur together would seem to indicate the formation of nickel sulfides. The high concentration of sulfur at the interface, combined with areas that seem to be chromium and nickel sulfides, raises the possibility that an oxidation-sulfidation reactions are taking place in addition to fluxing by molten AIT. The iron in this alloy is removed by transport across the chromium- and sulfur-rich zone into the ash. Figure 4.31 displays an RA85H specimen which has been exposed for 800 hours at 700°C. Intergranular attack has taken place to a point where grains are beginning to fall out.

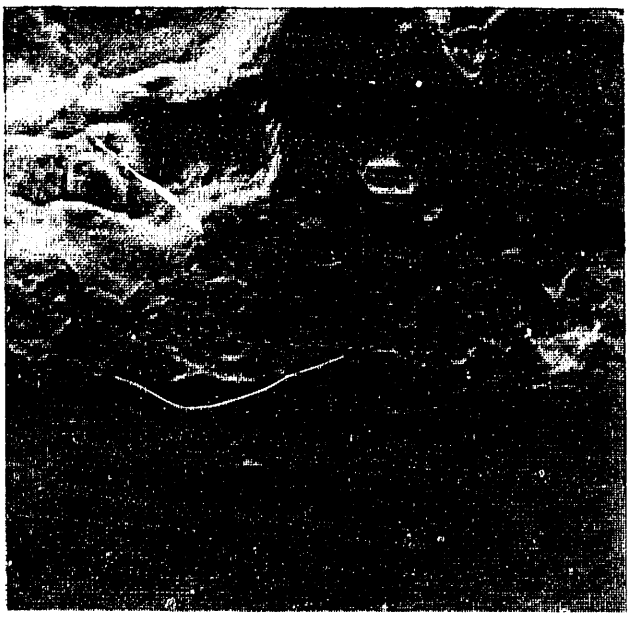

600X SEM Image

Figure 4.29 Corroded Surface of RA85H Specimen Coated With Ash Containing 10 wt% Alkali Sulfates After Exposure for 200 Hours at 700°C to Flue Gas Containing 1.0 vol% SO_2. (Top area of image shows ash coating; bottom area is specimen.)

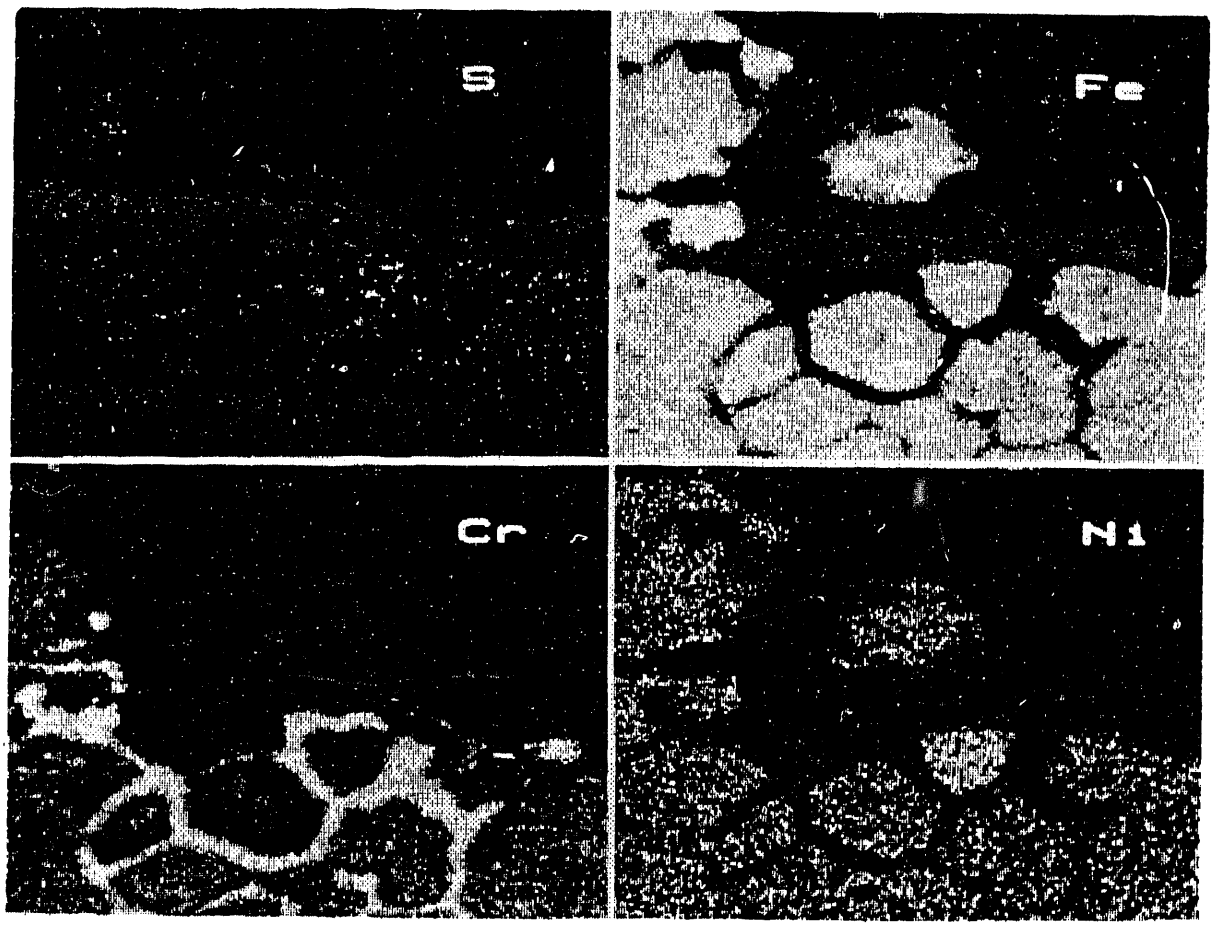

600X

Relative Concentration of Element

Figure 4.30 X-Ray Map of Corroded Surface of RA85H Specimen Coated With Ash Containing 10 wt% Alkali Sulfates After Exposure for 200 Hours at 700°C to Flue Gas Containing 1.0 vol% SO_2

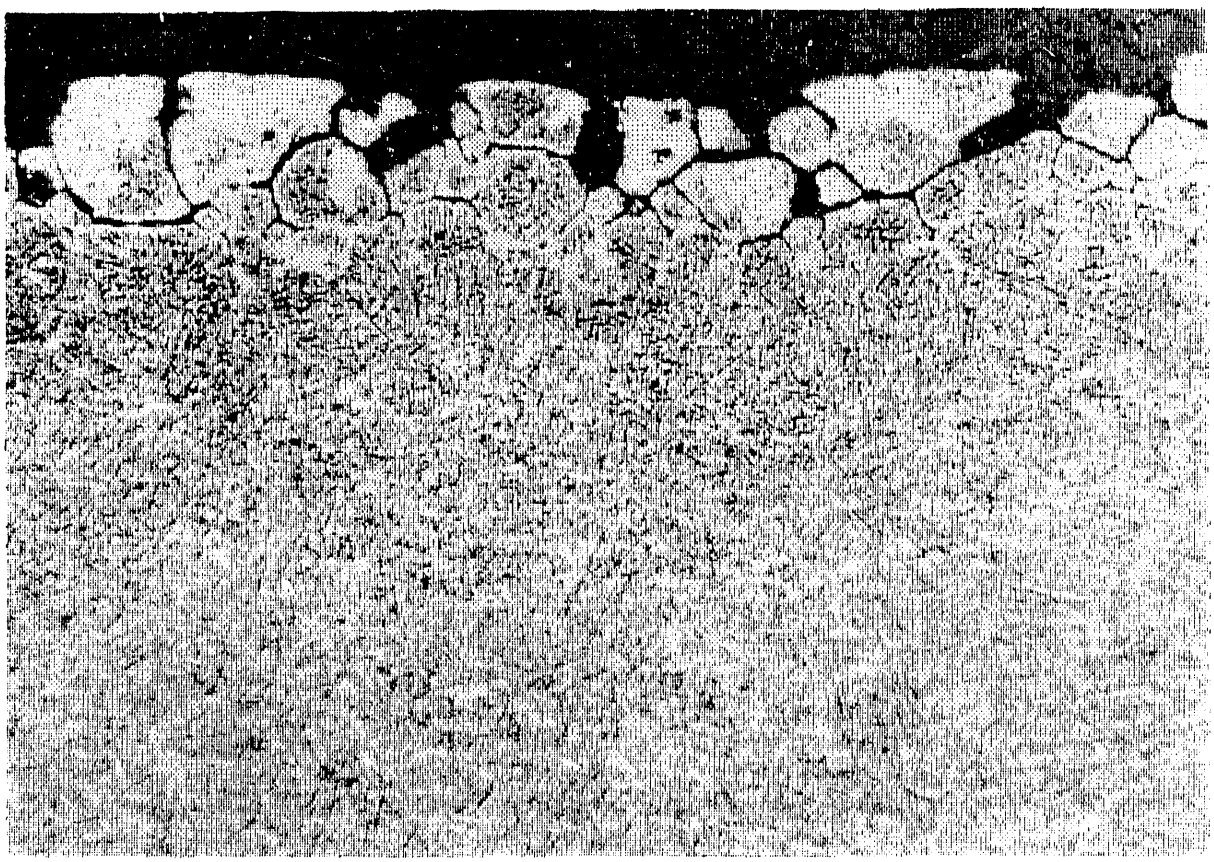

500X Oxalic Acid Etch

Figure 4.31 Corroded Surface of RA85H Specimen Coated With Ash Containing 10 wt% Alkali Sulfates After Exposure for 800 Hours at 700°C to Flue Gas Containing 1.0 vol% SO_2. (Note intergranular attack on specimen surface.)

A section through a corroding CR35A coupon exposed at 700°C for 200 hours is displayed in Figures 4.32 and 4.33. As Figure 4.32 shows, the metal surface is untouched except for one small blemish. The blemish seems to be enriched in chromium and sulfur in sections, while depleted in chromium in other sections. One explanation for this morphology is that the blemish was formed by chromium sulfidation. In areas of high oxygen activity, the sulfides were oxidized, recycling the sulfur into SO_2 and SO_3. Around and atop the blemish, chromium has depleted from the alloy to form a thin, dense layer. An iron-rich band has formed above this layer, and a small quantity of chromium has diffused into it.

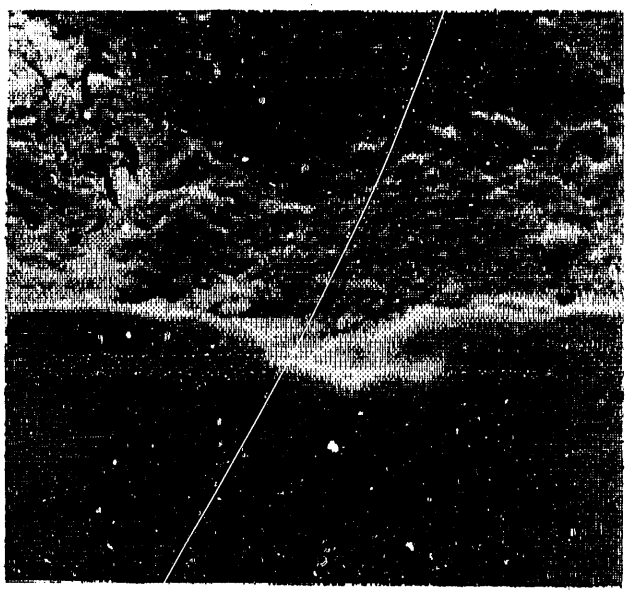

1200X SEM Image

Figure 4.32 Corroded Surface of CR35A Specimen Coated With Ash Containing 10 wt% Alkali Sulfates After Exposure for 200 Hours at 700°C to Flue Gas Containing 1.0 vol% SO_2. (Note beginning of pit in middle of photograph.)

The corroded surface of a monolithic 690 specimen after exposure at 700°C is shown in Figures 4.34 and 4.35, with an accompanying x-ray map of chemical composition shown in Figure 4.36. This specimen has been exposed for 800 hours, rather than the 200 hours of exposure for the previously shown specimens. As illustrated in both the optical photomicrograph and SEM image, the specimen is being attacked by a sulfidation and oxidation front moving down from the surface, depleting the surface metal of chromium. This depletion destroys the passive chromium oxide scale and allows AIT attack to occur. The attack morphology seen on this specimen could be the same form of attack seen on the CR35A specimen shown in Figures 4.32 and 4.33. This form of attack is only noticeable in higher-alloy specimens exposed for longer than 100 hours.

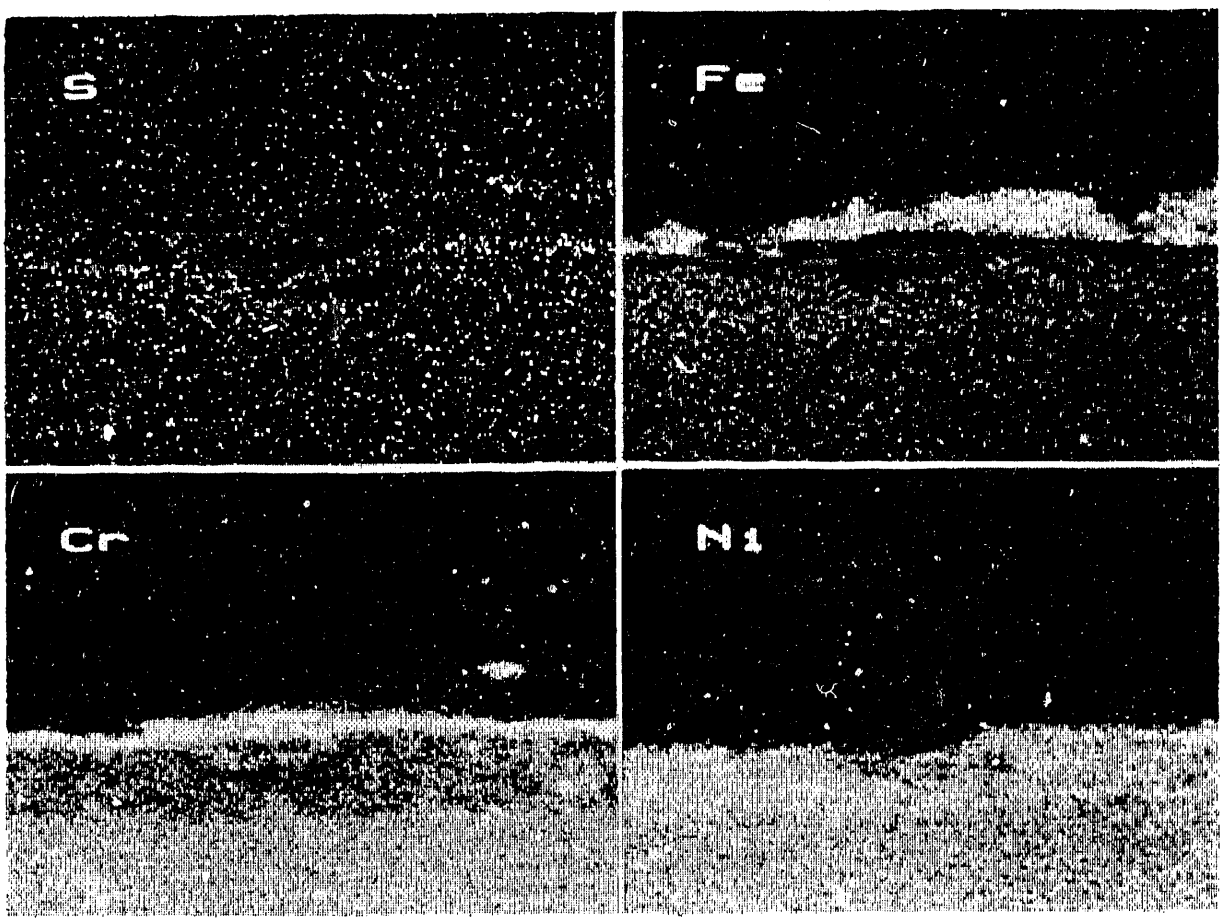

1200X

Relative Concentration of Element

Figure 4.33 X-Ray Map of Corroded Surface of CR35A Specimen Coated With Ash Containing 10 wt% Alkali Sulfates After Exposure for 200 Hours at 700°C to Flue Gas Containing 1.0 vol% SO_2

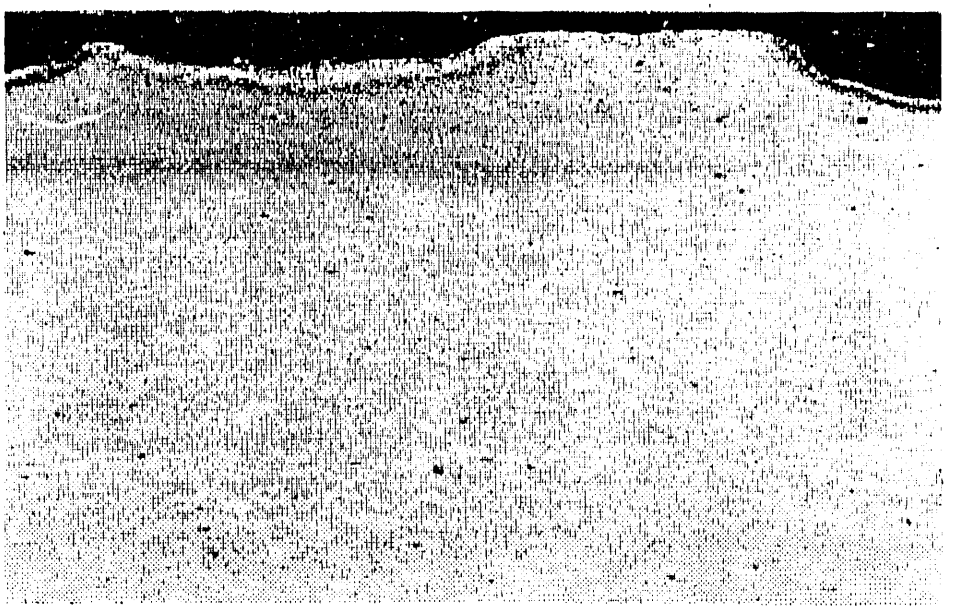

100X Oxalic Acid Etch

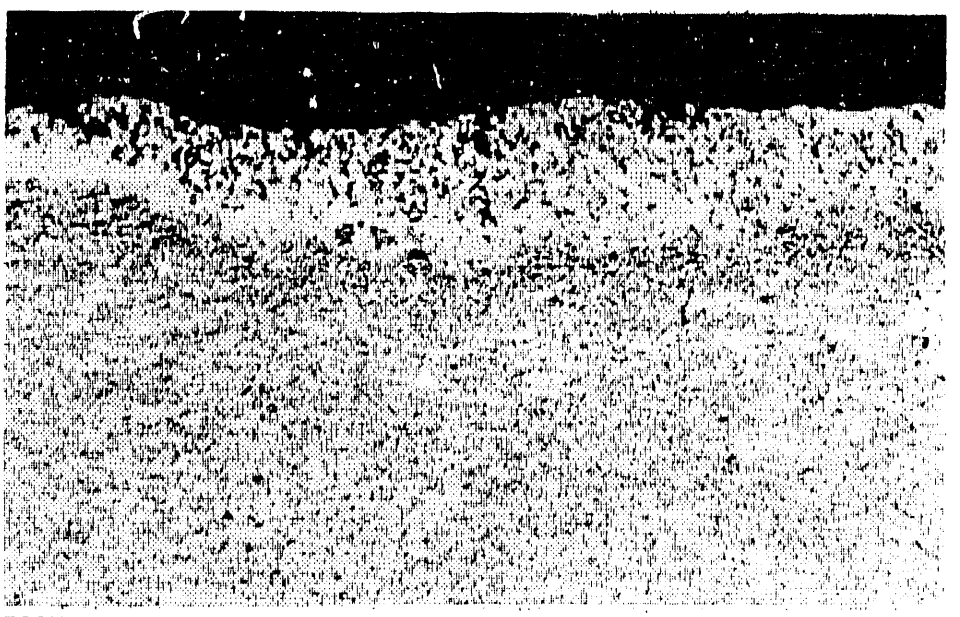

500X Oxalic Acid Etch

Figure 4.34 Corroded Surface of 690 Specimen Coated With Ash Containing 10 wt% Alkali Sulfates After Exposure for 800 Hours at 700°C to Flue Gas Containing 1.0 vol% SO_2. (Note chromium depletion and oxidation/sulfidation on specimen surface.)

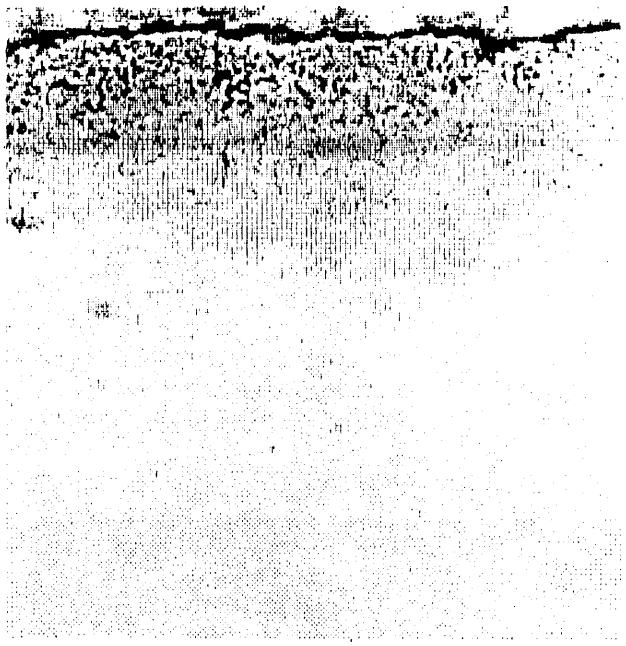

600X SEM Image

Figure 4.35 Corroded Surface of 690 Specimen Coated With Ash Containing 10 wt% Alkali Sulfates After Exposure for 200 Hours at 700°C to Flue Gas Containing 1.0 vol% SO_2. (Note chromium depletion and oxidation/sulfidation on specimen surface.)

A pit in iron aluminide, filled with corrosion products, is shown in Figure 4.37, with an accompanying x-ray map of the metal and deposit shown in Figure 4.38. The deposit appears to have a lamellar structure, with a thin layer containing a high concentration of sulfur, and a iron-rich region as the outermost layer. There appears to be no depletion in the alloy itself, in contrast to the stainless steels and nickel-based alloys. Rather, the corrosion front appears to be a sharp demarcation between corroded material and sound alloy.

For comparison with the laboratory specimens, an Alloy 310 Nb tube, which was exposed for 16,000 hours at the Tennessee Valley Authority's Gallatin Station, is shown in Figures 4.39 and 4.40 [5]. The corrosive attack on this specimen is fully developed and may be assumed to have reached steady state conditions. As illustrated in Figure 4.40, four attack mechanisms are occurring: chromium has been depleted from the area around the grain boundaries, subsurface metal has been depleted of chromium and enriched in nickel, chromium sulfides have formed in the subsurface metal, and AIT attack has occurred. All of these attack mechanisms are found on various specimens exposed during laboratory testing, indicating that exposures conducted under laboratory conditions provide similar conditions to those found in operating utility boilers.

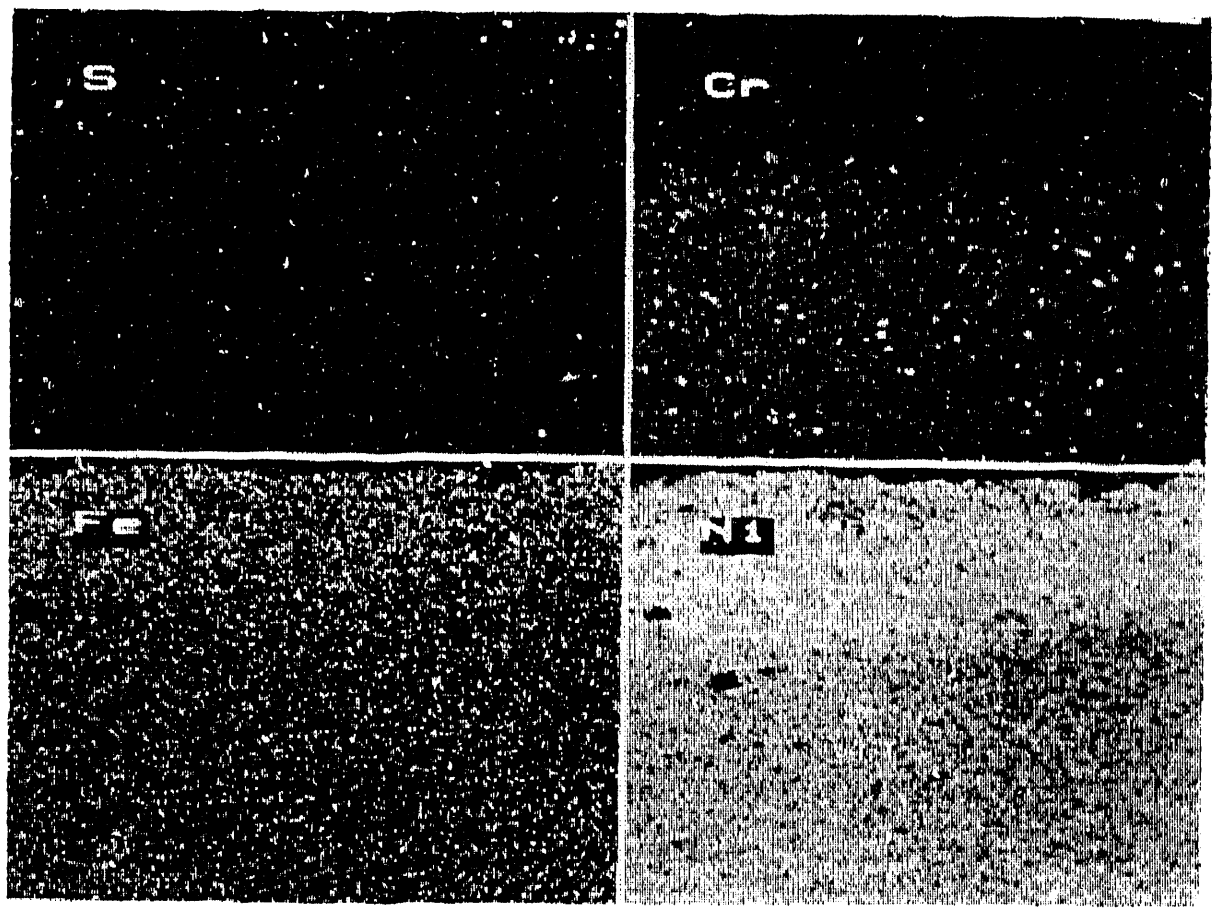

600X

Relative Concentration of Element

Figure 4.36 X-Ray Map of Corroded Surface of 690 Specimen Coated With Ash Containing 10 wt% Alkali Sulfates After Exposure for 200 Hours at 700°C to Flue Gas Containing 1.0 vol% SO_2

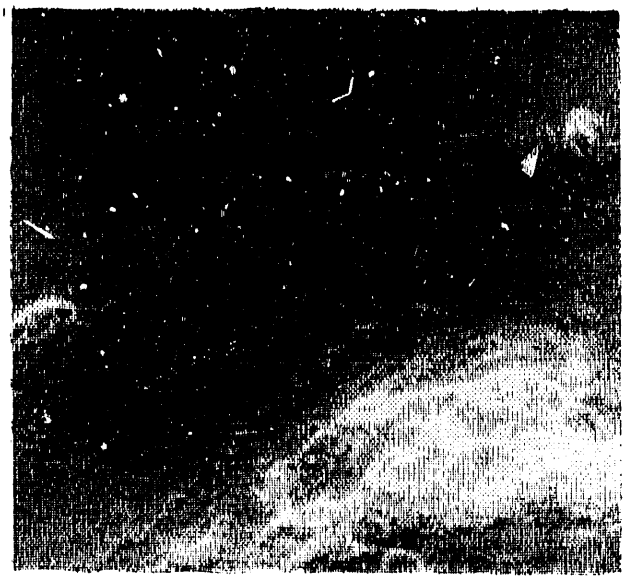

600X SEM Image

Figure 4.37 Corroded Surface of Iron Aluminide Specimen Containing 2% Chromium Chromium Coated With Ash Containing 10 wt% Alkali Sulfates After Exposure for 200 Hours at 700°C to Flue Gas Containing 1.0 vol% SO_2. (Note pit growing from specimen surface at bottom of photograph.)

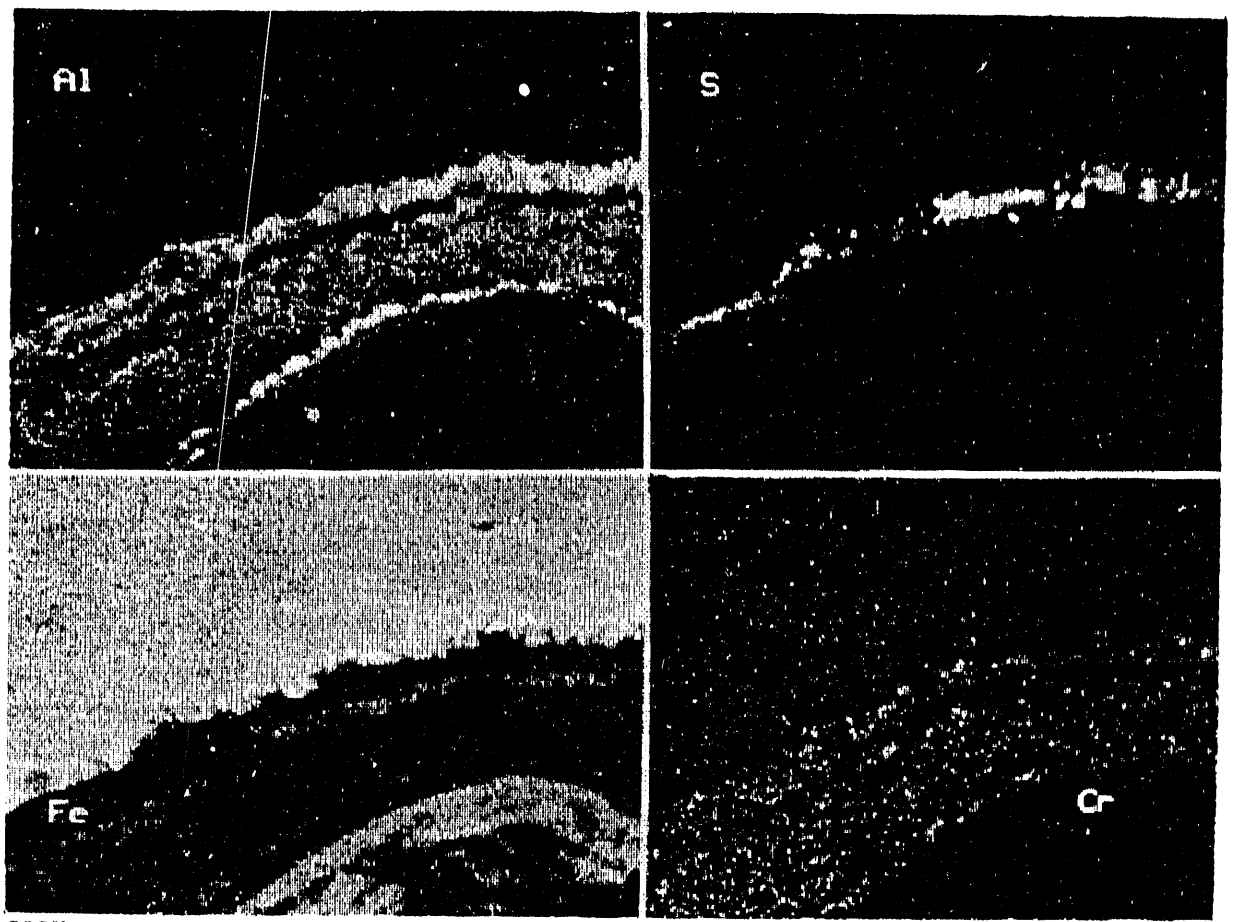

Figure 4.38 X-Ray Map of Corroded Surface of Iron Aluminide Specimen Containing 2% Chromium Coated With An Ash Containing 10 wt% Alkali Sulfates After Exposure for 200 Hours at 700°C to Flue Gas Containing 1.0 vol% SO_2

500X Unetched

Figure 4.39 Corroded Surface of 310 Nb Specimen After Exposure in Pulverized-Coal-Fired Boiler for 16,000 Hours. (Note general sulfidation/oxidation below layer of scale.)

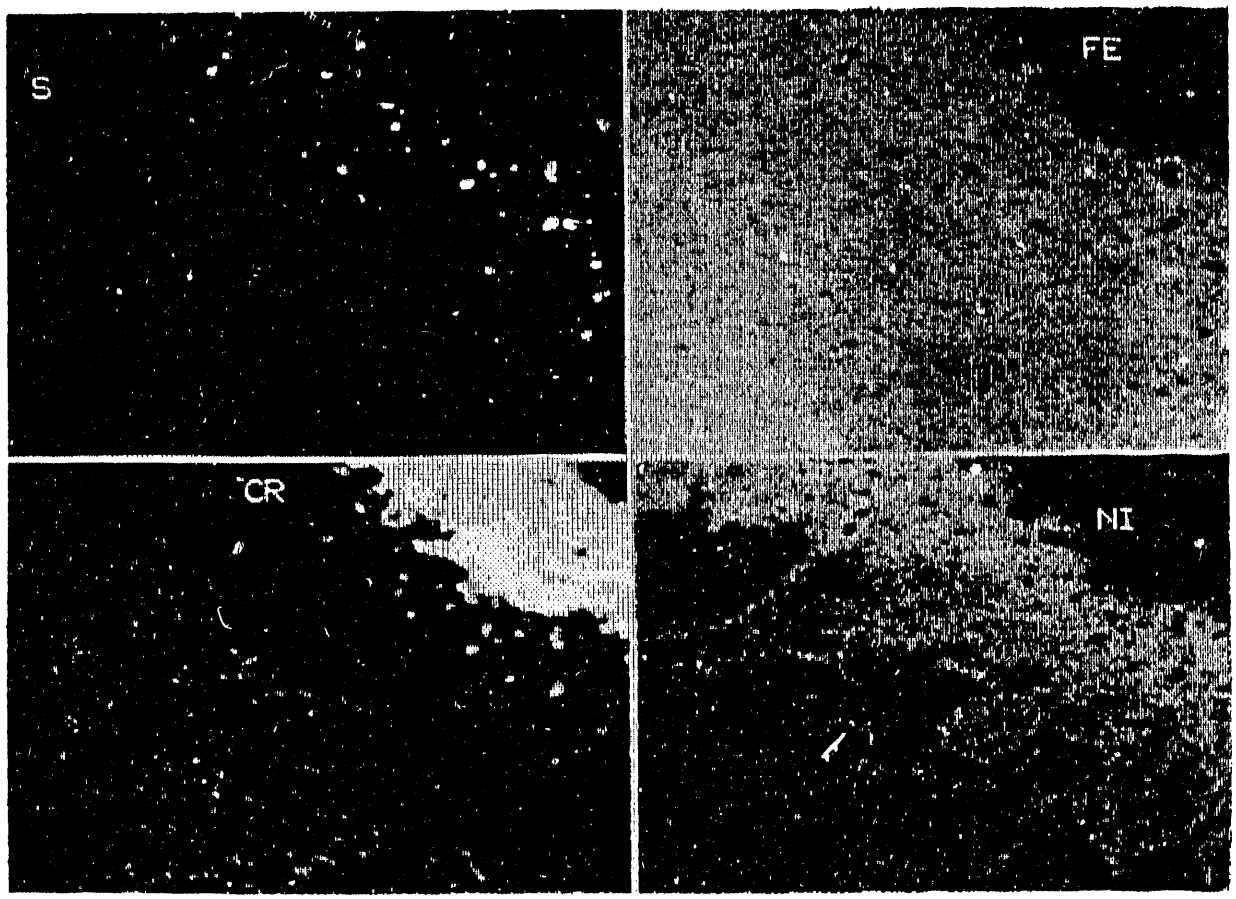

600X

Relative Concentration of Element

Figure 4.40 X-Ray Map of Corroded Surface of 310 Nb Specimen After Exposure for 16,000 Hours in Pulverized-Coal-Fired Boiler

4.8 ANALYSIS OF CLAD COUPONS

Comparing the corrosion morphologies described above, several trends become evident. Alloys with little intrinsic resistance to AIT attack, or alloys exposed to highly aggressive environments, do not show subsurface chromium depletion. Alloys that were resistant to attack and were exposed to moderately aggressive environments suffered subsurface chromium depletion below the attacked areas. Alloy 310 Nb, which was exposed in an operating utility boiler, also exhibited subsurface chromium depletion, indicating that this is not the result of the experiment. Intergranular attack also occurs to varying degrees along with generalized subsurface attack on the more highly resistant alloys. A fully developed example of this attack can be seen on Alloy 310 Nb, which has been exposed for 16,000 hours.

The unexpectedly high rate of corrosion in the modified Alloy 316 specimen clad with Alloy 690 may have been the result of the coalescence of chromium compounds at the grain boundaries, leading to intergranular attack. Figure 4.41 shows patches of grains falling from the specimen surface. What appears to be chromium carbides are "decorating" the grain boundaries. In addition to intergranular attack, oxidation/sulfidation and AIT attack are occurring on this specimen. Figure 4.42 shows a patch of this form of corrosion. A band of sulfidation and oxidation is preceding the AIT attack. Intergranular attack, generalized oxidation and sulfidation, and AIT attack may interact synergistically. If localized intergranular attack creates pitting on the surface of the specimen, a corrosion cell may form between the AIT in the pit and the AIT elsewhere, greatly enhancing corrosion rates in the pit.

The specimen of Alloy 800 clad with Alloy 72 (Figure 4.43) suffered a higher-than-expected rate of attack because of the presence of the Alloy 800H base material, which was not completely machined from the surface. The fusion line between the base metal on the top and the cladding on the bottom is clearly visible in the photograph.

500X Oxalic Acid Etch

Figure 4.41 Intergranular Attack on Corroded Surface of 690 Cladding/Type 316 Base Metal Coated With 10 wt% Alkali Sulfates After Exposure for 800 Hours at 700°C to 0.25 vol% SO_2

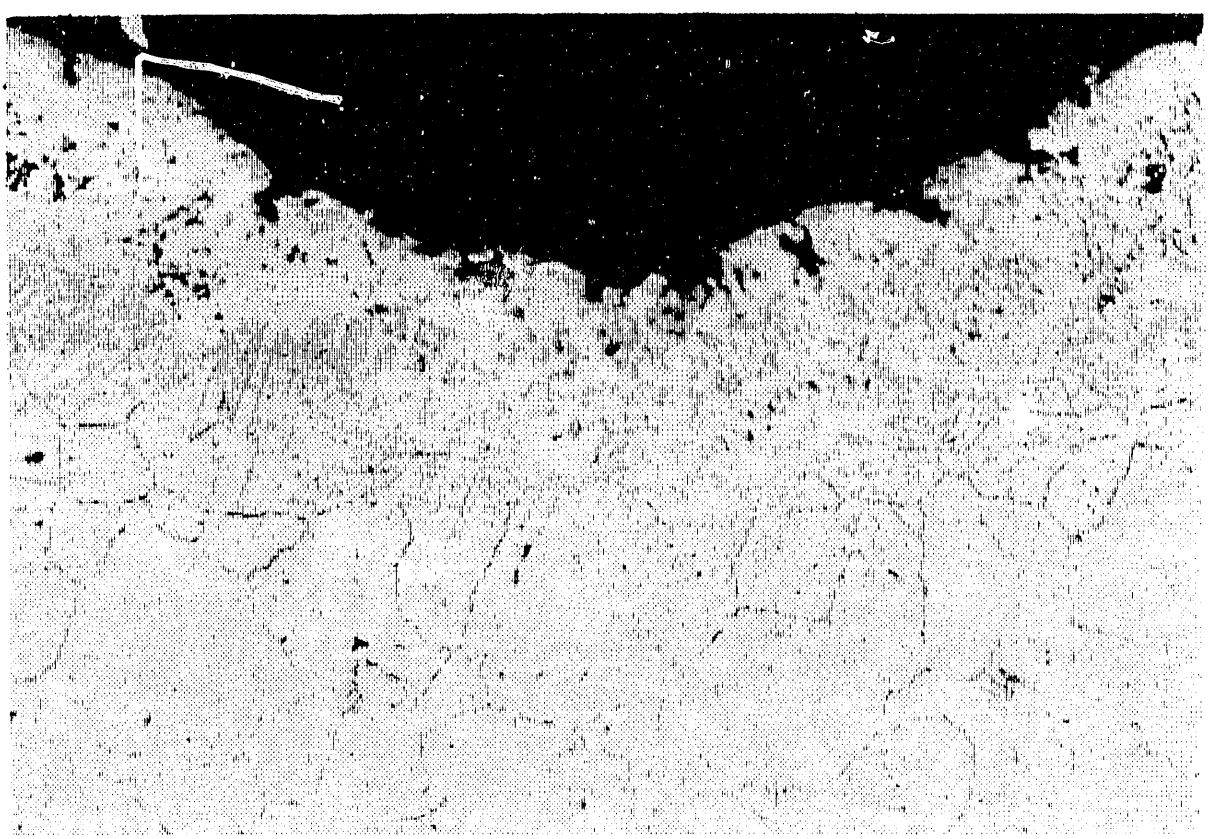

500X

Oxalic Acid Etch

Figure 4.42 Chromium Depletion and General Sulfidation/Oxidation Below Layer of Scale on Corroded Surface of 690 Cladding/Type 316 Base Metal Coated With 10 wt% Alkali Sulfates After Exposure for 800 Hours at 700°C to 0.25 vol% SO_2

100X Nital Etch

500X Nital Etch

Figure 4.43 Corroded Surface of 72 Weld Wire Deposited on Incoloy 800 Base Metal Coated With 10 wt% Alkali Sulfates After Exposure for 800 Hours at 700°C to 0.25 vol% SO_2. (Note thin layer of 800 on top of welded overlay.)

Section 5

DETERMINATION OF OBSERVED WASTAGE MECHANISMS

Since the 1970s, the prevailing theory regarding AIT attack has been the molten fluxing model. Articles by Stringer [6], Rapp [7], Hendry and Lees [8], and others cover this model in detail, so only a brief review will be given here. Above approximately 550 to 600°C, SO_3 reacts with Fe_2O_3 and $Na_2(SO_4)$ or $K_2(SO_4)$ to form molten AIT. This molten species is believed to promote metal wastage by fluxing the protective oxide scale from the metal surface. Degradation of the oxide film most likely occurs by an electrochemical mechanism, which may have broadly separated anodic and cathodic regions. Above approximately 725°C, ferric sulfate in the melt becomes unstable at nominal SO_3 pressures, and the AIT decomposes back into iron oxide and alkali sulfates.

5.1 POSSIBLE MECHANISMS OF MOLTEN AIT ATTACK ON IRON- OR NICKEL-BASED ALLOYS

Corrosion morphologies on iron- or nickel-based specimens attacked by AITs can be divided into two general categories: general attack and pitting. Since hot corrosion is an electrochemical phenomenon, one would expect to find many similarities between what is occurring in molten trisulfate films and the more familiar room-temperature aqueous corrosion. General attack occurs in aqueous corrosion when the metal being corroded develops little or no passivity. Similarly, general attack by molten AIT occurred on the lower-chromium stainless steels exposed to high concentrations of sulfate or SO_2. No passive layer of chromia could form under these harsh conditions; consequently, generalized attack resulted. In many cases, although the entire specimen was attacked, there were irregularities. Shallow, scalloped pits and depressions were common features on the attacked surface. These pits and depressions might have been caused by local electrochemical cells set up on the surface. The cells, in turn, may have been caused by local differences in SO_2 concentration or variations in the underlying metal.

In less-aggressive environments, molten trisulfate attack on moderate- to high-chromium alloys resulted in localized pitting rather than generalized attack over the entire surface. Pitting and crevice corrosion occur in alloys as a result of local breakdowns of passivity. Once local passivity is destroyed, an electrochemical corrosion cell may form, promoting further attack within the pit while cathodically protecting the surrounding area.

One mechanism for pitting attack in molten trisulfate could be as follows: At a given temperature, a minimum level of SO_2 is needed in the flue gas to convert the alkali sulfates and iron oxide in the ash into molten AITs. When the ash layer is laid down, either in the laboratory or from burning coal in a boiler, the ash layer will not be completely uniform. Gases diffuse to the metal surface more readily in areas where the ash layer is thinner than usual, or regions near the edge of the ash layer. The different levels of SO_2 concentration under the ash layer cause molten AITs to form at different rates. Different levels of SO_2 might also lead to different aggressiveness of the molten trisulfates. Once the molten trisulfate degrades the passive layer locally, an electrochemical corrosion cell can form (with the incompletely protected metal in the pit forming an anodic region), cathodically protecting

the area surrounding the pit. Active areas could also protect the rest of the metal surface by acting as a sink for reactants. The reaction products are oxides and sulfides of iron, nickel, and chromium; as the reaction proceeds, oxygen and sulfur are depleted from the melt surrounding the pit. This oxygen and sulfur depletion creates a diffusion gradient toward the already-active areas and away from the passive areas, helping them remain passive.

5.2 SUBSURFACE EFFECTS DURING MOLTEN AIT ATTACK

AIT corrosion on resistant alloys was often accompanied by subsurface attack on the alloy, taking the form of intergranular attack, subsurface penetration of sulfides and oxides, or selective depletion of elements from the alloy. Intergranular attack and subsurface penetration can be attributed to an oxidation/sulfidation mechanism, while selective depletion can be understood if a mass balance for elements consumed in sulfidation and oxidation is considered. Possible mechanisms for these attack modes have been discussed in the literature [9].

Both intergranular attack and the formation of subsurface oxides and sulfides can be explained by the migration of sulfur and oxygen through a thin passive layer. The sulfur concentration necessary to sustain a molten sulfate layer could be expected to provide high enough activity to drive sulfur through a thin film of chromia. Once in the metal, the sulfur combines with chromium and other sulfide formers. Depending upon the alloys microstructure, in particular whether the alloy is in a sensitized condition, sulfidation may occur--either as uniform sulfide penetration or as internal sulfidation along the grain boundaries. Oxygen may also diffuse through the passive layer, producing combined oxidation/sulfidation attack.

The depletion of elements from a thin band next to the surface can be understood by considering that chromium-rich features such as a passive layer on the surface and subsurface sulfides and oxides must get chromium from somewhere--and that "somewhere" is the rest of the specimen. Because of the limited diffusivity of chromium, only a small volume of metal is available from which to draw the chromium, leading to a thin, depleted band of material underneath the chromium-rich passive layer.

5.3 MECHANISMS OF ATTACK ON INTERMETALLIC ALUMINIDES

Much of what has been discussed about iron- and nickel-based alloys also applies to intermetallic aluminides. Like stainless steels, the mechanism of attack for these alloys appears to be electrochemical in nature. X-ray mapping of corroded specimens indicates that attack occurs by the fluxing off of a passive film composed primarily of alumina. Several specimens showed evidence of intergranular attack; however, there was no indication of subsurface penetration or selective depletion of elements.

The aluminides appeared to have also suffered gas-phase attack, in addition to AIT attack. Several nickel-containing specimens suffered catastrophic corrosion, apparently the result of the gas-phase attack. One corrosion mechanism appeared to be gas-phase attack into preexisting cracks and rolling laps, causing the specimen to swell and crack further. In several cases this swelling and cracking completely destroyed nickel aluminide

specimens within 800 hours. Iron aluminides, based on Fe_3Al, showed general pitting attack, which was somewhat greater for the 2% Cr alloy than for the alloy containing 5% Cr.

5.4 HOW MATERIAL AND ENVIRONMENTAL VARIABLES AFFECT CORROSION RESISTANCE

From the background presented in the preceding two sections, we can gauge the effects that various alloying elements or changes to the environment have on the corrosion resistance of an alloy. For an alloy to be successful in a boiler environment, it must be resistant to both AIT attack and various forms of sulfidation attack. As the graph in Figure 4.1 showed, chromium is the element primarily responsible for resistance against AIT attack. This resistance is widely believed to be due to a passive layer of chromia formed on the metal surface. Other elements that appear to improve resistance to AIT attack include aluminum and silicon, both of which form stable oxides and may improve stability of the passive layer. Aluminum and silicon have also been found to improve resistance to sulfidation.

Higher concentrations of either the alkali sulfates in the ash or the SO_2 in the flue gas increased the corrosion rate. This increase was most likely the result of greater activity of the reactants in the molten trisulfate layer. Higher concentrations of SO_2 in the flue gas would be expected to increase sulfur diffusion into the metal, tying up chromium and accelerating the corrosion rate. The delayed effects of sulfidation may explain why some alloys suffered breakaway corrosion during longer exposure times. Degradation and attack may occur in high-chromium alloys by sulfidation tying up chromium, and AIT can attack the chromium-depleted layer. This mechanism would require an incubation period for the depletion of chromium from the alloy. The incubation period is determined by the rate that sulfur diffuses into the metal and combines with chromium. Sulfidation is well known to have long incubation periods, possibly lasting for thousands of hours. However, once chromium is depleted, breakaway corrosion may start. The possibility that this incubation period exists would suggest that short-term laboratory tests may be overly optimistic. Alloys that perform satisfactorily in the laboratory do not always hold up as well under service conditions.

Section 6

CONCLUSIONS AND RECOMMENDATIONS

The general nature of AIT attack is well understood, and there is a consensus on the basic mechanisms of attack. The attack rates and morphologies observed on specimens exposed to conditions simulating the superheater section of a PC-fired boiler were similar to those found by previous investigators. The attack appeared to be caused by a molten trisulfate layer forming on the metal surface. Examination of the ash layer after exposure revealed a fused band next to the metal surface, which appeared to have been molten during exposure.

In addition to the molten AIT attack, a number of specimens show evidence of subsurface sulfidation and oxidation in the form of either intergranular attack or uniform penetration. Sulfidation and oxidation occurred primarily on the more-resistant alloys exposed for 800 hours, the longest exposure time. Examination of a Type 310 Nb probe specimen taken from an operating PC-fired boiler after 2 years of exposure showed similar forms of sulfur penetration and intergranular attack, adding support that this is a operating attack mode and not the result of laboratory testing. Several specimens exhibiting sulfidation suffered breakaway corrosion at longer exposure times, indicating that sulfidation and AIT attack may be synergistic.

In the alloys evaluated, resistance to attack appeared to be determined primarily by the chromium content of the alloy. Up to 30-percent chromium appears to improve resistance to attack in these alloys. Above 30 percent, resistance does not seem to improve. Additions of silicon and aluminum also appear to be beneficial in resisting AIT attack. Molybdenum, on the other hand, may be detrimental to resistance.

While there is no complete solution to AIT attack, incremental improvements are being made. Alloys and claddings with a chromium content above 30 percent appear to have substantial resistance to attack, validating previous research. A new alloy, CR35A, had excellent resistance to attack. The claddings tested generally performed as well as the base alloy. Two cases of breakaway corrosion occurred on clad specimens; however, these were anomalies. Although further testing is needed to determine long-term suitability, both CR35A and the claddings tested appear quite promising.

Alloy RA85H may provide better resistance than alloys with similar chromium contents, such as Alloy 347. RA85H suffered less wastage than alloys containing similar chromium levels; however, intergranular attack was found on several of the RA85H specimens, possibly leading to breakaway corrosion. Although RA85H holds promise, long-term exposures are needed to determine whether breakaway corrosion will occur.

The aluminide alloys tested showed wide variance in their resistance to both molten trisulfate attack and gas-phase attack. Neither the nickel aluminide nor the iron aluminide containing 2-percent chromium held up as well as the more conventional stainless steels. The iron aluminide containing 5-percent chromium performed as well as Alloy 347. Given the low chromium content of the iron aluminides and their newness, further development of this alloy system may lead to alloys with improved molten trisulfate attack resistance.

Section 7

REFERENCES

1. I. M. Rehn, "Corrosion Problems in Coal-Fired Boiler Superheater and Reheater Tubes," EPRI CS-1653, Project 644-1, Final Report, November 1980.

2. I. M. Rehn, "Laboratory Fireside Corrosion Evaluation of Improved Superheater Tube Alloys and Coatings," EPRI CS-3134, Project 644-1, Final Report, June 1983.

3. I. M. Rehn, "Fireside Corrosion of Superheater Alloys for Advanced-Cycle Steam Plants," EPRI CS-5195, Project 1403-11, Final Report, May 1987.

4. S. Kihara, W. Wolowodiuk, K. Nakagawa, "Laboratory Coal Ash Corrosion Tests," EPRI GS-6449, Project 1403-19, Final Report, July 1989.

5. J. Blough and W. T. Bakker, "Measurement of Superheater Corrosion by Molten Alkali Sulfates," Heat-Resistant Materials, Proceedings of the First International Conference, Fontana, Wisconsin, ASM International, Materials Park, Ohio, September 1991, pp. 567-576.

6. J. Stringer, "High Temperature Corrosion Problems in the Electric Power Industry and Their Solution," High Temperature Corrosion, International Corrosion Conference Series—Volume 6, National Association of Corrosion Engineers, Houston, Texas, 1983.

7. R. A. Rapp, "Chemistry and Electrochemistry of the Hot Corrosion of Metals," Corrosion—NACE, Volume 42, Number 10, October 1986.

8. A. Hendry and D. J. Lees, "Corrosion of Austenitic Steels in Molten Sulphate Deposits," Corrosion Science, Volume 20, Permagon Press Ltd, England, 1980.

9. G. Y. Lai, High Temperature Corrosion of Engineering Alloys, ASM International, Materials Park, Ohio, 1990.

APPENDIX A

Recoated Between Exposures:

Fe_3Al-8
Fe_3Al-5Cr-27

Steam Cleaned and Recoated Between Exposures:

Fe_3Al-9
Fe_3Al-5Cr-28

Gas Content:	1.0 vol% SO_2
Temperature:	700°C
Exposure Time:	800 hours
Sulfate Content:	10 wt%

Recoated Between Exposures:

556-27
671/316-14
17-14 CuMo-14
690/316-27

Steam Cleaned and Recoated Between Exposures:

72/800H-29
72/LSS-29
347-22
690-9
690/316-28
316-23

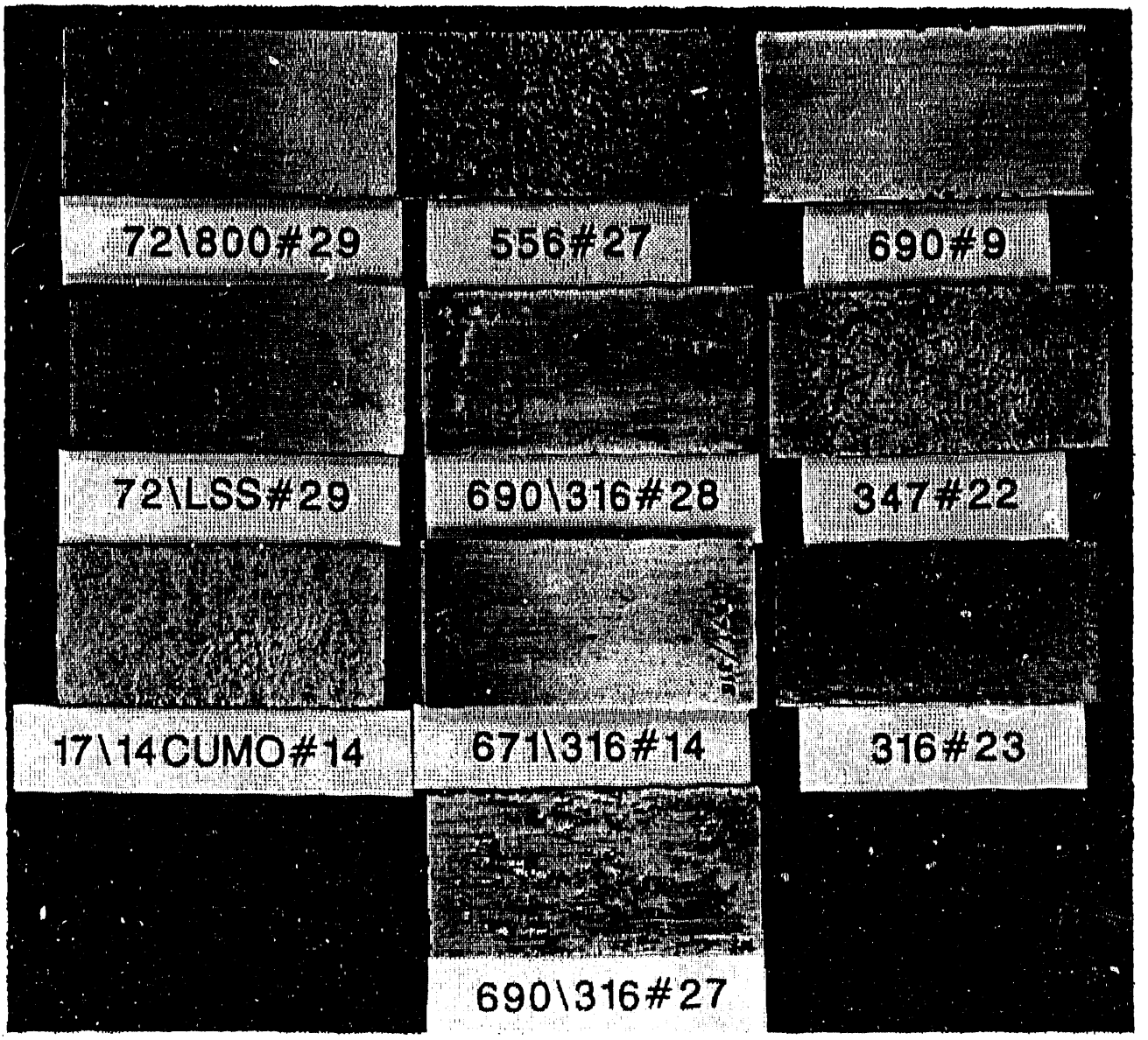

Gas Content:	1.0 vol% SO_2
Temperature:	700°C
Exposure Time:	800 hours
Sulfate Content:	10 wt%

Recoated Between Exposures:

72/800H-28
RA85H-21
800H-27
671-8
347-21
HR3C-27

Steam Cleaned and Recoated Between Exposures:

690/800H-28
556-28
CR35A-25
671/316-15
17-14 CuMo-15

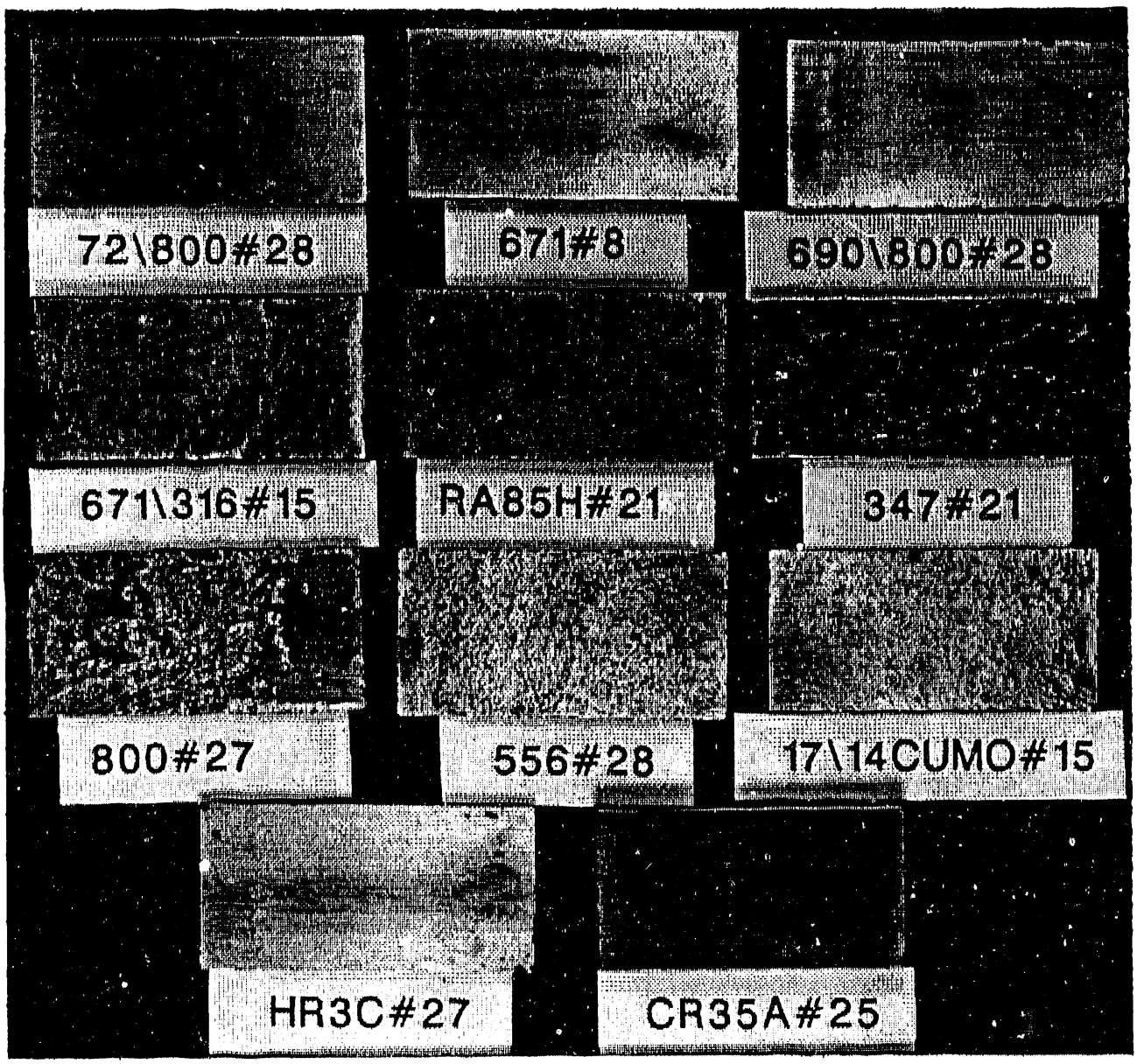

Gas Content:	1.0 vol% SO_2
Temperature:	700°C
Exposure Time:	800 hours
Sulfate Content:	10 wt%

Recoated Between Exposures:

Fe_3Al-11
Fe_3Al-5Cr-31

Steam Cleaned and Recoated Between Exposures:

Fe_3Al-12
Fe_3Al-5Cr-32

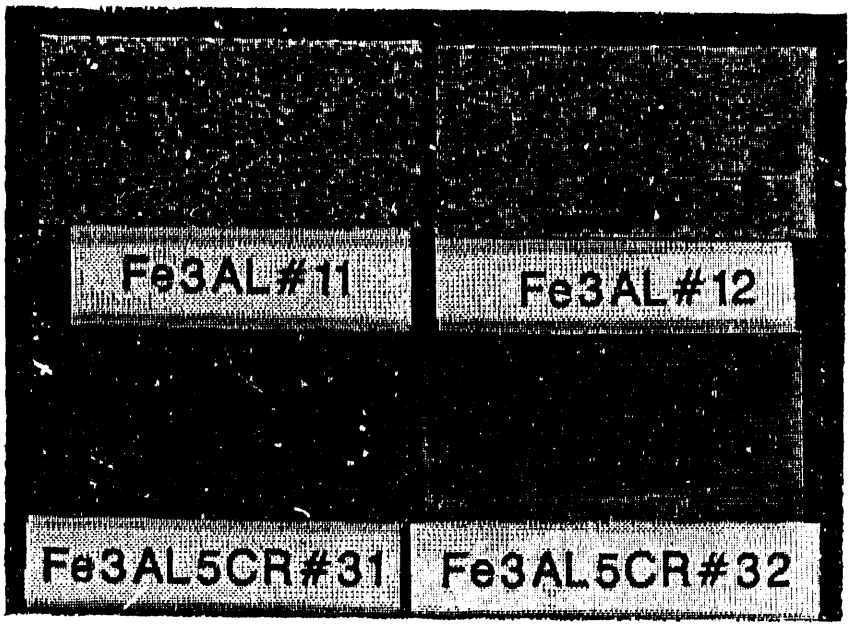

Gas Content:	1.0 vol% SO_2
Temperature:	650°C
Exposure Time:	800 hours
Sulfate Content:	10 wt%

Recoated Between Exposures:

690/316-30
690-11
17-14 CuMo-17
NF709-5
HR3C-30

Steam Cleaned and Recoated Between Exposures:

556-31
HR3C-31
800H-31
72/800H-32

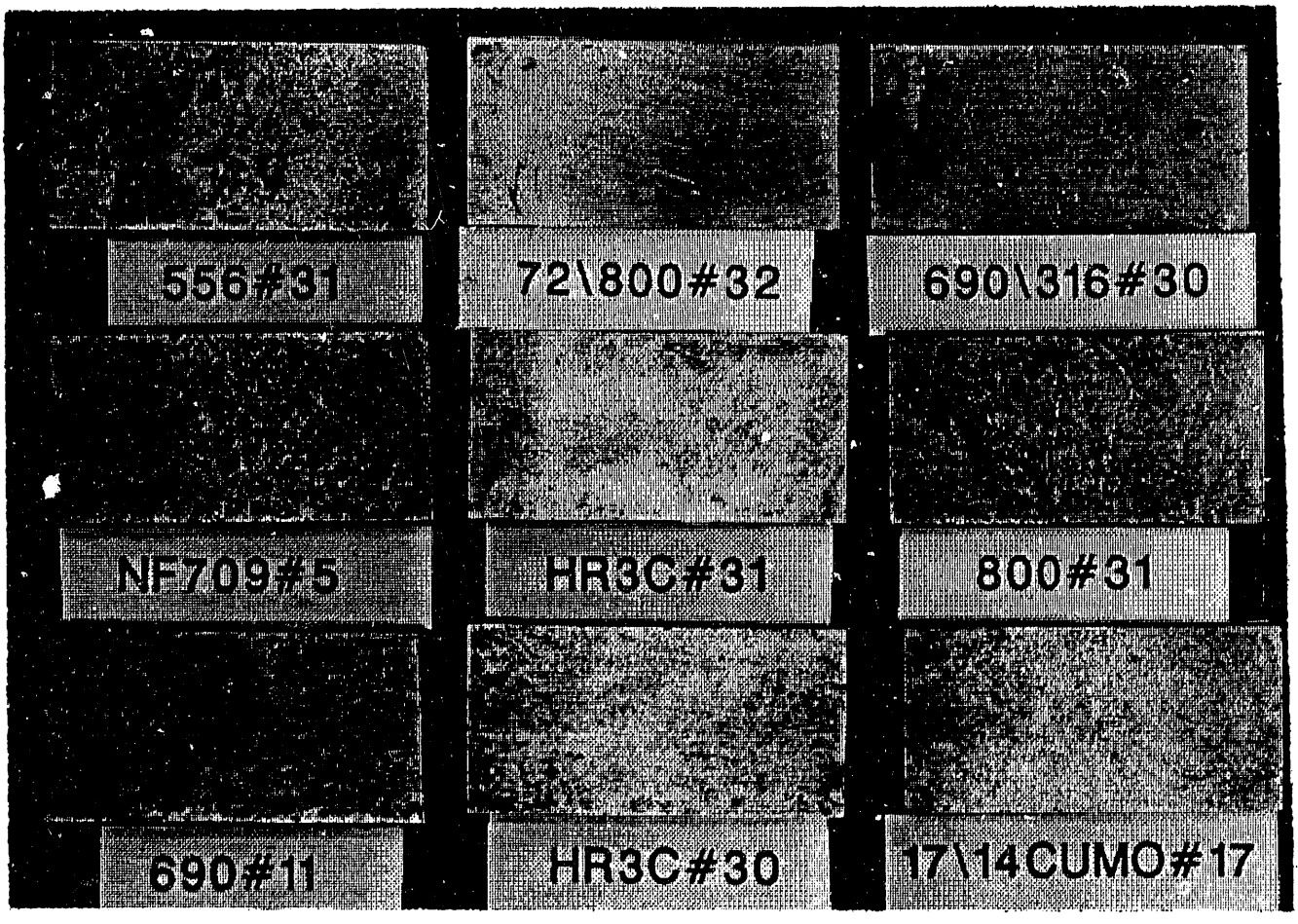

Gas Content:	1.0 vol% SO_2
Temperature:	650°C
Exposure Time:	800 hours
Sulfate Content:	10 wt%

Recoated Between Exposures:

347-24
556-30
CR35A-27
690/800H-30

Steam Cleaned and Recoated Between Exposures:

NF709-6
72/LSS-32
17-14 CuMo-18
690-12
690/800H-31
RA85H-25
690/316-31
316-26

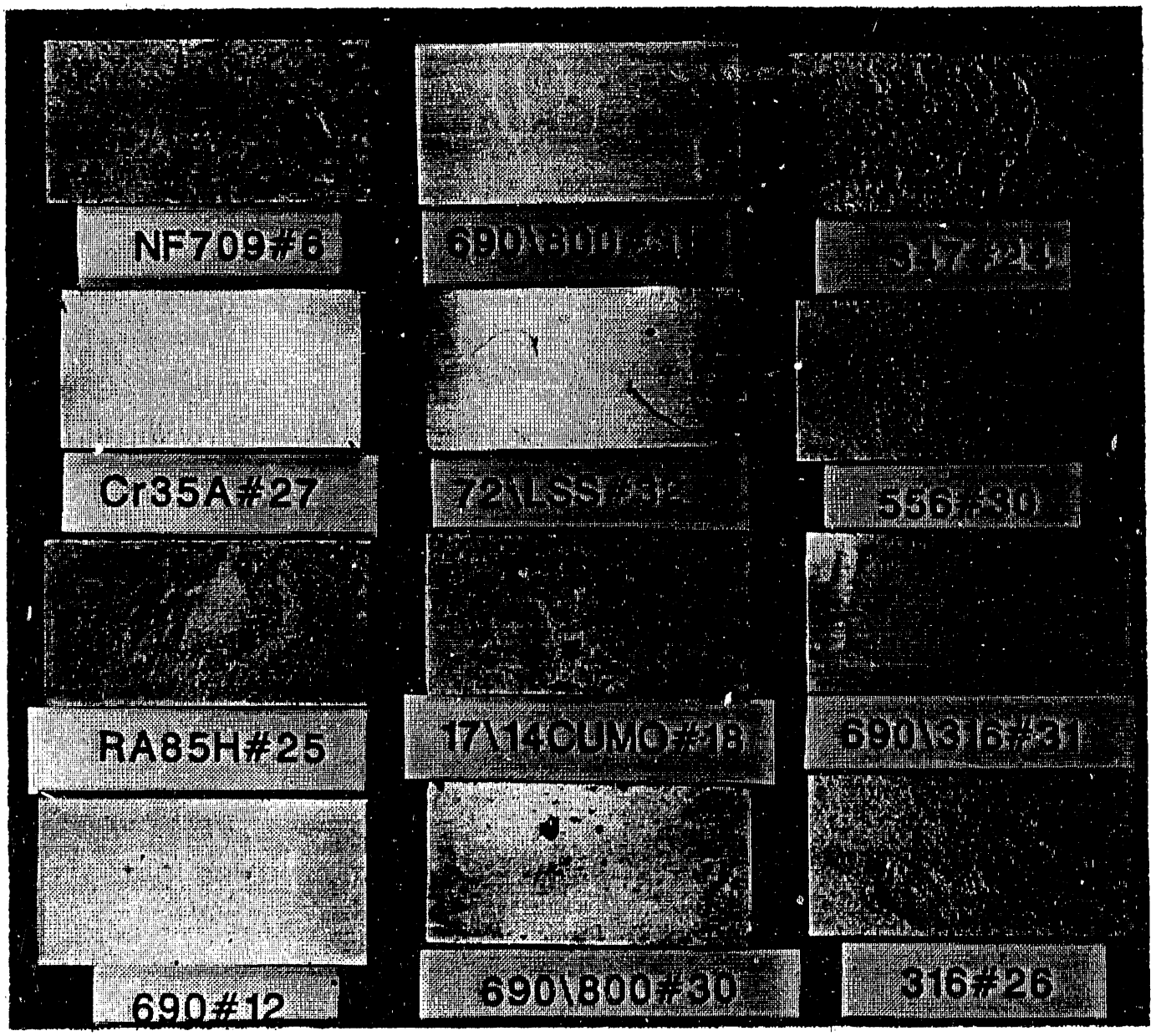

Gas Content:	1.0 vol% SO_2
Temperature:	650°C
Exposure Time:	800 hours
Sulfate Content:	10 wt%

Recoated Between Exposures:

690-8
316-22
CR35A-24
NF709-2
671/316-14
72/LSS-28

Steam Cleaned and Recoated Between Exposures:

HR3C-28
671-9
RA85H-22
800H-28
NF709-3

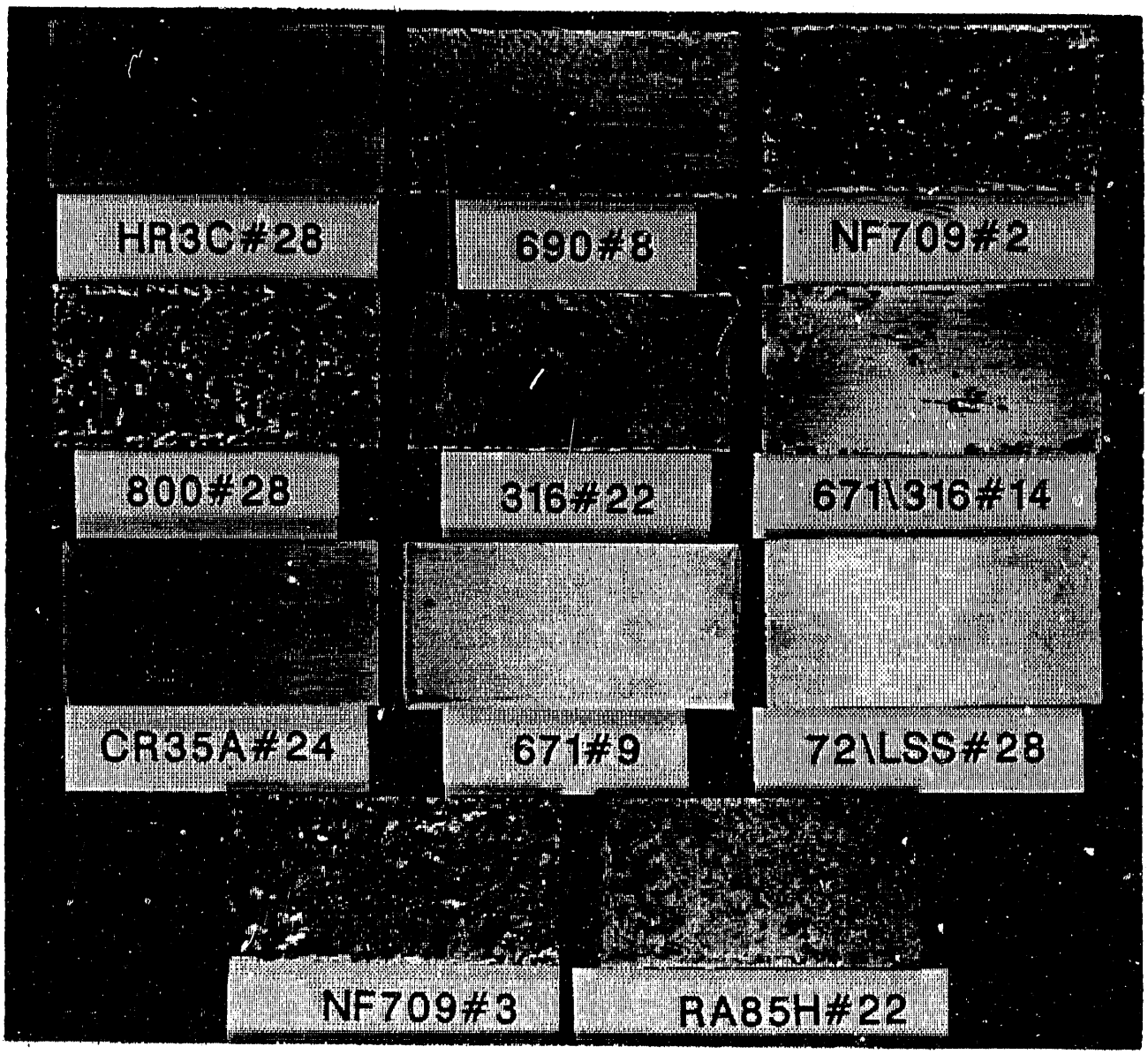

Gas Content:	1.0 vol% SO_2
Temperature:	650°C
Exposure Time:	800 hours
Sulfate Content:	10 wt%

Recoated Between Exposures:

RA85H-24
316-25
671-11
72/800H-31
72/LSS-31

Steam Cleaned and Recoated Between Exposures:

347-25
CR35A-28
671-12

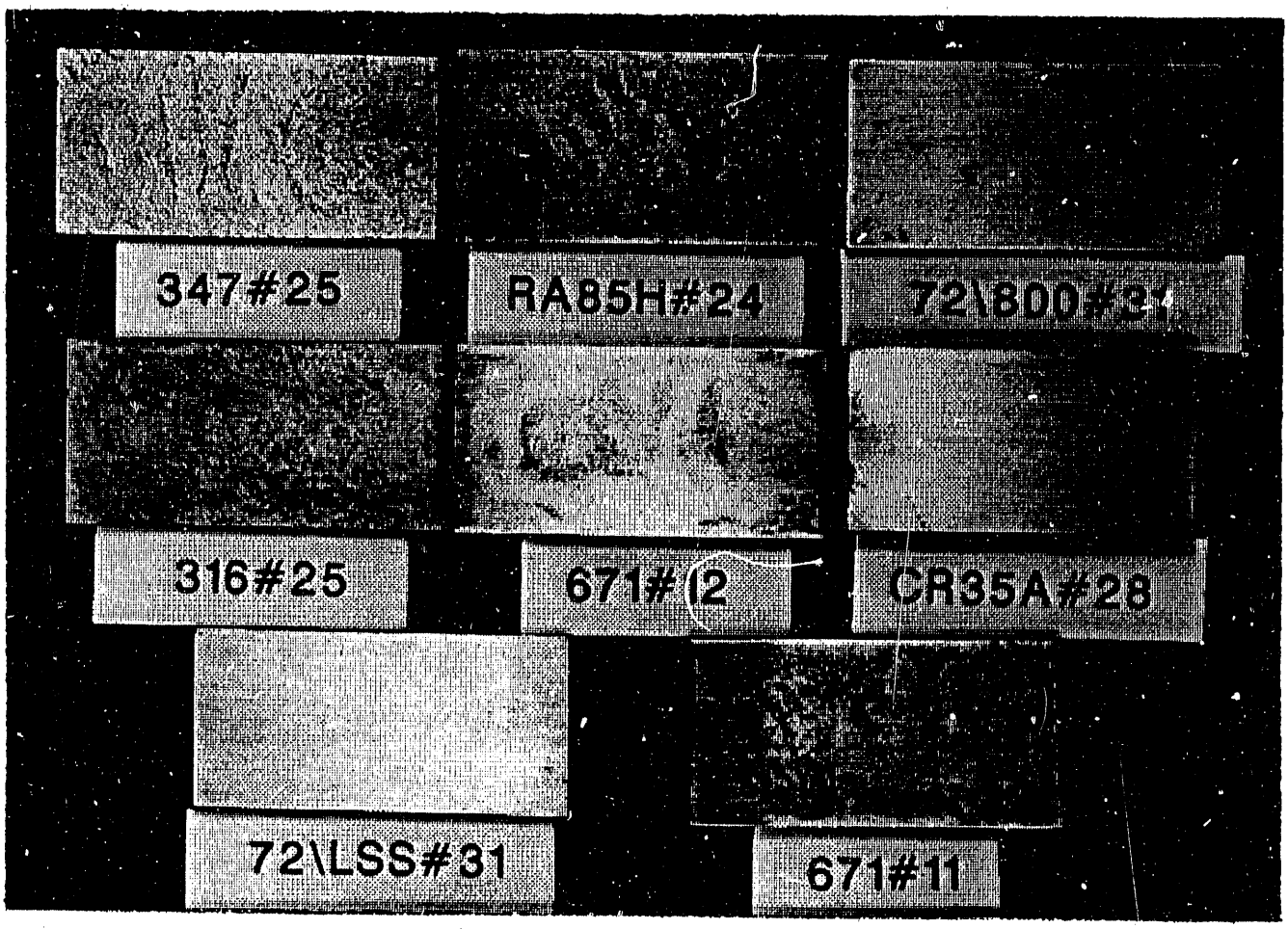

Gas Content:	1.0 vol% SO_2
Temperature:	700°C
Exposure Time:	800 hours
Sulfate Content:	10 wt%

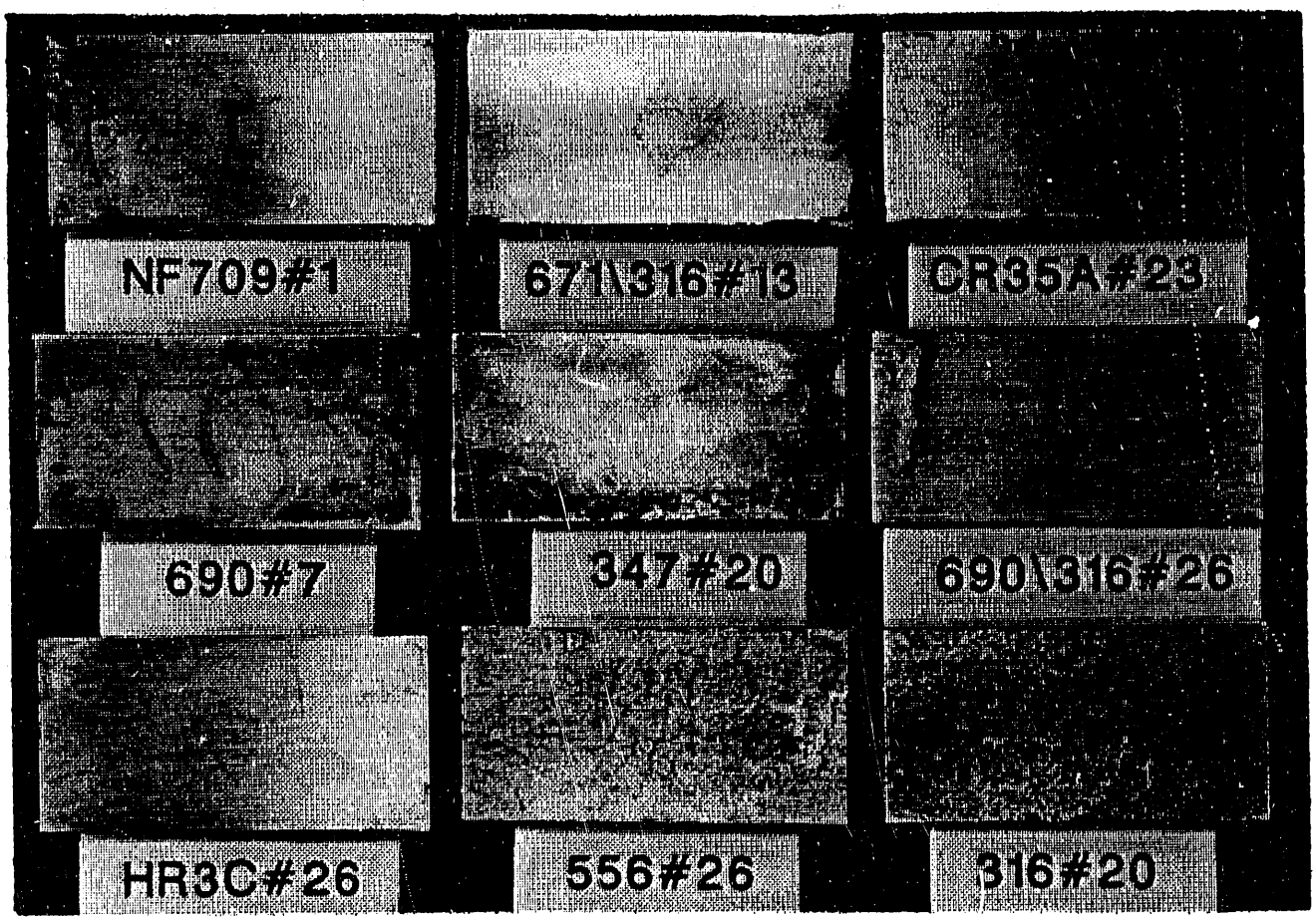

Gas Content:	1.0 vol% SO_2
Temperature:	700°C
Exposure Time:	100 hours
Sulfate Content:	10 wt%

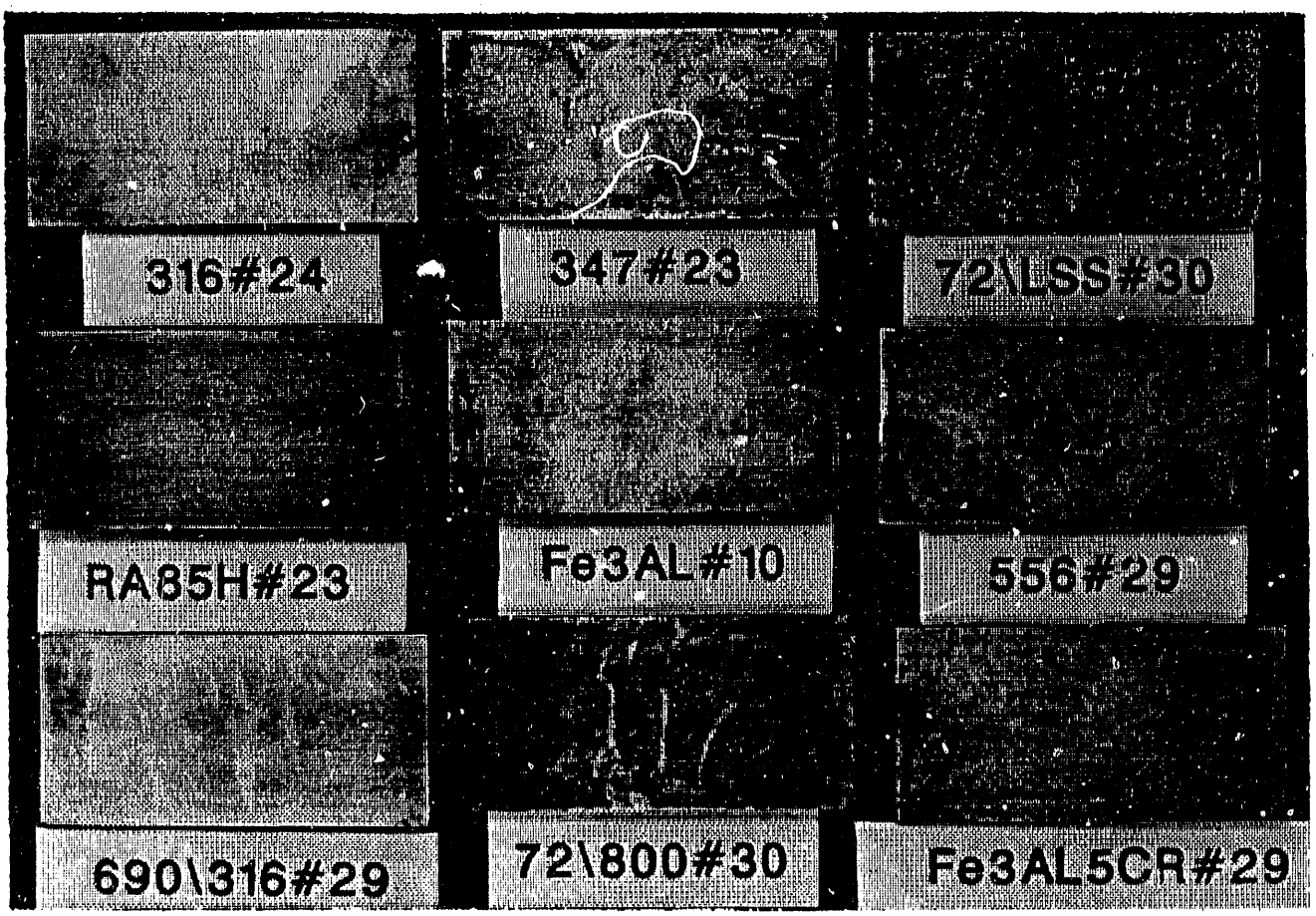

Gas Content:	1.0 vol% SO_2
Temperature:	650°C
Exposure Time:	100 hours
Sulfate Content:	10 wt%

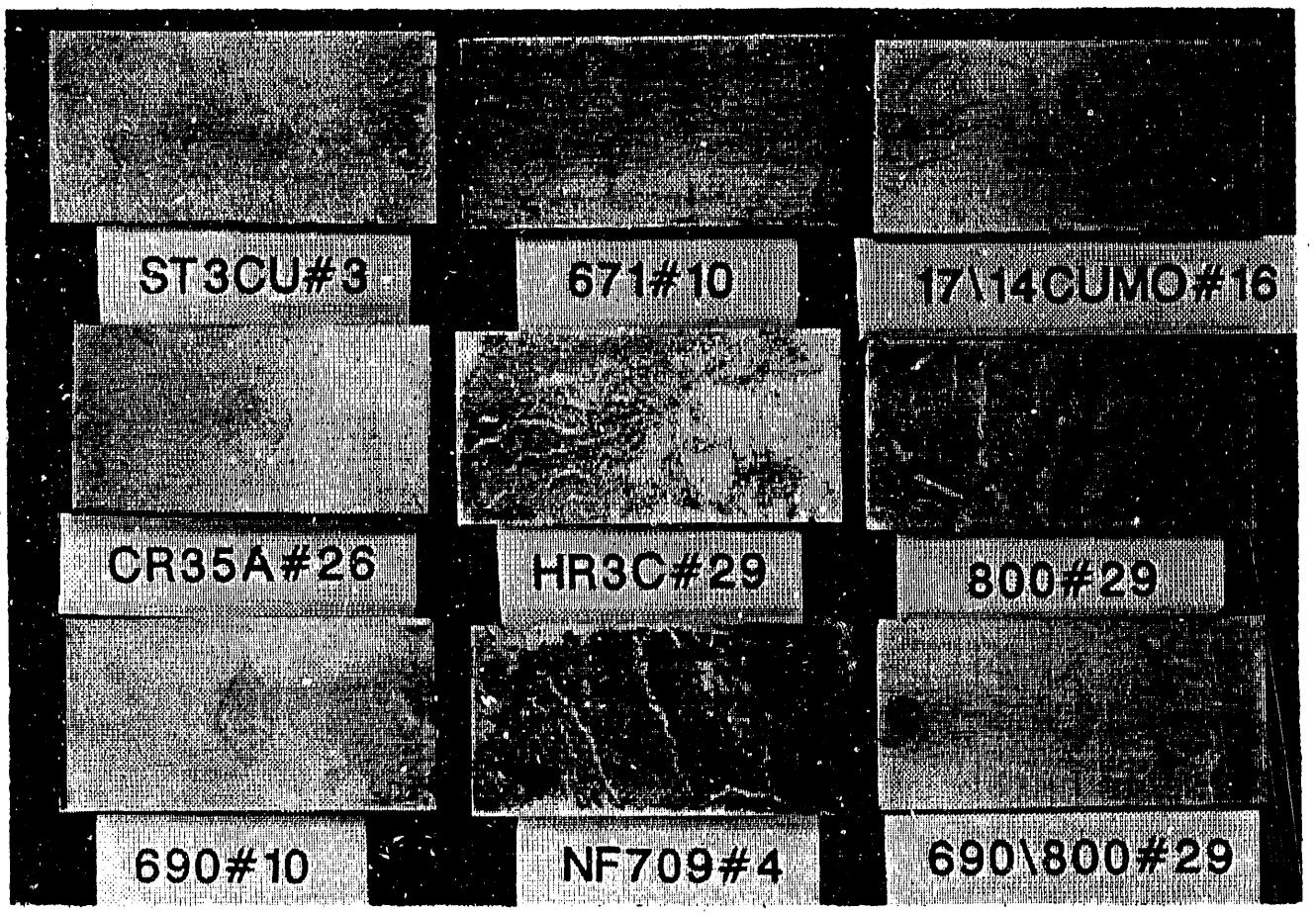

Gas Content:	1.0 vol% SO_2
Temperature:	650°C
Exposure Time:	100 hours
Sulfate Content:	10 wt%

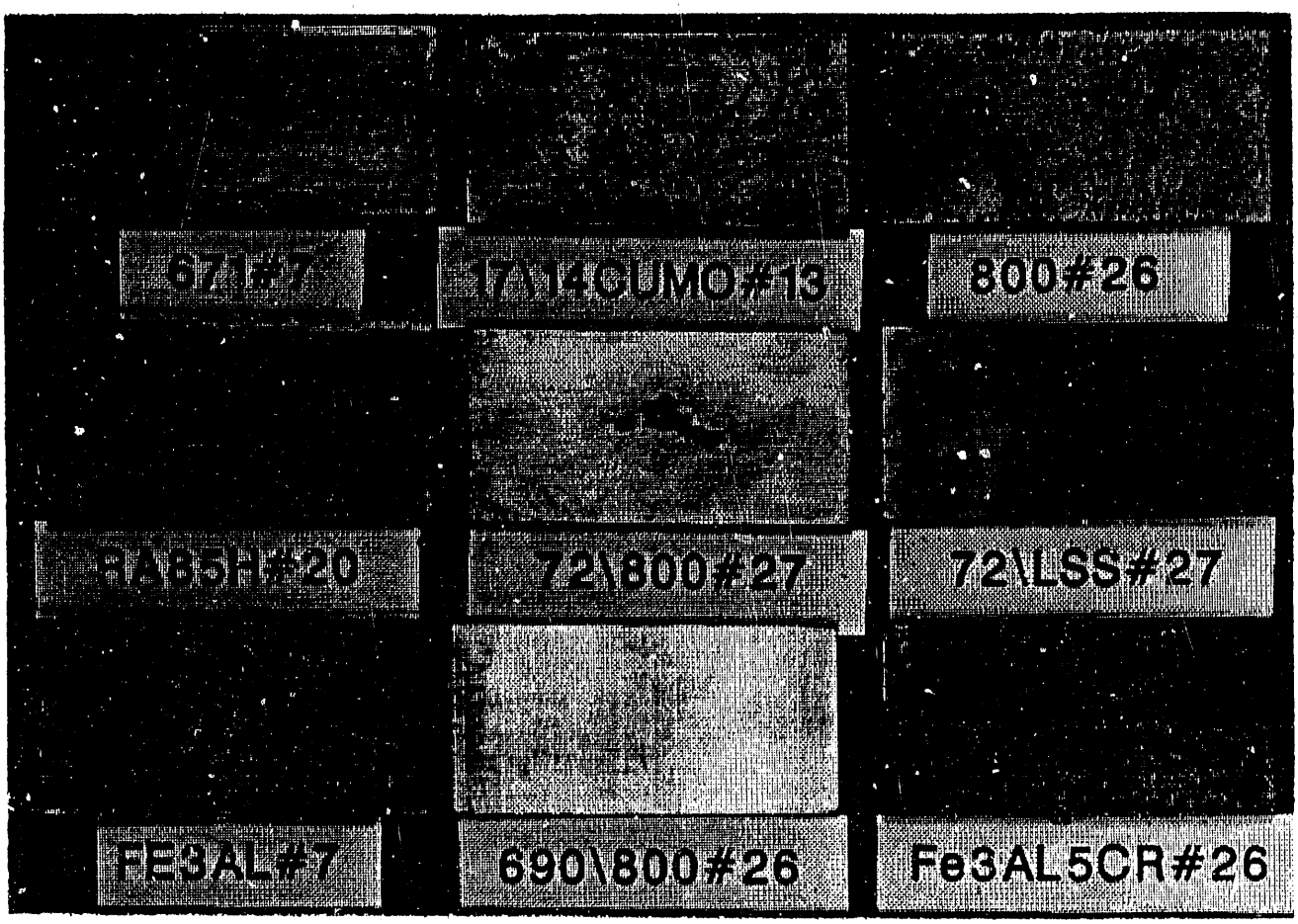

Gas Content:	1.0 vol% SO_2
Temperature:	700°C
Exposure Time:	100 hours
Sulfate Content:	10 wt%

Recoated Between Exposures:

Fe_3Al-5Cr-21	556-20	72/800H-21
671/316-7	HR3C-20	690/316-20
SAN28-1	690-21	

Steam Cleaned and Recoated Between Exposures:

NF709-8	671/316-8	CR35A-21
$(FeNi)_3Al$-8	800H-21	316-8

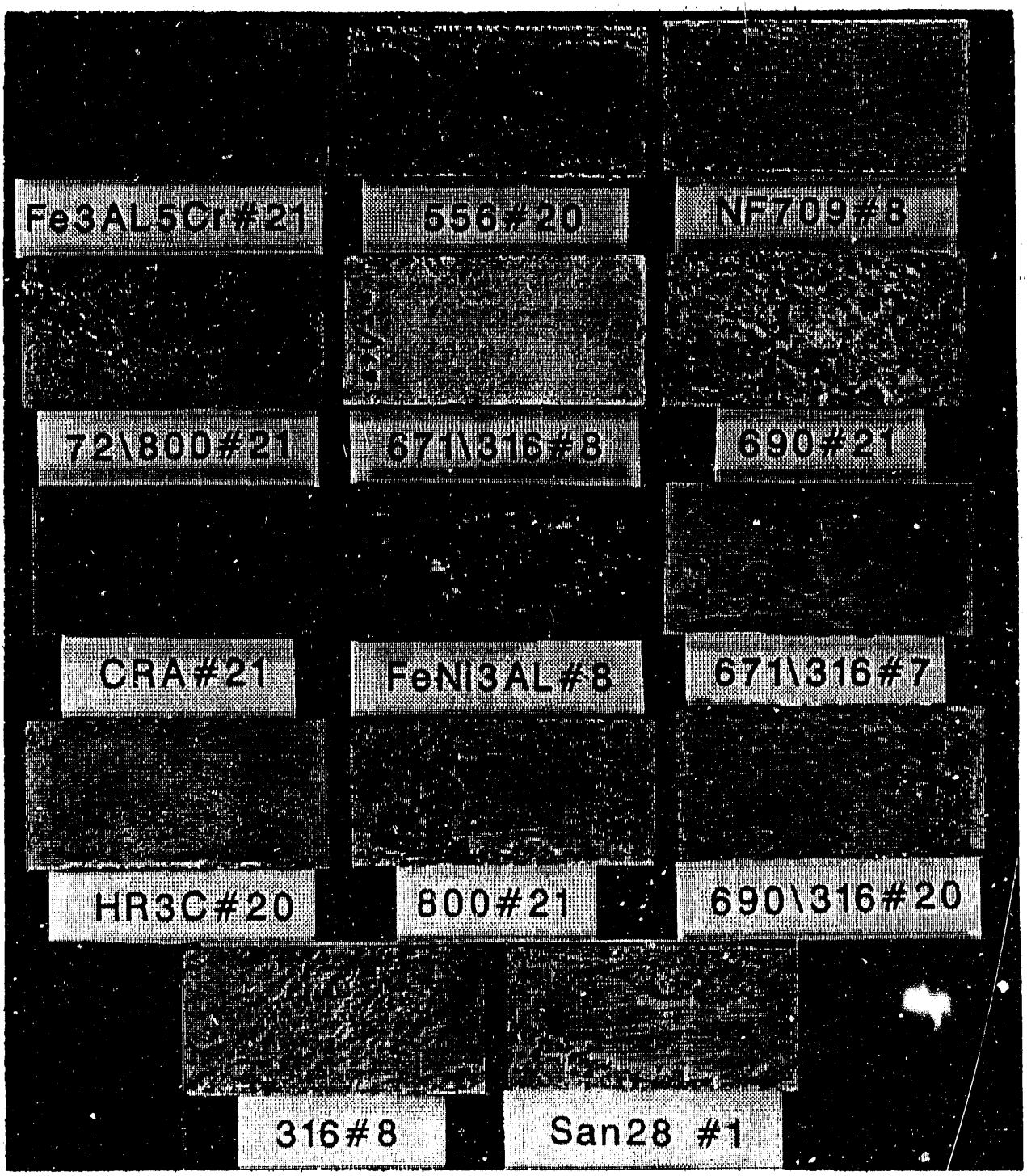

Gas Content:	0.25 vol% SO_2
Temperature:	700°C
Exposure Time:	800 hours
Sulfate Content:	10 wt%

Recoated Between Exposures:

17-14 CuMo-7
OSU-10
Fe_3Al-5Cr-20
671-21

Steam Cleaned and Recoated Between Exposures:

OSU-11
671-22
RA85H-8
690/316-21
347-8
17-14 CuMo-8
72/800H-22
72/LSS-22

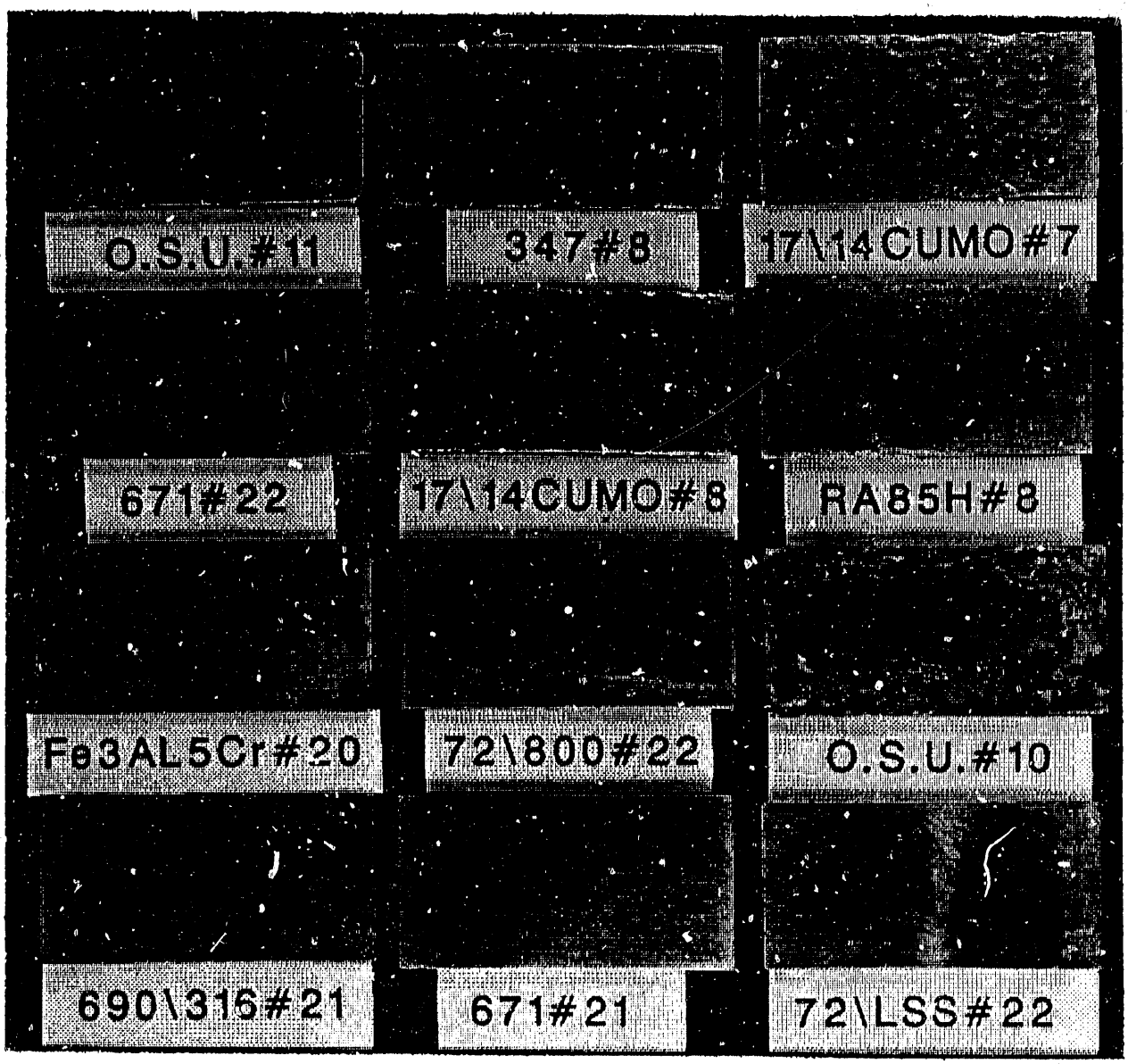

Gas Content: 0.25 vol% SO_2
Temperature: 700°C
Exposure Time: 800 hours
Sulfate Content: 10 wt%

Recoated Between Exposures:

690/800H-20	CR35A-20
RA85H-7	347-7
316-7	NF709-7
$(FeNi)_3Al$-7	72/LSS-21

Steam Cleaned and Recoated Between Exposures:

HR3C-21	690/800H-21
556-21	690-22

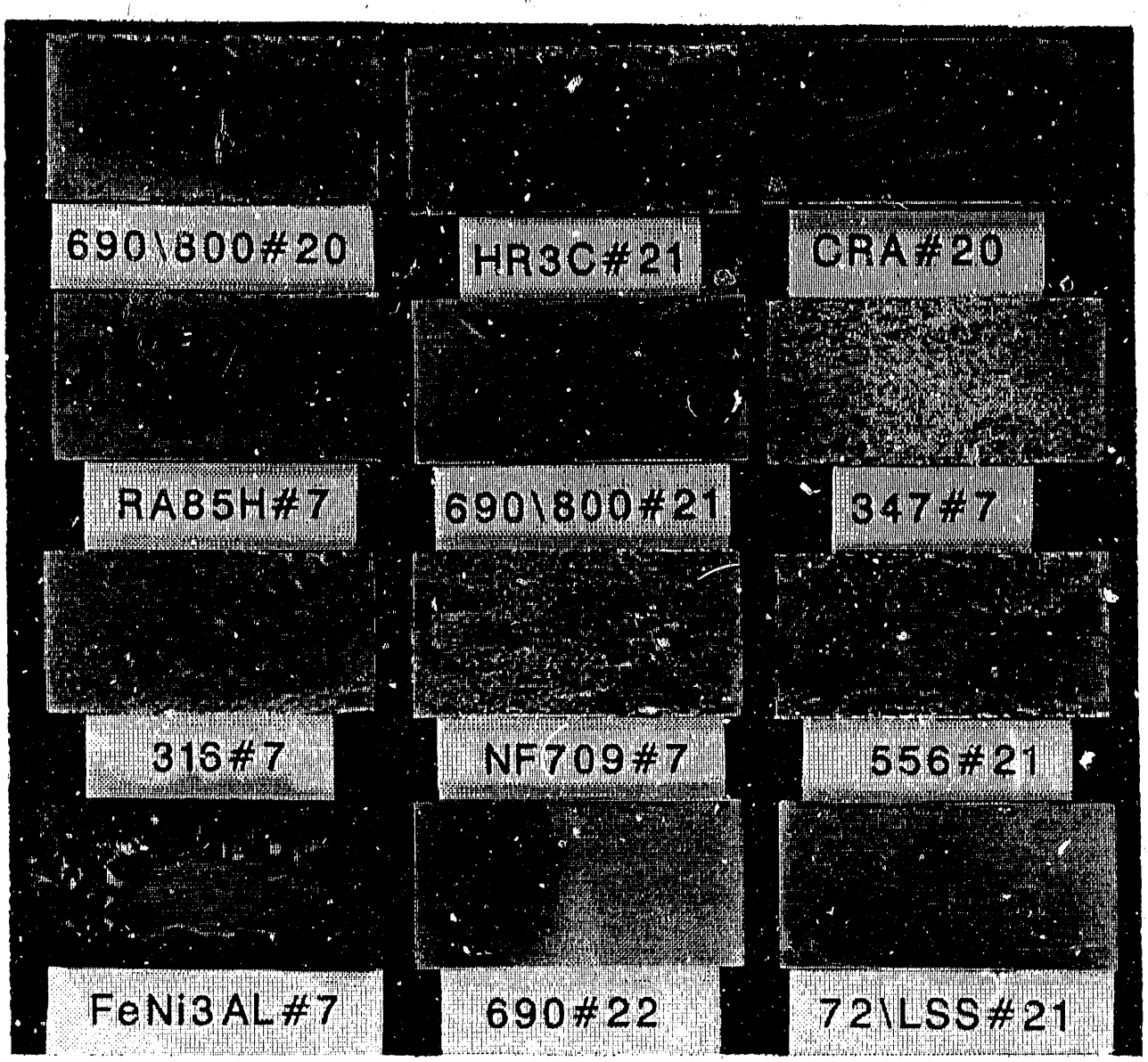

Gas Content:	0.25 vol% SO_2
Temperature:	700°C
Exposure Time:	800 hours
Sulfate Content:	10 wt%

Recoated Between Exposures:

RA85H-4
NF709-4
SAN28-4
OSU-2

Steam Cleaned and Recoated Between Exposures:

RA85H-5
NF709-5
SAN28-5

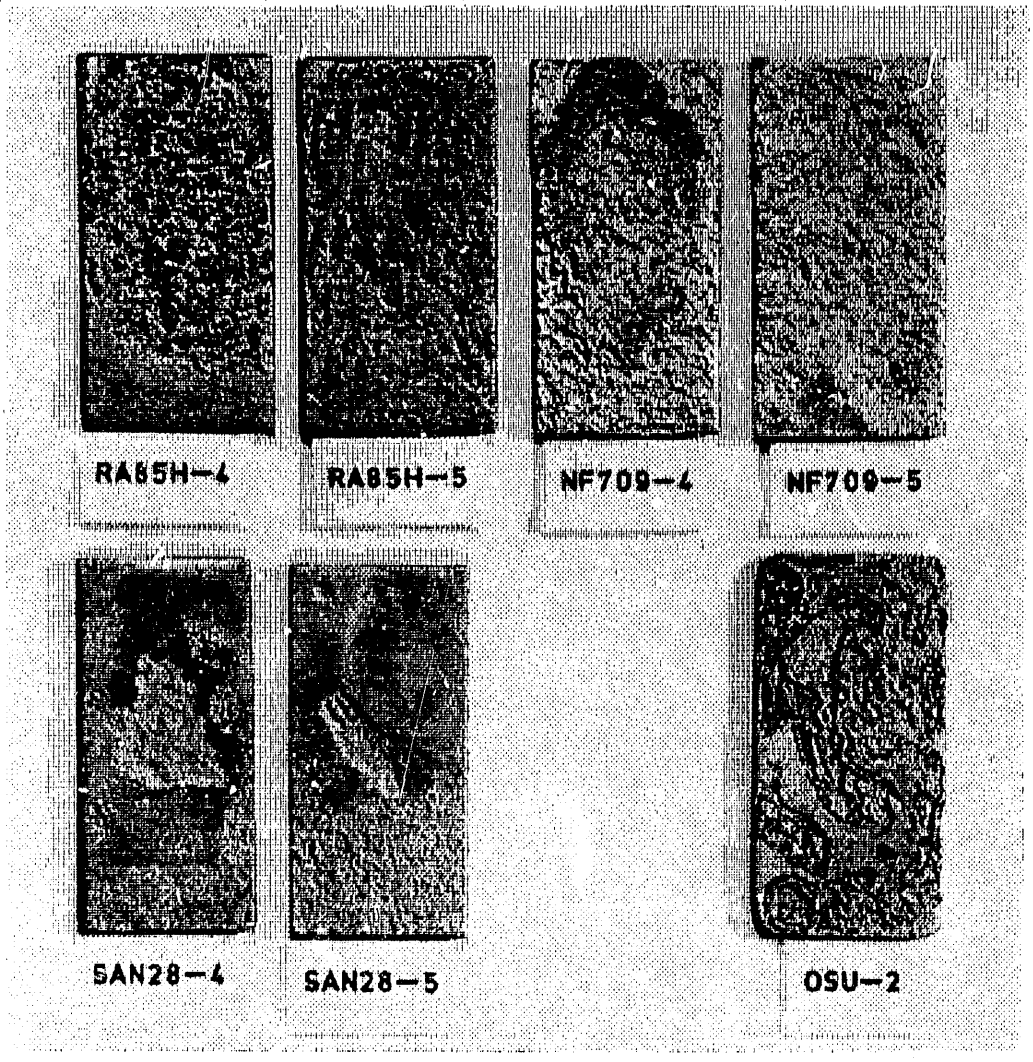

Gas Content:	0.25 vol% SO_2
Temperature:	650°C
Exposure Time:	200 hours
Sulfate Content:	75 wt%

Recoated Between Exposures:

671/316-4
671-4
690/316-4
690-4

Steam Cleaned and Recoated Between Exposures:

671/316-5
671-5
690/316-5
690-5

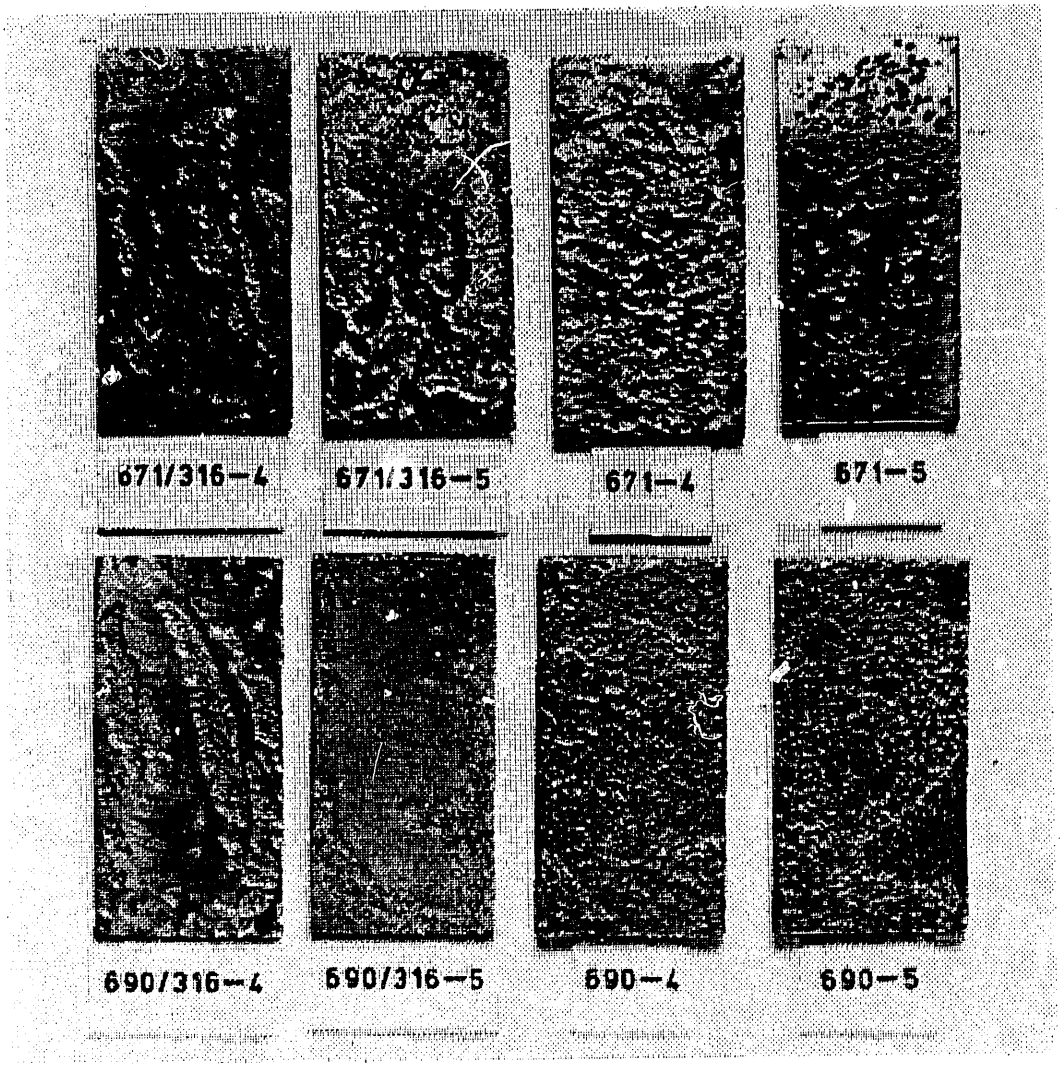

Gas Content:	0.25 vol% SO_2
Temperature:	650°C
Exposure Time:	200 hours
Sulfate Content:	75 wt%

Recoated Between Exposures:

Fe_3Al-4 $(FeNi)_3Al$-4

Steam Cleaned and Recoated Between Exposures:

Fe_3Al-5 $(FeNi)_3Al$-5

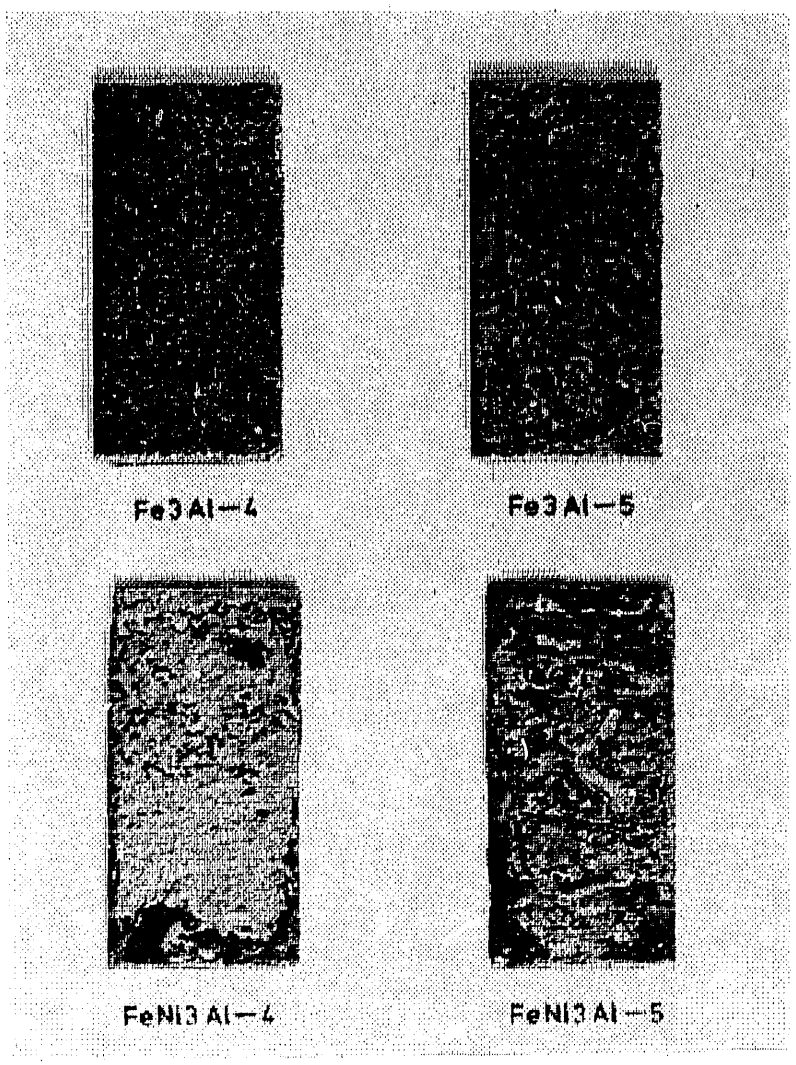

Gas Content:	0.25 vol% SO_2
Temperature:	650°C
Exposure Time:	200 hours
Sulfate Content:	75 wt%

Recoated Between Exposures:

17-14 CuMo-4
347-4
CR35A-4
316-4

Steam Cleaned and Recoated Between Exposures:

17-14 CuMo-5
347-5
CR35A-5
316-5

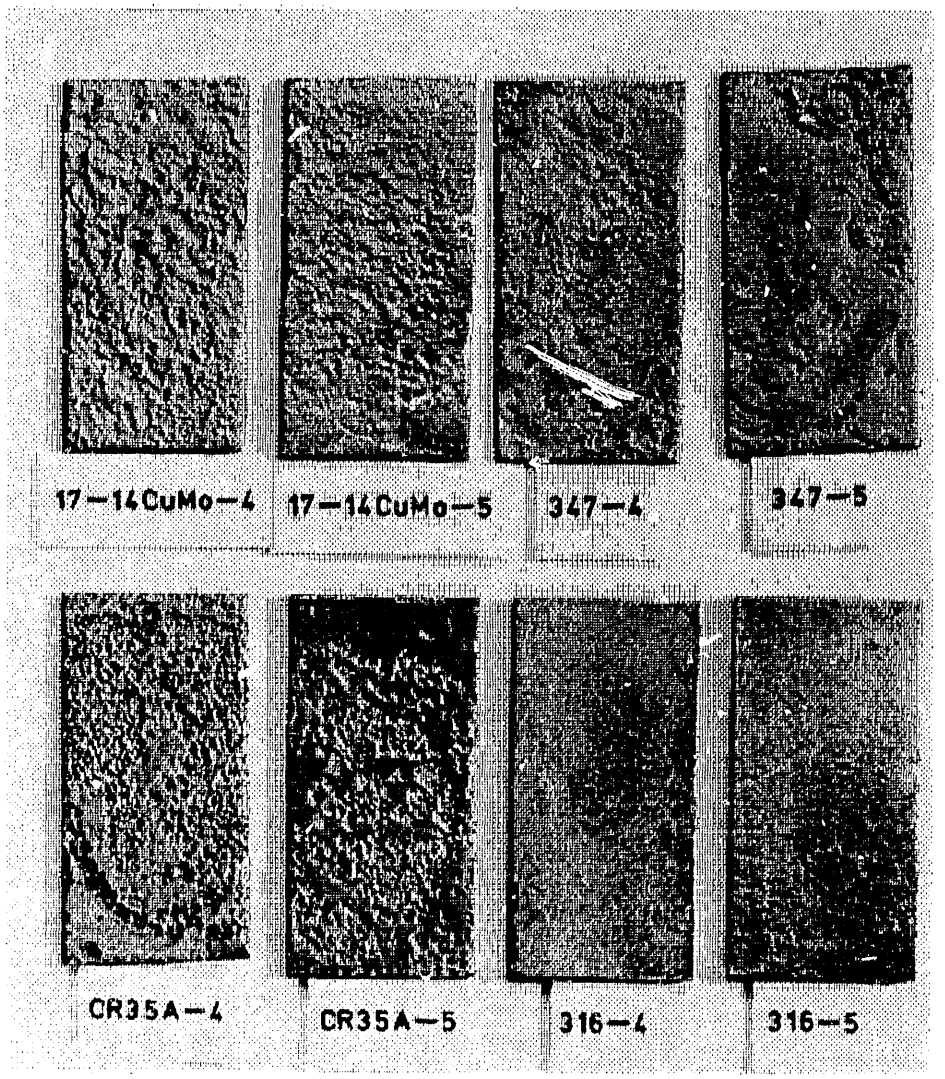

Gas Content:	0.25 vol% SO_2
Temperature:	650°C
Exposure Time:	200 hours
Sulfate Content:	75 wt%

Recoated Between Exposures:

800H-7
800H-10*
690/800H-4
72/800H-4

Steam Cleaned and Recoated Between Exposures:

800H-8
800H-11*
690/800H-5
72/800H-5

[*Coated with a coal ash containing 10 wt% alkali sulfates.]

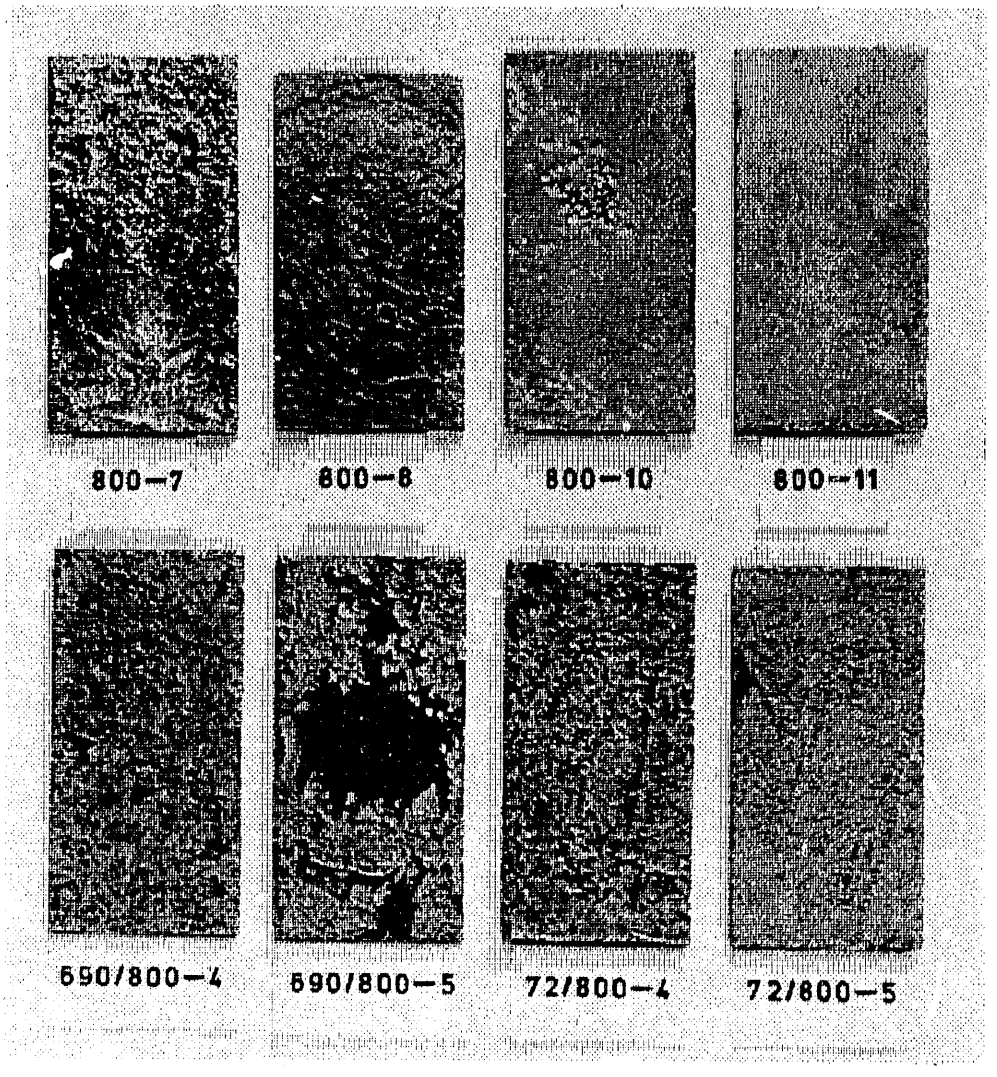

Gas Content: 0.25 vol% SO_2
Temperature: 650°C
Exposure Time: 200 hours
Sulfate Content: 75 wt%

Recoated Between Exposures:

72/800H-25	72/LSS-24
556-23	OSU-13
RA85H-10	SAN28-2
690/800H-23	$(FeNi)_3Al$-9

Steam Cleaned and Recoated Between Exposures:

NF709-10	72/LSS-25
800H-24	$(FeNi)_3Al$-10

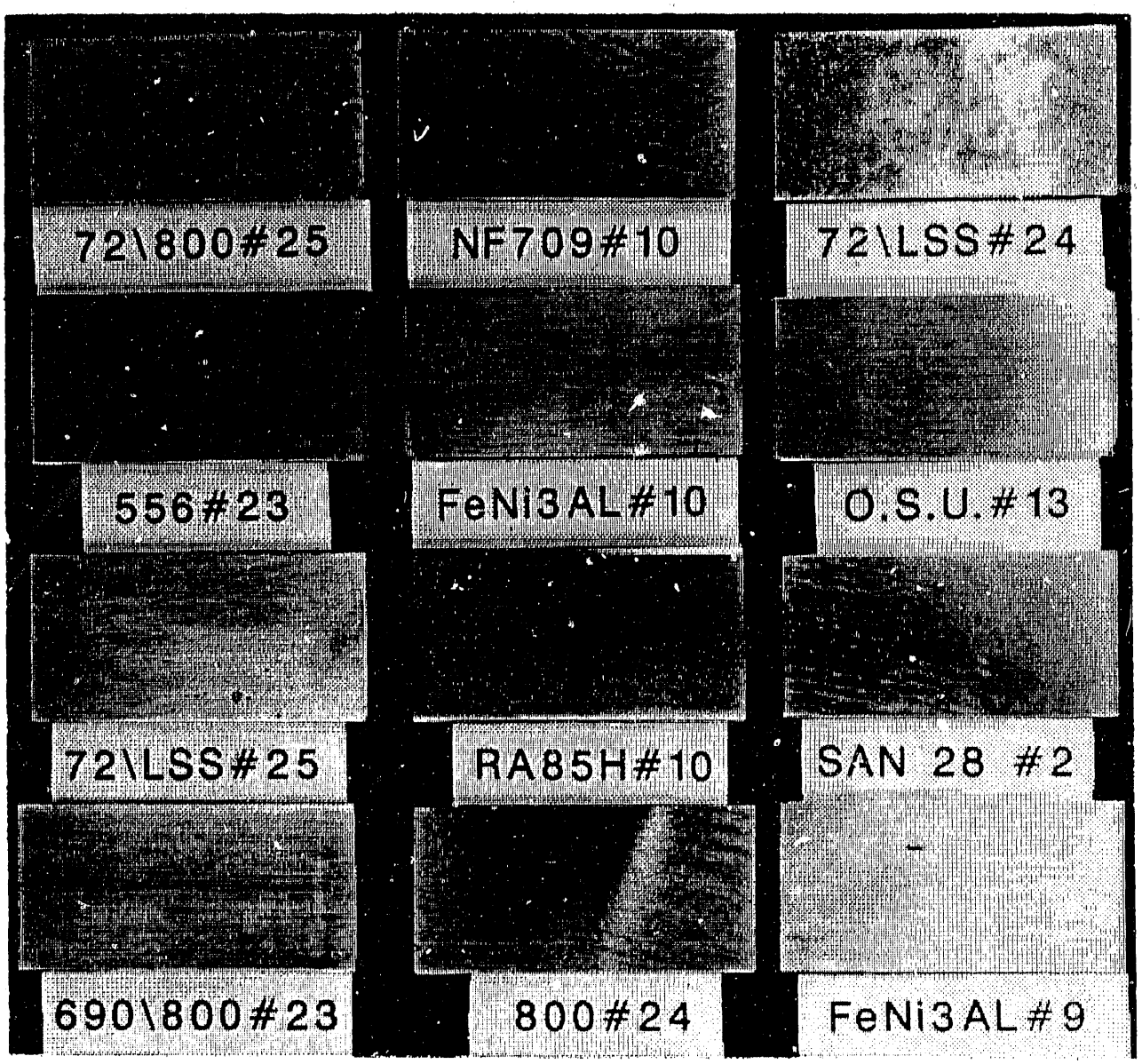

Gas Content:	0.25 vol% SO_2
Temperature:	650°C
Exposure Time:	800 hours
Sulfate Content:	10 wt%

Recoated Between Exposures:

Fe_3Al-5Cr-23	671/316-10	72/800H-24
NF709-9	347-10	17-14 CuMo-10

Steam Cleaned and Recoated Between Exposures:

CR35A-8	OSU-14	556-24
HR3C-24	HR3C-23	690/800H-24
17-14 CuMo-11	671-25	690/316-24

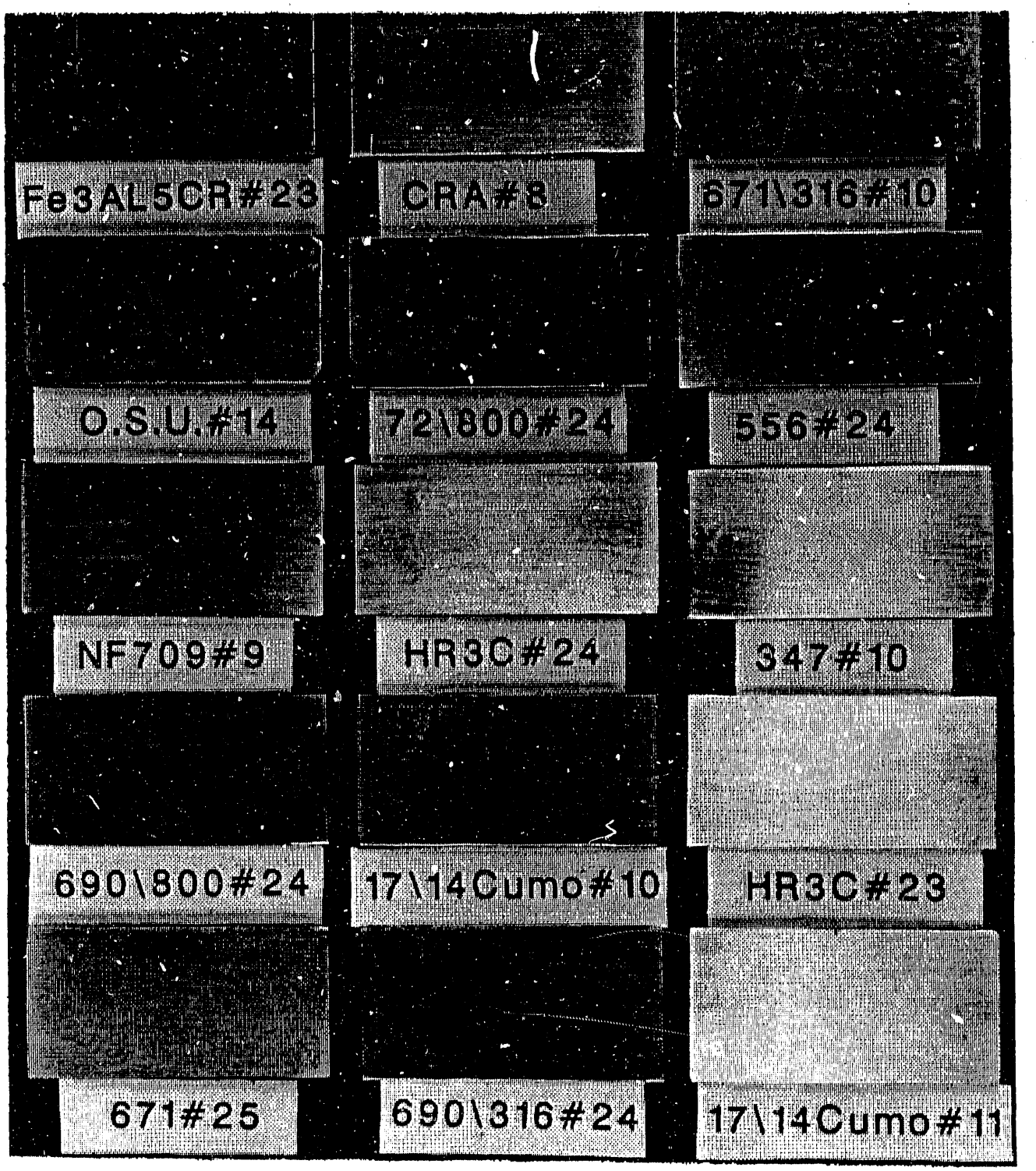

Gas Content:	0.25 vol% SO_2
Temperature:	650°C
Exposure Time:	800 hours
Sulfate Content:	10 wt%

Recoated Between Exposures:

690-24	CR35A-7
316-10	800H-23
671-24	690-316-23

Steam Cleaned and Recoated Between Exposures:

316-11	347-11
690-25	Fe_3Al-5Cr-24
RA85H-11	671/316-23

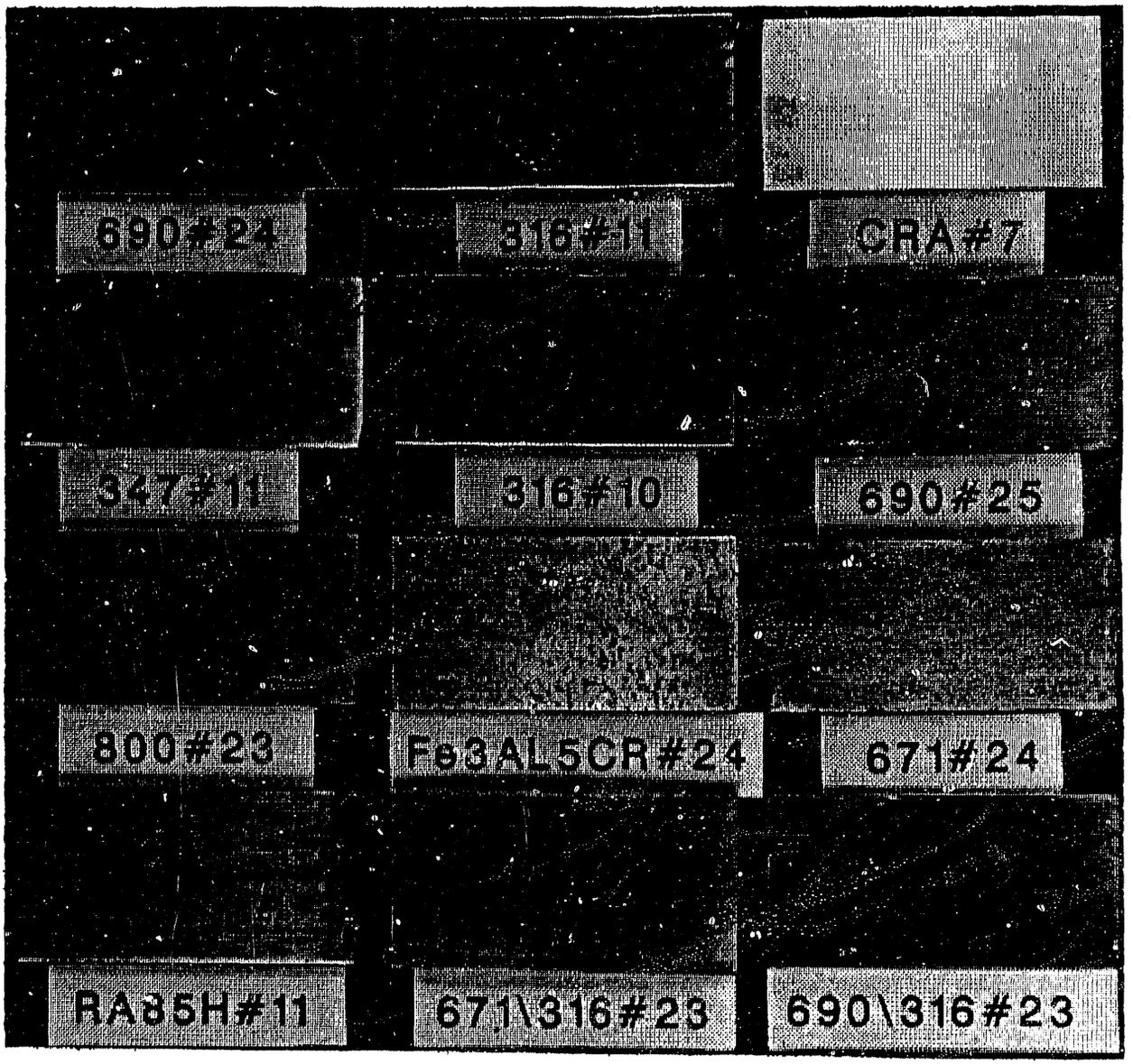

Gas Content:	0.25 vol% SO_2
Temperature:	650°C
Exposure Time:	800 hours
Sulfate Content:	10 wt%

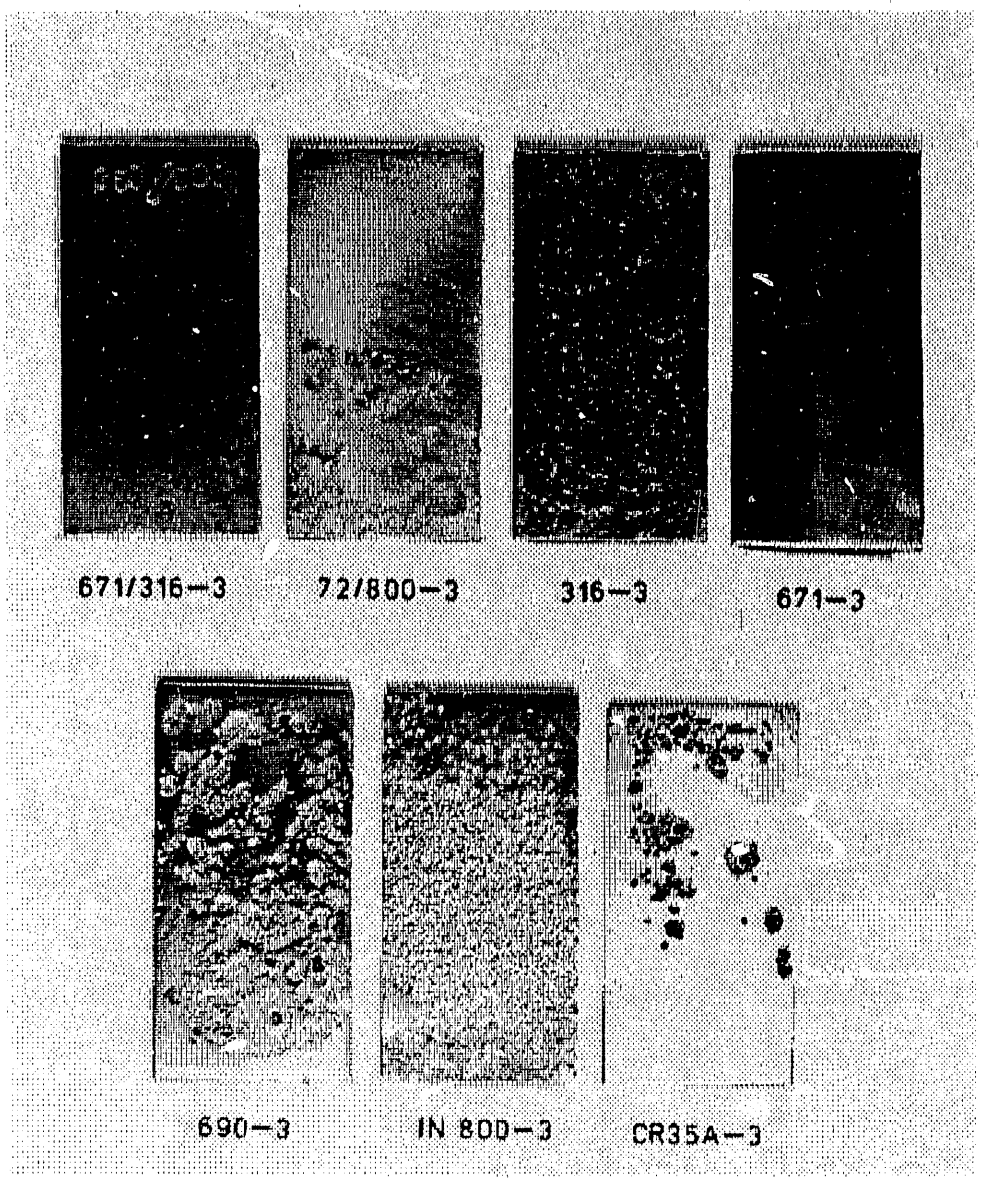

Gas Content:	0.25 vol% SO_2
Temperature:	700°C
Exposure Time:	100 hours
Sulfate Content:	75 wt%

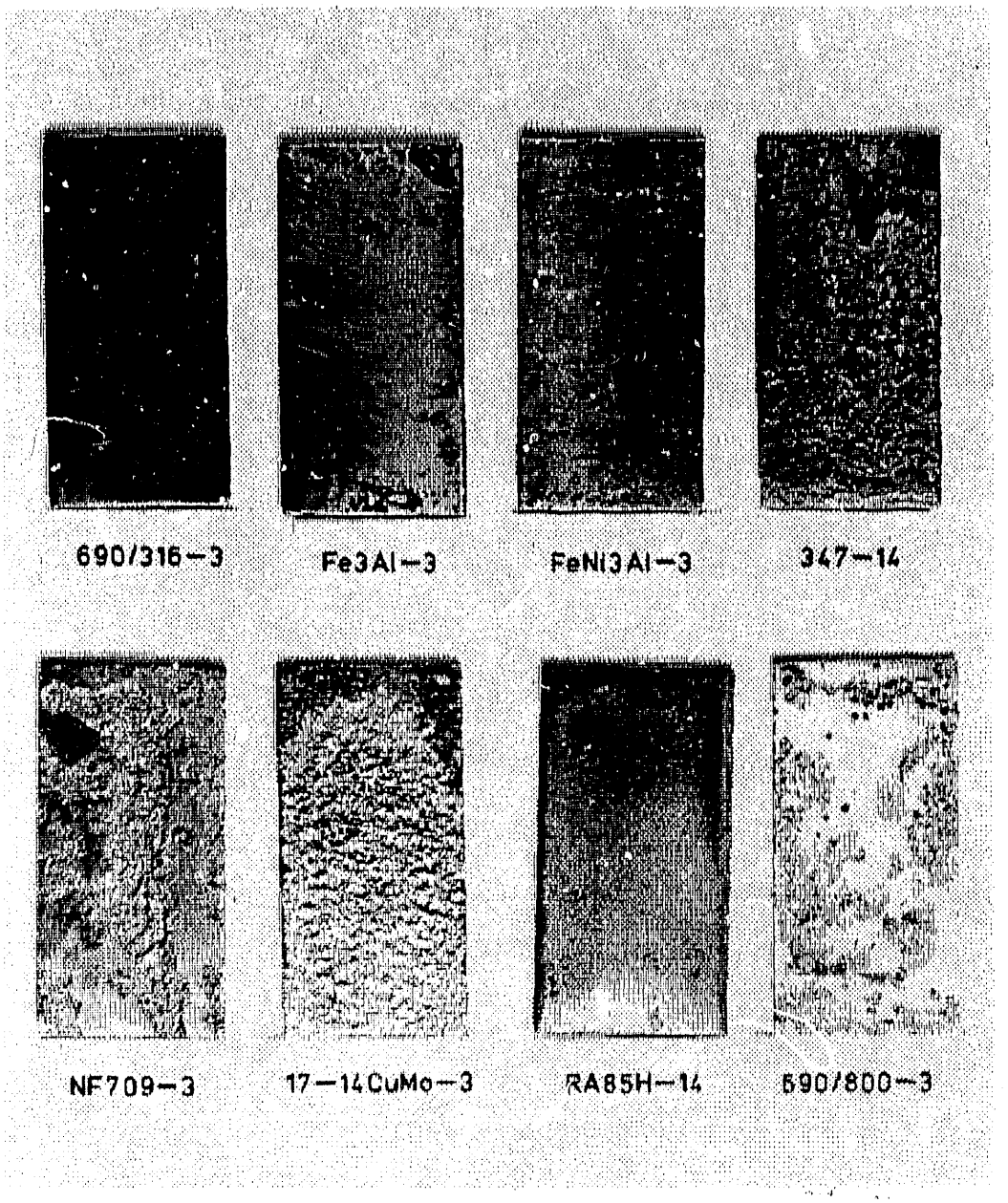

Gas Content:	0.25 vol% SO_2
Temperature:	700°C
Exposure Time:	100 hours
Sulfate Content:	75 wt%

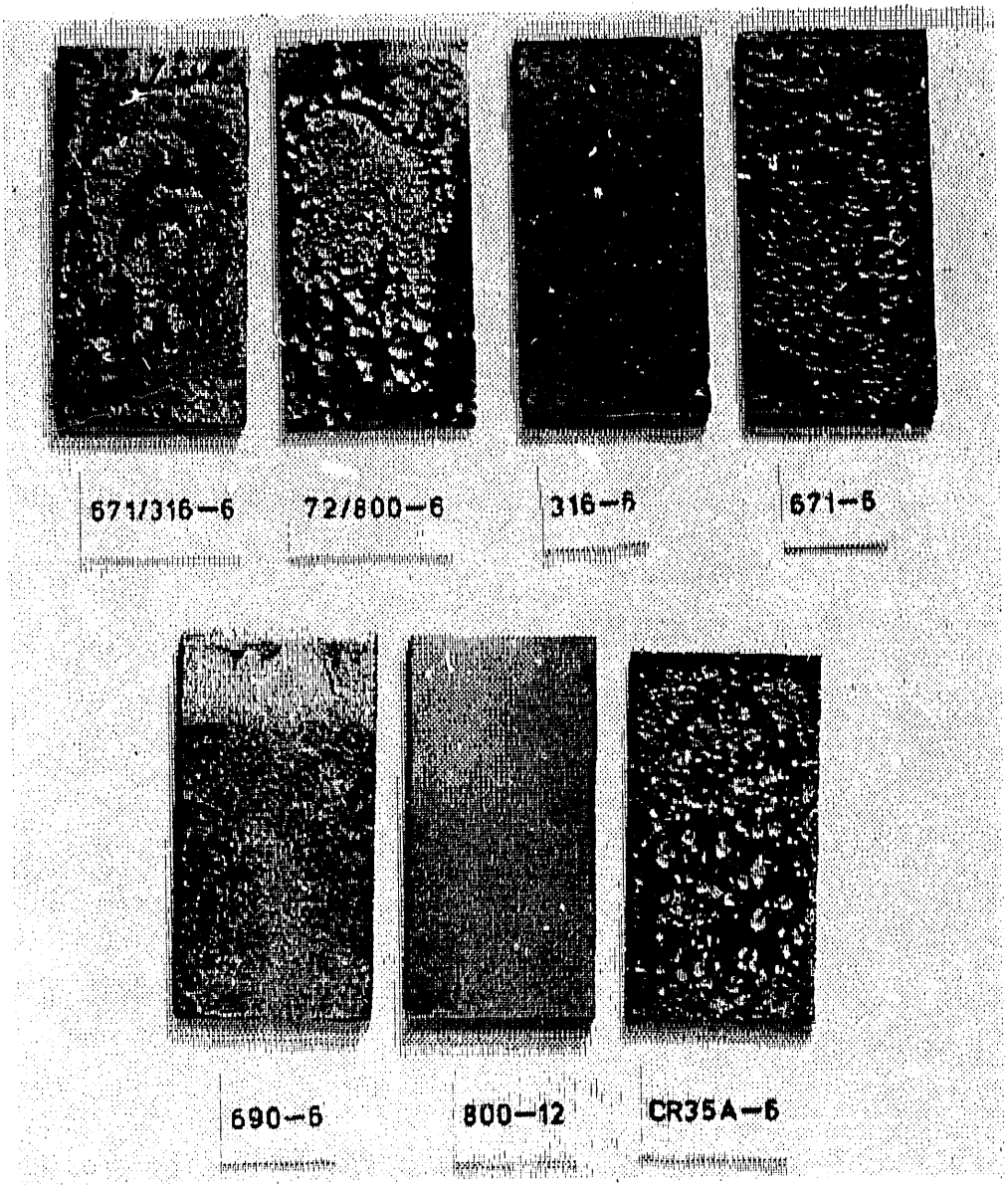

Gas Content:	0.25 vol% SO_2
Temperature:	650°C
Exposure Time:	100 hours
Sulfate Content:	75 wt%

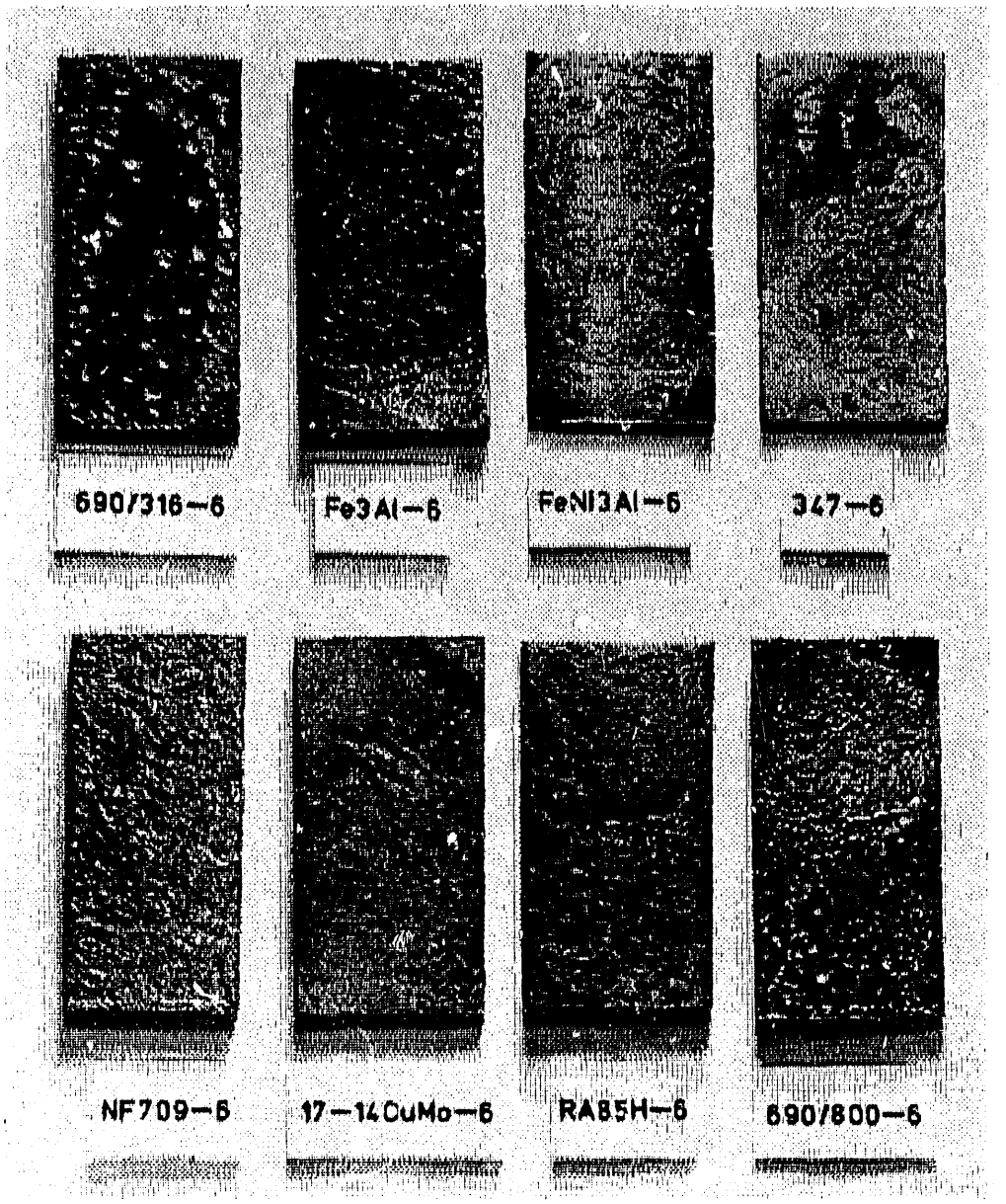

Gas Content: 0.25 vol% SO_2
Temperature: 650°C
Exposure Time: 100 hours
Sulfate Content: 75 wt%

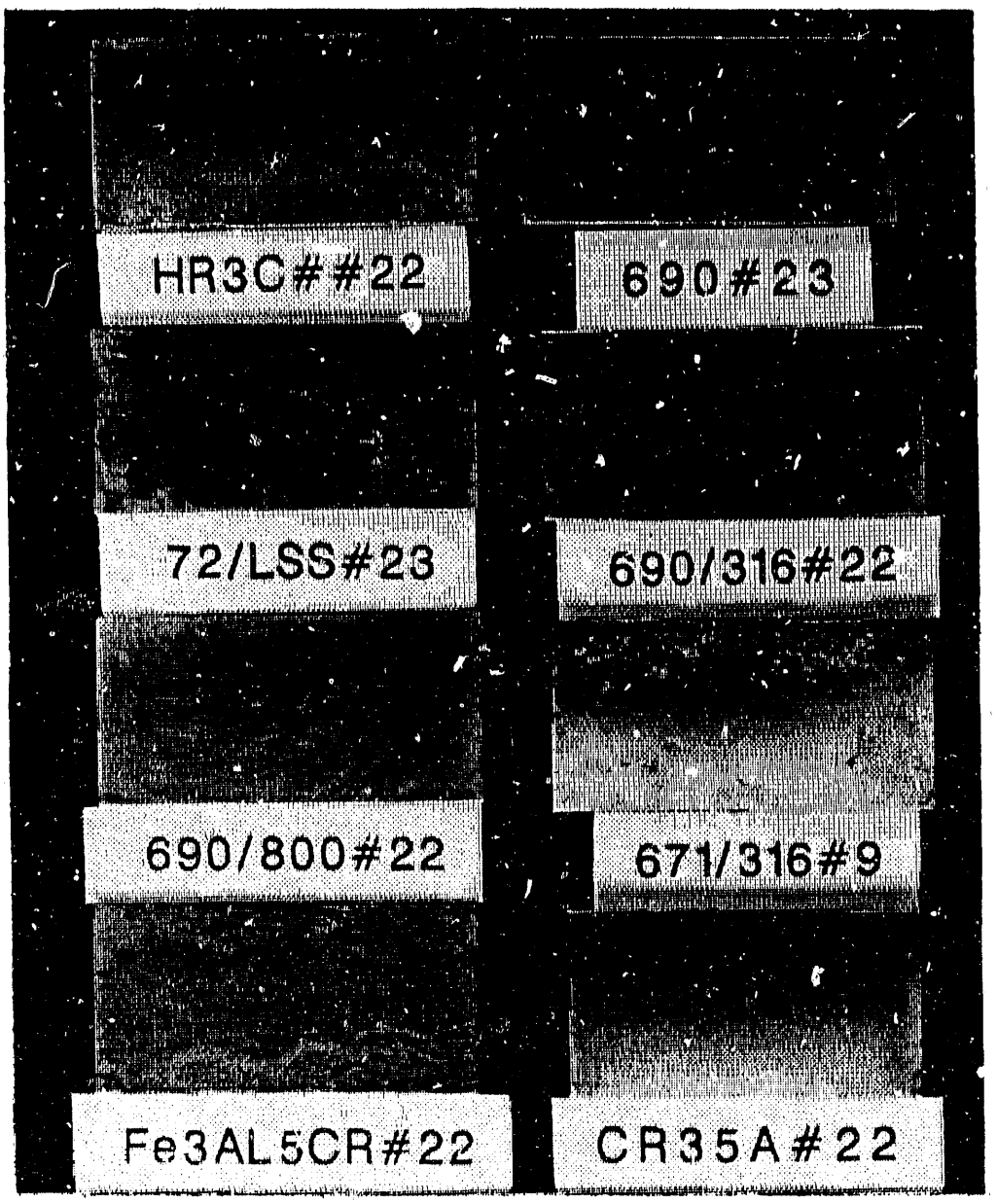

Gas Content:	0.25 vol% SO_2
Temperature:	700°C
Exposure Time:	100 hours
Sulfate Content:	10 wt%

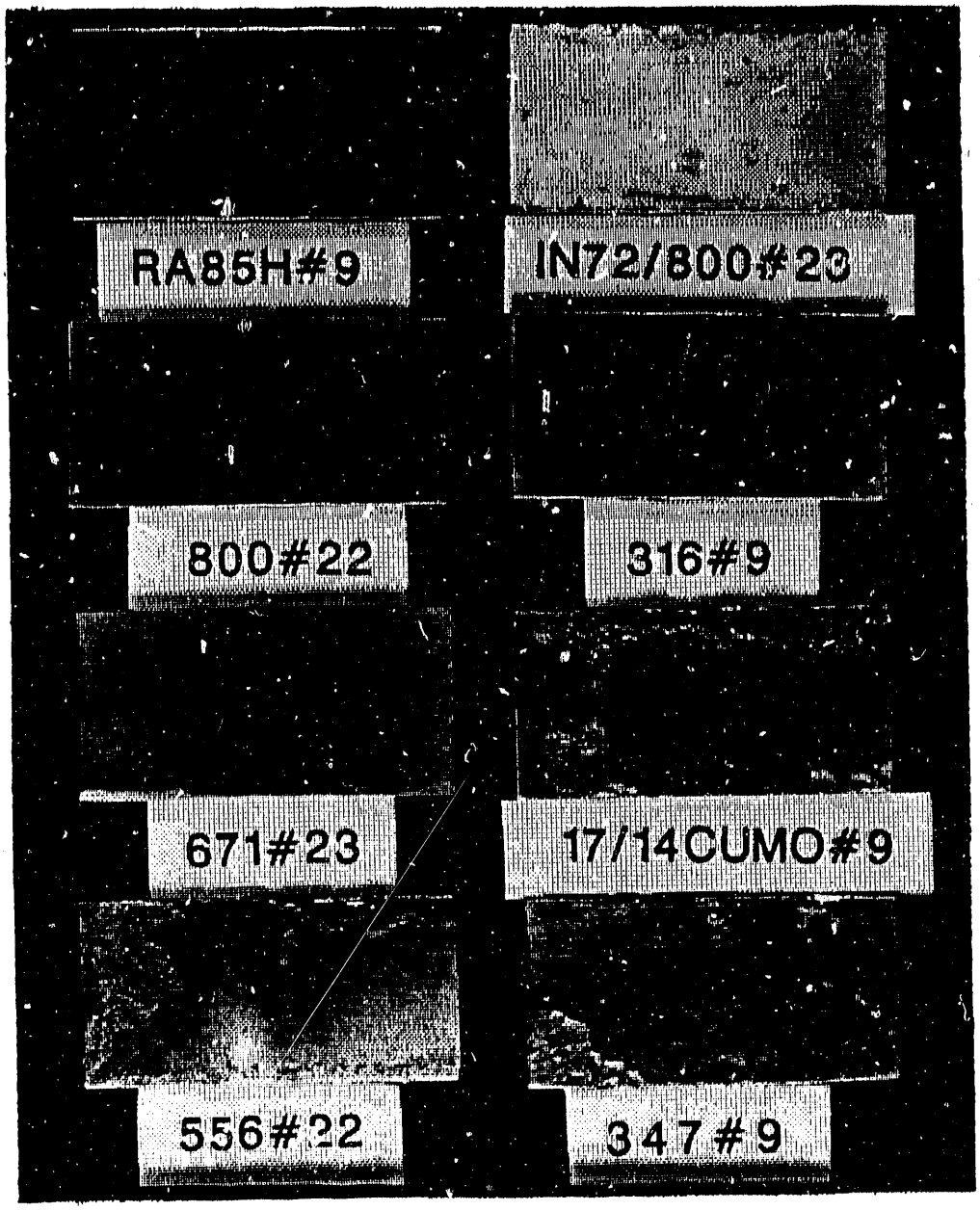

Gas Content:	0.25 vol% SO_2
Temperature:	700°C
Exposure Time:	100 hours
Sulfate Content:	10 wt%

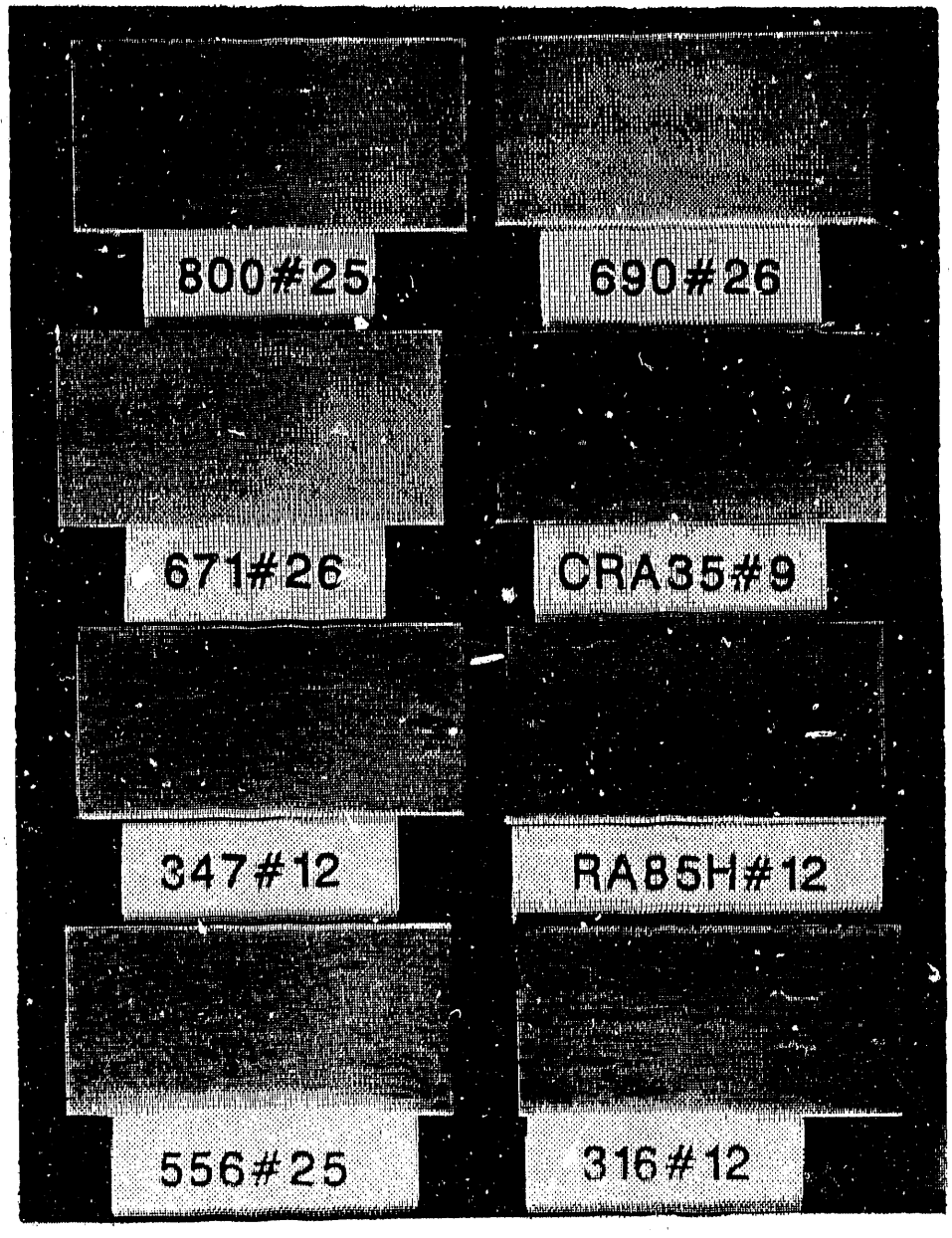

Gas Content:	0.25 vol% SO_2
Temperature:	650°C
Exposure Time:	100 hours
Sulfate Content:	10 wt%

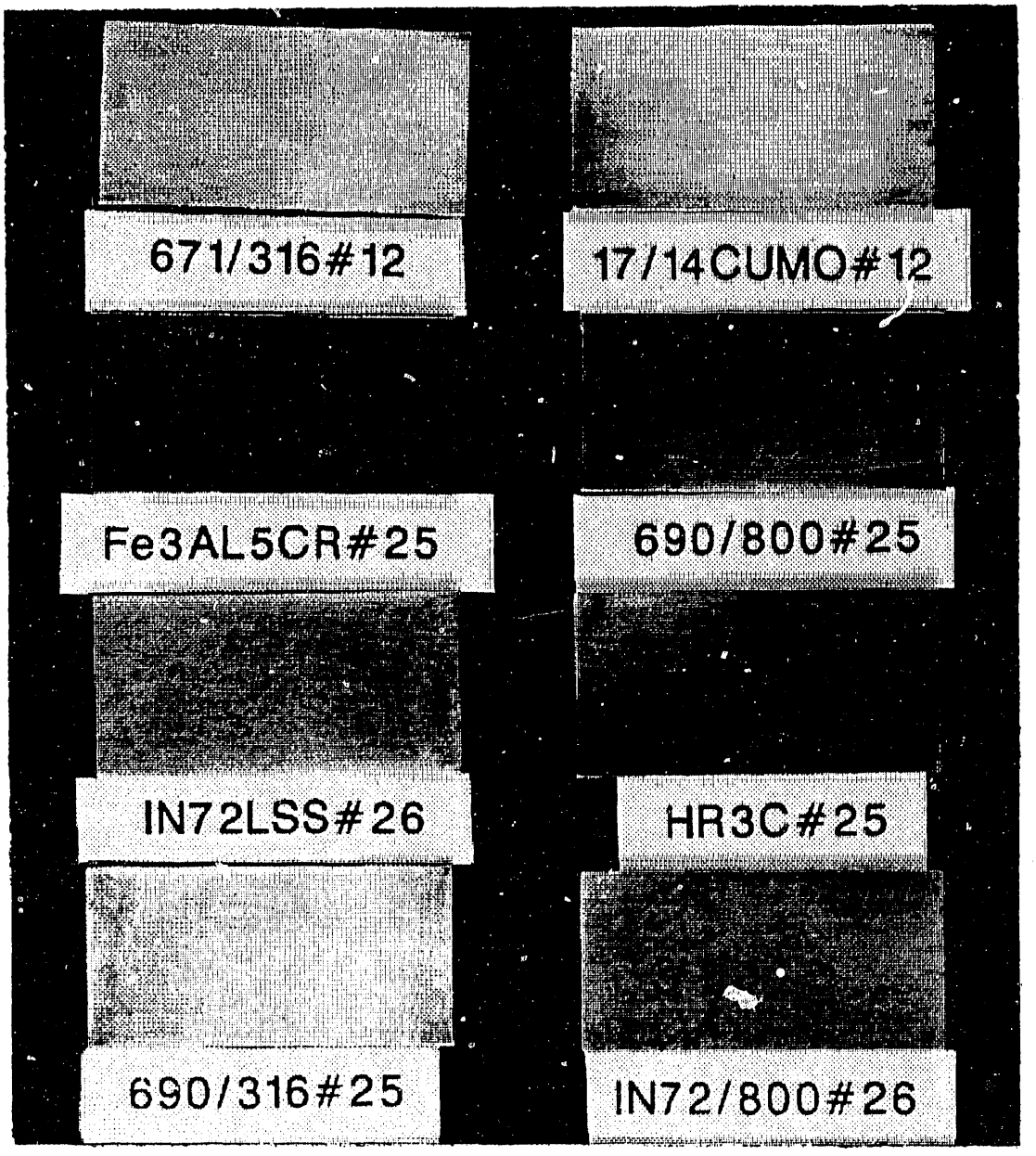

Gas Content:	0.25 vol% SO_2
Temperature:	650°C
Exposure Time:	100 hours
Sulfate Content:	10 wt%

APPENDIX B

DISTRIBUTION

AIR PRODUCTS AND CHEMICALS
P. O. Box 538
Allentown, PA 18105
S. W. Dean
S. C. Weiner

ALBERTA RESEARCH COUNCIL
Oil Sands Research Department
P.O. Box 8330, Postal Station F
Edmonton, Alberta
Canada T6H5X2
L. G. S. Gray

ALLISON GAS TURBINE DIVISION
P. O. Box 420
Indianapolis, IN 46206-0420
P. Khandelwal (Speed Code W-5)
R. A. Wenglarz (Speed Code W-16)

AMAX R&D CENTER
5950 McIntyre Street
Golden, CO 80403
T. B. Cox

ARGONNE NATIONAL LABORATORY
9700 S. Cass Avenue
Argonne, IL 60439
W. A. Ellingson
K. Natesan

ARGONNE NATIONAL LABORATORY-WEST
P. O. Box 2528
Idaho Falls, ID 83403-2528
S. P. Henslee

AVCO RESEARCH LABORATORY
2385 Revere Beach Parkway
Everett, MA 02149
R. J. Pollina

BABCOCK & WILCOX
1562 Beeson St.
Alliance, OH 44601
T. I. Johnson

BABCOCK & WILCOX
Domestic Fossil Operations
20 South Van Buren Ave.
Barberton, OH 44023
M. Gold

BATTELLE-COLUMBUS LABORATORIES
505 King Avenue
Columbus, OH 43201
V. K. Sethi
I. G. Wright

BETHLEHEM STEEL CORPORATION
Homer Research Laboratory
Bethlehem, PA 18016
B. L. Bramfitt
J. M. Chilton

BRITISH COAL CORPORATION
Coal Research Establishment
Stoke Orchard, Cheltenham
Glouchester, England GL52 4RZ
M. Arnold
C. Bower
A. Twigg

BRITISH GAS CORPORATION
Westfield Development Centre
Cardenden, Fife
Scotland KY50HP
J. E. Scott

BROOKHAVEN NATIONAL LABORATORY
Department of Applied Science
Upton, Long Island, NY 11973
T. E. O'Hare

CANADA CENTER FOR MINERAL & ENERGY TECHNOLOGY
568 Booth Street
Ottawa, Ontario
Canada K1A OG1
R. Winston Revie
Mahi Sahoo

COLORADO SCHOOL OF MINES
Department of Metallurgical Engineering
Golden, CO 80401
G. R. Edwards

COMBUSTION ENGINEERING
911 W. Main Street
Chattanooga, TN 37402
D. A. Canonico

EC TECHNOLOGIES INC.
3614 Highpoint Drive
San Antonio, TX 78217
D. J. Kenton

ELECTRIC POWER RESEARCH INSTITUTE
P.O. Box 10412
3412 Hillview Avenue
Palo Alto, CA 94303
W. T. Bakker
J. T. Stringer
H. Wolk

EUROPEAN COMMUNITIES JOINT RESEARCH CENTRE
Petten Establishment
P. O. Box 2
1755 ZG Petten
The Netherlands
M. Van de Voorde

FOSTER WHEELER DEVELOPMENT CORPORATION
Materials Technology Department
John Blizard Research Center
12 Peach Tree Hill Road
Livingston, NJ 07039
J. L. Blough

IDAHO NATIONAL ENGINEERING LABORATORY
P.O. Box 1625
Idaho Falls, ID 83415
D. W. Keefer
R. N. Wright

LAWRENCE LIVERMORE LABORATORY
P.O. Box 808, L-325
Livermore, CA 94550
W. A. Steele

NATIONAL INSTITUTE OF STANDARDS AND TECHNOLOGY
Materials Building
Gaithersburg, MD 20899
L. K. Ives

NATIONAL MATERIALS ADVISORY BOARD
National Research Council
2101 Constitution Avenue
Washington, DC 20418
K. M. Zwilsky

NEW ENERGY AND INDUSTRIAL TECHNOLOGY DEVELOPMENT ORGANIZATION
Sunshine 60 Bldg.
P.O. Box 1151, 1-1
Higashi-Ikebukuro 3-chrome
Toshima-Ku, Tokyo, 170
Japan
H. Narita/S. Ueda

OAK RIDGE NATIONAL LABORATORY
P. O. Box 2008
Oak Ridge, TN 37831
P. T. Carlson
N. C. Cole
J. H. DeVan
R. R. Judkins
J. L. Langford (8 copies)
R. W. Swindeman

RESEARCH TRIANGLE INSTITUTE
P. O. Box 12194
Research Triangle Park, NC 27709
T. W. Sigmon

SHELL DEVELOPMENT COMPANY
P. O. Box 1380
Houston, TX 77251-1380
L. W. R. Dicks

THE JOHNS HOPKINS UNIVERSITY
Materials Science & Engineering
Maryland Hall
Baltimore, MD 21218
R. E. Green, Jr.

THE MATERIALS PROPERTIES COUNCIL, INC.
United Engineering Center
345 E. Forty-Seventh Street
New York, NY 10017
M. Prager

THE TORRINGTON COMPANY
Advanced Technology Center
59 Field Street
Torrington, CT 06790
W. J. Chmura

UNION CARBIDE CORPORATION
Linde Division
P. O. Box 44
175 East Park Drive
Tonawanda, NY 14151-0044
Harry Cheung

UNIVERSITY OF NOTRE DAME
Department of Materials Science
and Engineering
P. O. Box E
Notre Dame, IN 46556
T. H. Kosel

UNIVERSITY OF TENNESSEE AT KNOXVILLE
Materials Science and Engineering Dept.
Knoxville, TN 37996
R. A. Buchanan
C. D. Lundin

UNIVERSITY OF TENNESSEE SPACE INSTITUTE
Tullahoma, TN 37388
J. W. Muehlhauser

UNIVERSITY OF WASHINGTON
Department of Materials Science
and Engineering
101 Wilson, FB-10
Seattle, WA 98195
T. G. Stoebe

WESTINGHOUSE ELECTRIC CORPORATION
Research and Development Center
1310 Beulah Road
Pittsburgh, PA 15235
S. C. Singhal

WESTINGHOUSE HANFORD COMPANY
P.O. Box 1970, W/A-65
Richland, WA 99352
R. N. Johnson

DOE
IDAHO OPERATIONS OFFICE
P. O. Box 1625
Idaho Falls, ID 83415
R. B. Loop

DOE
DOE FIELD OFFICE, OAK RIDGE
P. O. Box 2001
Oak Ridge, TN 37831
Assistant Manager for Research and Development

DOE
DOE FIELD OFFICE, OAK RIDGE
P. O. Box 2008
Building 4500N, MS 6269
Oak Ridge, TN 37831
E. E. Hoffman

DOE
OFFICE OF BASIC ENERGY SCIENCES
Materials Sciences Division
ER-131 GTN
Washington, DC 20545
J. B. Darby

DOE
OFFICE OF CONSERVATION AND RENEWABLE ENERGY
CE-12 Forrestal Building
Washington, DC 20545
J. J. Eberhardt

DOE
OFFICE OF FOSSIL ENERGY
Washington, DC 20545
D. J. Beecy (FE-14) GTN
J. P. Carr (FE-14) GTN
F. M. Glaser (FE-14) GTN

DOE
MORGANTOWN ENERGY TECHNOLOGY CENTER
P. O. Box 880
Morgantown, WV 26505
R. A. Bajura
R. C. Bedick
D. C. Cicero
F. W. Crouse, Jr.
N. T. Holcombe
W. J. Huber
M. J. Mayfield
J. E. Notestein
J. S. Wilson

DOE
PITTSBURGH ENERGY TECHNOLOGY CENTER
P. O. Box 10940
Pittsburgh, PA 15236
A. H. Baldwin
G. V. McGurl
R. Santore
T. M. Torkos

END

DATE
FILMED
4/01/92